JOURNAL OF THE AERONAUTICAL SCIENCES

VOLUME 16 JULY, 1949 NUMBER 7

A Study of the Bending-Torsion Aeroelastic Modes for Aircraft Wings

MARTIN GOLAND* AND YUDELL L. LUKE†

Midwest Research Institute

SUMMARY

The manner of arriving at the stability determinant for natural motions of a bending vs. torsion aeroelastic system is outlined. This permits determination of the characteristics of the natural modes of the system at any chosen air speed. Sample calculations are presented for a series of wings subject to bending vs. torsion flutter, showing how the natural mode dampings and frequencies change as the flutter speed is approached. It is found that the damping in the critical mode increases with air speed until at least 85 per cent of the critical speed is attained; it then rapidly decreases to the flutter value of zero. The noncritical mode encounters a sharp increase in stability in the proximity of flutter. A comparison is also made between the normal mode characteristics and the system response due to forced excitation; it is found that the latter usually affords an earlier indication of the approach to a critical state. From this it appears that flight-flutter testing is best carried out using the forced vibration technique.

INTRODUCTION

A SIGNIFICANT TREND in current aeronautical engineering practice is the growing detail with which a variety of dynamical problems must be treated. Whereas in the past it has been possible to approach a design almost solely on the basis of satisfying certain pseudostatic operating conditions, when modern high-performance aircraft are involved, many instances arise where this point of view must be discarded; in its place, a realistic consideration of the craft as a free body in three-dimensional motion is necessary. This trend is particularly evident in certain problems in the fields of stability and structures, where the complexity of questions relating to handling qualities, maneuverability, and dynamic loads has increased to the point where the simplified pseudostatic approximations no longer apply. Examples of such problems are found in the study of the aircraft behavior in gusty air, the dynamical loads induced during landing, and the effects of aeroelasticity during high-performance operation.

The present paper is concerned with the dynamic characteristics of an aircraft while in flight at an air speed close to a critical wing bending-torsion flutter speed. The study is of interest for several reasons: The nature of the dynamic behavior of the craft near flutter is of importance in deciding on the maximum allowable flight speed consistent with safe operation. Also, one procedure for experimentally determining the flutter speed of a craft is by the method of forced oscillation;[1] to utilize this procedure with safety, the performance near flutter should be thoroughly understood. Finally, the results obtained here shed light on the aeroelastic mechanism of the bending-torsion flutter mode. Since it appears that many high-performance aircraft will of necessity operate at speeds that are relatively close to a flutter speed, questions of the kind discussed here assume an increased significance.

Considering now an elastic aircraft in free flight, it follows that the motions of the craft result from the simultaneous action of inertia, elastic, and aerodynamic forces, all of which are a consequence of the motion of the craft itself; if only small departures from a pseudostatic state of motion are considered, as is the usual case in theoretical aeroelastic treatments, then the magnitudes of these forces are linearly dependent on the disturbances themselves. From the general theory for linear dynamic systems, the result then appears that the disturbed motion is compounded from a number of natural modes, whose descriptions follow from a knowledge of the roots of the pertinent stability determinant. In addition to the forces mentioned, dissipative forces

Presented at the Session on Structures—Dynamic Loads, Seventeenth Annual Meeting, I.A.S., New York, January 24–27, 1949.

* Chairman, Engineering Mechanics Division.

† Research Mathematician.

are encountered in all physical systems; while these are of considerable practical importance, their influence on the dynamic behavior of the system is well understood, and it is permissible to neglect their effects for the purposes of the present theoretical discussion.

The nature of the response mechanism for the case of forced oscillations in flight is also disclosed by the general theory. The response is composed of two parts: one is the natural response arising from the complementary solution to the equations of motion and involving the natural modes, while the second part is the forced response and corresponds to the particular solution to the equations.

The present paper is devoted to a study of the natural modes only. The character of the forced response has received the attention of numerous previous authors,[2, 3] of which the cited references are examples. Myklestad[2] derives the forced response resulting from the application of an external force of harmonically oscillating magnitude, while Smilg and Wasserman[3] investigate the hypothetical structural damping required to maintain constant amplitude oscillations at chosen air speeds. Studies of this kind, while informative in their own right, do not disclose the character of the natural modes.

In the present work, the general stability determinant for an aeroelastic system involving wing bending vs. wing torsion is established. The equations of motion are derived by making use of the Wagner air forces,[4, 5] which presume a potential flow of an incompressible fluid past a thin, two-dimensional airfoil in unsteady motion. It is then shown how the roots of the stability determinant can be extracted in a relatively simple manner, enabling a description of the natural modes. Sample calculations for a number of aircraft wings are presented over speed ranges from zero air speed up to the flutter speed. Finally, the results of the natural mode study are compared with the character of the forced response under conditions of harmonic oscillation to determine to what extent the two display a common mechanism.

The preparation of the present paper was suggested by certain findings by the authors in connection with a program sponsored by the Dynamics Branch, Aircraft Laboratory, Air Materiel Command, U.S. Air Force. Messrs. Smilg, Spielberg, and Wasserman, all of that agency, have contributed toward the development of many of the ideas.

Derivation of the Aeroelastic Modes

Since the concern here is with the natural modes at air speeds below the flutter speed, it follows that the analysis must be of sufficient generality to embrace nonharmonic motions of the system; for example, it is to be expected that the natural modes will be characterized by decaying oscillatory motions, and the air forces introduced in the equations of motion must embrace this circumstance. While structural damping is not included in the work here for reasons already given, it is of passing interest to note that no physically substantiated description of the dissipation mechanism for general kinds of motion is at present available to the analyst.

The Wagner air forces,[4, 5] which apply under the conditions mentioned in the previous section of the paper, are employed in the present analysis. For the convenience of the reader, a brief description of these air forces is now given. Throughout the analysis in this paper, a nondimensional coordinate system is used, according to the following scheme: Physical lengths are referred to the reference length b_r, where b_r is a reference semichord length of the wing; physical times are referred to b_r/U_0, where U_0 is the forward speed of the craft, considered to remain constant in the present study; physical masses are referred to ρb_r^3, where ρ is the mass density of the air; physical forces are then referred to the force $\rho U_0^2 b_r^2$.

Consider now an airfoil with a semichord b moving horizontally to the left with a uniform forward velocity in a two-dimensional field of flow. Let $w_h(\tau)$ be the time history of the downward velocity of the airfoil measured at the rear quarter-chord point, and let $\theta(\tau)$ be the time history of the nose-up pitching motions (τ is the nondimensional time). The forces and moments acting per unit of span as a result of unsteady motion are then as follows:

(a) A *lift* force with center of pressure at the forward quarter-chord point and of amount

$$L_1 = 2\pi b \int_0^\tau \kappa\left(\frac{\tau - \tau_1}{b}\right)\{\dot{w}_h(\tau_1) + \dot{\theta}(\tau_1)\}d\tau_1 + 2\pi b\kappa\left(\frac{\tau}{b}\right)\{w_h(0) + \theta(0)\} \quad (1)$$

where the function $\kappa(\tau)$ describes the growth of lift on an airfoil of physical semichord b_r due to a sudden (step-function) change in angle of attack and is equal to

$$\kappa(\tau) = 1 - \Phi(\tau) \quad (2)$$

where $\Phi(\tau)$ is the Wagner "lift deficiency" function calculated by von Kármán and Sears.[5] Jones[6] suggests that $\kappa(\tau)$ can be approximated with sufficient accuracy for practical purposes by the expression

$$\kappa(\tau) \approx 1 - a_1 e^{-\beta_1 \tau} - a_2 e^{-\beta_2 \tau} \quad (3)$$

where $a_1 = 0.165$, $a_2 = 0.335$, $\beta_1 = 0.0455$, and $\beta_2 = 0.3$. For convenience, this approximation is retained in the work reported here.

(b) A *lift* force with center of pressure at the midchord and of amount

$$L_2 = \pi b^2\{\dot{w}_h(\tau) + \dot{\theta}(\tau)\} \quad (4)$$

(c) A *downward* force with center of pressure halfway between the forward quarter-chord and the midchord and of amount

$$L_3 = (\pi/2)b^3\{\ddot{\theta}(\tau)\} \quad (5)$$

(d) Finally, a *nose-down* moment of amount

$$M_1 = (\pi/2)b^3\{\dot{\theta}(\tau)\} \tag{6}$$

It is evident that L_1 describes the circulatory component of lift; L_2 and L_3 are "apparent mass" contributions, while M_1 is a rotational damping component.

The total lift on the airfoil per unit of span is then

$$L = L_1 + L_2 - L_3 \tag{7}$$

and the total moment about the forward quarter-chord, positive when nose-up, is

$$M = -(1/2)L_2 + (1/4)L_3 - M_1 \tag{8}$$

In the analysis to follow, interest is centered on the air forces that arise from a damped, oscillatory motion of the airfoil. A general motion of this kind is defined by the time histories

$$z = Ae^{\lambda\tau}; \quad \theta = Be^{\lambda\tau}; \quad \lambda = -\alpha + j\omega \tag{9}$$

where z is a complex coordinate, the real (or imaginary) part of which represents the vertical displacement at the forward quarter-chord point; θ is now taken to be a complex coordinate, the real (or imaginary) part of which describes the pitch of the airfoil, positive when nose-up; and A and B are complex constants. The parameter α describes the degree of the decay of the motion, while ω refers to the circular frequency; evidently, by proper choice of α and ω, the time histories can be made to apply to harmonic, as well as to aperiodic, motions. It follows at once that $w_h(\tau)$ can be represented in complex form as

$$w_h(\tau) = \dot{z} + b\dot{\theta} = \lambda(z + b\theta) \tag{10}$$

The air forces due to the motion Eq. (9) are readily obtained from an application of Eqs. (1) through (10). Treating first the circulatory component, this is most easily derived with the aid of operational methods. The Laplace transform of L_1 is shown by the standard procedures to be[7]

$$\bar{L}_1 = 2\pi b \frac{\delta_1 p^2 + \delta_2 p + \delta_3}{(bp + \beta_1)(bp + \beta_2)(p - \lambda)} \times [\lambda A + (b\lambda + 1)B] \tag{11}$$

where p is the Laplace operator,

$$\delta_1 = [1 - a_1 - a_2]b^2$$
$$\delta_2 = [\beta_1(1 - a_2) + \beta_2(1 - a_1)]b$$
$$\delta_3 = \beta_1\beta_2$$

For the problem at hand, the aperiodic air force components arising from the poles $p = -\beta_1/b$ and $p = -\beta_2/b$ are not of interest; only the air forces due to the pole $p = \lambda$ are required, and these are

$$L_1 = 2\pi b \frac{(\delta_1\lambda^2 + \delta_2\lambda + \delta_3)}{(b\lambda + \beta_1)(b\lambda + \beta_2)} [\lambda z + (b\lambda + 1)\theta] \tag{12}$$

It is convenient to set

$$c(\lambda) = (\delta_1\lambda^2 + \delta_2\lambda + \delta_3)/[(b\lambda + \beta_1)(b\lambda + \beta_2)] \tag{13}$$

and then the circulatory component of the wing lift becomes

$$L_1 = 2\pi b\{c(\lambda)\}[\lambda z + (b\lambda + 1)\theta] \tag{14}$$

The remaining lift and moment components L_2, L_3, M_1 are derived without difficulty by direct substitution of the z, θ forms.

It is then found that the total wing lift and the wing moment about the forward quarter-chord point, each per unit of span, can be written as

$$L = l_z z + l_\theta \theta \tag{15}$$

$$M = m_z z + m_\theta \theta \tag{16}$$

where

$$l_z = \pi b[2\lambda c(\lambda) + b\lambda^2] \tag{17}$$

$$l_\theta = \pi b[2(b\lambda + 1)c(\lambda) + b\lambda(b\lambda + 1) - (b^2/2)\lambda^2] \tag{18}$$

$$m_z = -(\pi/2)b^2\lambda^2 \tag{19}$$

$$m_\theta = \pi b^2\left[-\frac{1}{2}\lambda(b\lambda + 1) + \frac{b}{2}\lambda\left(\frac{\lambda}{4} - 1\right)\right] \tag{20}$$

Before concluding this résumé of the air forces induced by the unsteady motion of the airfoil, it is of interest to note how the present descriptions reduce to the well-known results for certain limiting cases. For the pseudostatic case, when $\lambda = 0$, the familiar expressions for the air forces arise (note that the static angle of attack is $\lambda z + \theta$). Considering next harmonic motion with the circular frequency Ω, so that $\alpha = 0$ and $\lambda = j\Omega$, it is seen that Eqs. (15) through (20) reduce to the Theodorsen results,[3, 8] with the function $c(\lambda)$ fulfilling the role of his $C(k)$ function. If Eq. (13) is examined with this in mind, it is found that the function $c(\lambda)$ agrees to within a few per cent with the corresponding values of $C(k)$ over the entire range of values of Ω.

Attention is now given to the derivation of the equations of motion for the bending vs. torsion aeroelastic system. Consider first a two-dimensional system of unit span. Letting z_e be the downward displacement at the elastic axis, then the kinetic energy for the system can be written as

$$2T = m\dot{z}_e^2 + 2S\dot{z}_e\dot{\theta} + I\dot{\theta}^2 \tag{21}$$

where m is the airfoil mass, S is the mass static unbalance about the elastic axis (positive for a rearward c.g.), and I is the mass moment of inertia about the elastic axis. The potential energy of the system is written as

$$2V = m\omega_b^2 z_e^2 + I\omega_t^2\theta^2 \tag{22}$$

where ω_b and ω_t are the uncoupled wing bending and torsion frequencies, respectively. The air forces, Eqs. (15) and (16), are next referenced to the elastic axis displacement, so that the lift and the nose-up moment about the elastic axis are written as

$$L = l_1 z_e + l_2\theta \tag{23}$$

$$M_e = m_1 z_e + m_2\theta \tag{24}$$

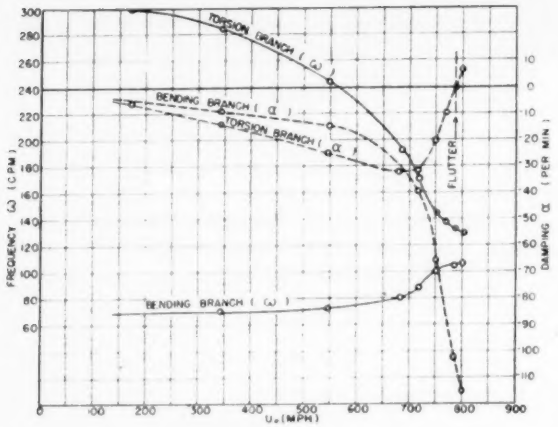

FIG. 1. Natural mode characteristics plotted vs. air speed for the wing bending-torsion system with $\omega_b = 69$ cycles per min. and $\omega_t = 304$ cycles per min.

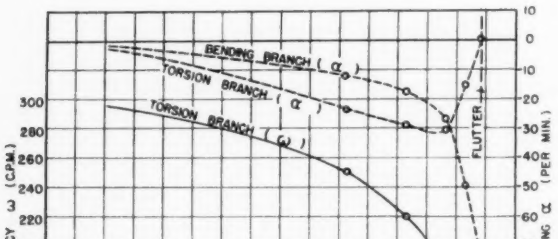

FIG. 2. Natural mode characteristics plotted vs. air speed for the wing bending-torsion system with $\omega_b = 103.5$ cycles per min. and $\omega_t = 304$ cycles per min.

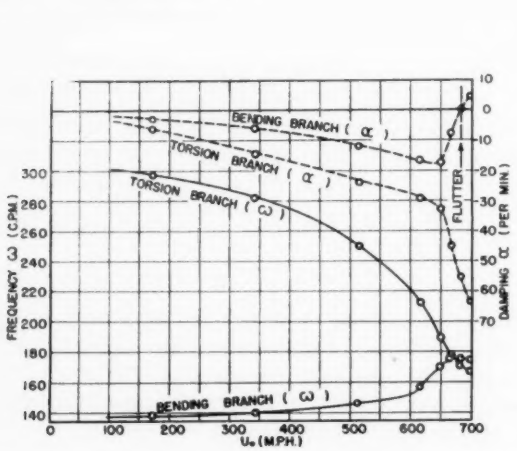

FIG. 3. Natural mode characteristics plotted vs. air speed for the wing bending-torsion system with $\omega_b = 138$ cycles per min. and $\omega_t = 304$ cycles per min.

where

$$l_1 = l_z; \quad l_2 = l_\theta - el_z \tag{25}$$

$$m_1 = m_z + el_z \tag{26}$$

$$m_2 = m_\theta + e(l_\theta - m_z) - e^2 l_z \tag{27}$$

and where e is the rearward distance from the quarter-chord point to the elastic axis.

An application of the Lagrange equations of motion, using Eqs. (9) and (21) through (24) then leads to the equations of motion for the system,

$$\{m(\lambda^2 + \omega_b^2) + l_1\}z_e + \{S\lambda^2 + l_2\}\theta = 0 \tag{28}$$

$$\{S\lambda^2 - m_1\}z_e + \{I(\lambda^2 + \omega_t^2) - m_2\}\theta = 0 \tag{29}$$

Those values of λ which are the roots of the stability determinant arising from Eqs. (28) and (29) describe the natural modes of the aeroelastic system. With the roots λ known, the mode shapes are determined from the equations of motion in the usual manner.

In the interests of clarity, consideration has thus far been confined to a two-dimensional system. The air forces, however, are derived for a wing strip of arbitrary chord b, so that the tools necessary for a three-dimensional aeroelastic analysis are at hand. The procedure for extending the argument to a three-dimensional system is well-known[3] and is not repeated here. The sample calculations described later are carried out for a three-dimensional wing.

Method of Solution

For the purposes of the present study, attention is centered on those aeroelastic modes that have their zero air-speed origins in the two ground vibration modes that are composed of fundamental wing bending and torsion. As the air speed is gradually increased, the character of these modes also changes in a continuous fashion, so that a space plot of λ vs. U_0 can be visualized as having two branches: The "bending branch" has its zero air-speed origin in the ground mode which is primarily wing bending, while the "torsion branch" has an analogous interpretation.

Since the parameters l_1, l_2, m_1, and m_2 are themselves complex functions of λ, it is evident that obtaining a straightforward solution for λ from the stability determinant of Eqs. (28) and (29) is a tedious operation; it is necessary that the roots of an eighth degree polynomial be found. Fortunately, however, the amount of labor required to effect a solution is considerably reduced by employing an iterative procedure for evaluating the stability roots. This procedure is described as follows:

It is to be noted that the numerical values of ω_b and ω_t are dependent on the magnitude of U_0; hence, a separate solution must be carried out for each air speed. To start a particular solution, attention is centered on one of the modes, say the bending branch, and a reasonable estimate for the mode frequency is made.

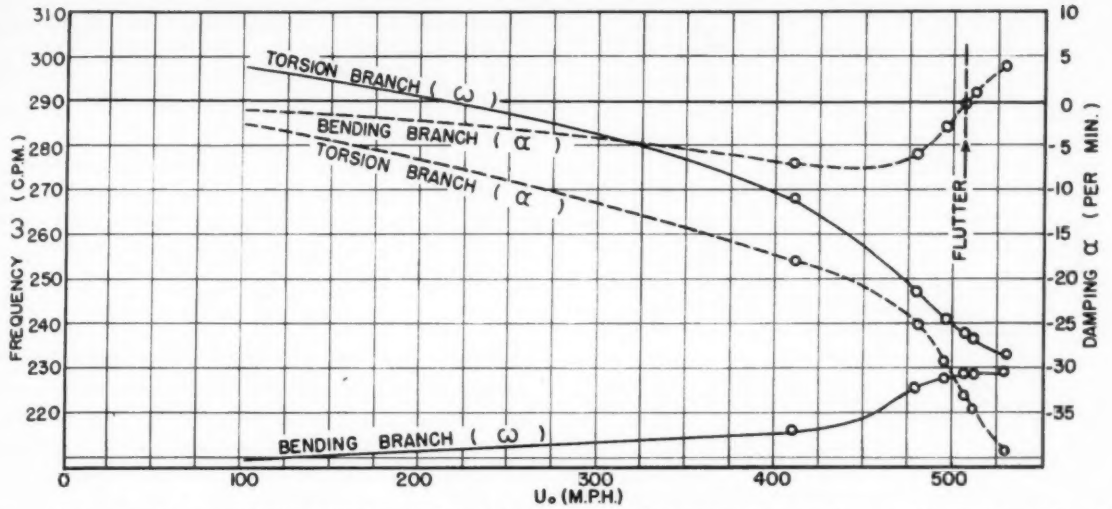

FIG. 4. Natural mode characteristics plotted vs. air speed for the wing bending-torsion system with $\omega_b = 207$ cycles per min. and $\omega_t = 304$ cycles per min.

Assuming that $\alpha = 0$ and setting ω equal to the estimated frequency [see Eq. (9)], the associated value of $c(\lambda)$ is computed from Eq. (13), and then l_1, l_2, m_1, and m_2 are evaluated from Eqs. (25) through (27). The trial values for the latter four coefficients are next introduced into the stability determinant, which now takes the form of a quadratic in λ^2. The roots of the quadratic are found, and a refined value for the λ corresponding to the bending branch is thus obtained; four roots λ are obtained from the quadratic, and the root of interest is readily chosen by inspection and on the basis of physical reasoning.

Based on the refined λ value, a new value for $c(\lambda)$ is computed, and then the four air-force coefficients l_1, l_2, m_1, m_2 are recalculated. The new quadratic in λ^2 corresponding to these coefficients is written and the roots derived. A second refinement for the value of the bending branch λ is thus obtained. The process is repeated until the values of λ computed by successive iterations agree with each other within reasonable limits—i.e., the process is continued until convergence is attained. In order to compute the torsion branch λ, the entire iteration process is repeated from the beginning.

It is found that convergence is usually attained within a surprisingly few iteration cycles, three or four such cycles generally being sufficient for each λ determination. The numerical operations involved in the work are relatively convenient to handle with desk-type calculating machines, so that solutions can be obtained rapidly and without tedious effort.

Calculations for Sample Wings

To illustrate the kind of results to be expected from an aeroelastic study of the type described here, a series of calculations are now presented which bring to light the effect of a change in the ratio ω_b/ω_t on the aeroelastic behavior of a fighter-class wing. A series of wings are studied, each being dynamically identical with the next except that the natural frequency of the normal bending mode is varied. The frequency of the normal (uncoupled) torsion mode is kept at 304 cycles per min., and wings with the following (uncoupled) bending mode frequencies are dealt with: 69, 103.5, 138, 207, and 276 cycles per min. The corresponding ratios of ω_b/ω_t for the wings are 0.227, 0.341, 0.454, 0.682, and 0.909. The wings are taken as supported in the "free-free" sense and carry a fuselage at the root and a substantial concentrated weight at the wing tip (arising from a tip tank installation). The detailed data for the wing system with the 138 cycles per min. bending frequency are drawn from the description of an actual model of a modern fighter aircraft, the system being fully described in a previous paper by the present authors;[9] see the Case I aircraft, Table I, of that paper. All of the wings dealt with here are assumed to have the same generalized masses as the 138 cycle per min. wing, as well as the same geometric and mode shape characteristics. Hence, the wings are dynamically identical, save for the bending frequency parameter.

The results of the calculations for the bending branch and torsion branch stability roots for the five wings are shown in Figs. 1–5. The calculations extend from zero air speed up to the flutter speed, and the plots are of α and ω as a function of the air speed U_0. The air speeds quoted are uncorrected for compressibility effects—i.e., they refer to flight in "incompressible" air.

The first point of interest to be noted in Figs. 1–5 concerns the variation of the mode damping α with air speed. For the branch that leads to flutter, it is seen

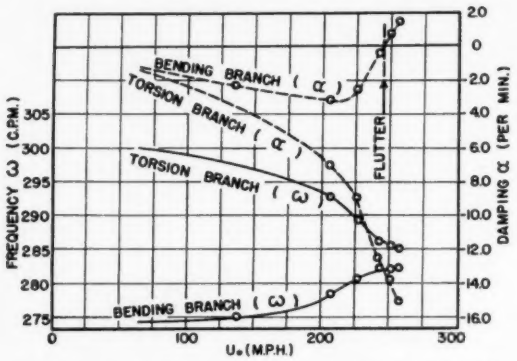

FIG. 5. Natural mode characteristics plotted vs. air speed for the wing bending-torsion system with $\omega_b = 276$ cycles per min. and $\omega_t = 304$ cycles per min.

that in each of the five cases the mode damping at first gradually increases with air speed; however, at some point in the region of from 85 to 95 per cent of the flutter speed, the mode stability suddenly starts to decrease and the damping rapidly drops to the flutter value ($\alpha = 0$). For the mode that does not lead to flutter, the damping gradually increases with the air speed until the region near flutter is reached. Then, as the critical speed is approached and the one mode goes to flutter, the damping in the second mode suddenly increases at a rapid rate. This substantial improvement in the stability of the nonflutter mode as the critical speed is approached is a matter of considerable interest.

Experience with wing bending-torsion flutter has shown it to be a precipitous phenomenon, the transition from stability to instability occurring within a narrow speed range; it is to be noted that this type of behavior is indicated by the present calculations. Also, it is a generally accepted design specification within the industry that the maximum flight speed for a model shall not exceed 85 per cent of its flutter speed. For wing bending-torsion flutter this is seen to be a reasonable requirement, since a decrease in mode stability is not to be expected until this limit speed is surpassed.

Turning now to a consideration of the mode frequencies, it follows from Figs. 1–5 that the bending branch frequency remains approximately the same and equal to the ground frequency at all air speeds, although a sudden slight increase is observed in the immediate vicinity of the flutter speed. The frequency of the torsion branch mode falls appreciably, however, as the air speed increases; at the flutter speed, the frequencies of both branches lie fairly close to each other for all five cases investigated. As in the three other curves in each figure, a sudden change in the nature of the torsion branch frequency variation with air speed occurs when the flutter speed is approached.

It should be noted that, for the systems with a low ω_b/ω_t ratio, it is the torsion branch mode that leads to flutter; for the higher ratios of the bending to torsion frequencies, the mode connected with the bending branch results in flutter. The well-known drop in critical speed as the bending and torsion frequencies approach each other in value is also observed in the present calculations.

As a final point of interest, the logarithmic decrements for the critical modes in the five cases are compared. It is readily shown that the logarithmic decrement for the natural oscillations at a particular air speed is given by

$$\log \Delta = 2\pi(\alpha/\omega)$$

Compare now the logarithmic decrements for the critical modes for the five wings at that air speed where the value of α is a maximum; this corresponds closely to the air speed at which a maximum of mode stability is indicated. In the order of ascending bending frequency, the values are roughly 1.08, 1.06, 0.67, 0.21 and 0.074.

It is thus seen that, as the ratio ω_b/ω_t increases, the rate of decay of the natural oscillations in the critical mode tends to decrease—i.e., the mode gives the appearance of relatively lesser stability. As ω_b/ω_t approaches unity, the natural oscillations disappear at an extremely slow rate, regardless of air speed. Hence, the severity of flutter decreases as the normal bending and torsion frequencies approach each other in value.

The Behavior Near Flutter: A Comparison with the Air Materiel Command and Myklestad Methods

A proper analysis of the behavior of an aeroelastic system in the immediate vicinity of flutter is of considerable importance when, for example, a program of flight-flutter testing is undertaken. The results of the analysis must be used to appraise the safety of the procedure in general and must also serve as a basis for fixing a safe increment of air speed for successive tests.[1] In the simplest kind of flight-flutter testing, the aircraft is disturbed from steady flight by the pilot, and the resulting rate of decay is observed; here, only the natural modes are of interest. For more elaborate tests employing forced vibration, the nature of the forced response is of primary interest, although the presence of a poorly damped natural mode adds to the difficulty of obtaining accurate test data.

It is now of interest to compare the behavior of the natural modes near flutter with the responses that result from forced excitation, the primary object being to determine which of the two mechanisms is best adapted to flight-flutter studies. As has already been mentioned, the Air Materiel Command method[3] investigates the damping required to sustain steady oscillations at the various air speeds, while Myklestad[2] studies the response induced by an oscillatory applied force. The results afforded by these two procedures are now com-

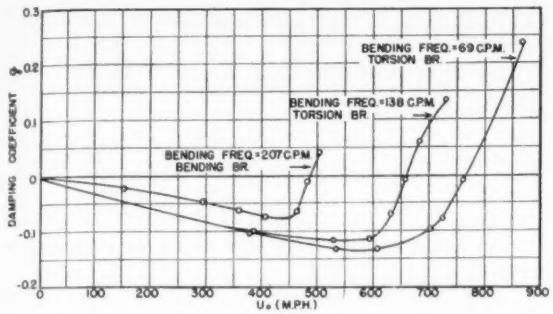

FIG. 6. Curves of g vs. U_0 calculated by the A.M.C. method for the wing bending-torsion systems with ω_b = 69, 138, and 207 cycles per min. and ω_t = 304 cycles per min.

pared with those obtained from an analysis of the natural modes as outlined in this paper.

Fig. 6 shows the U_0 vs. g curves derived by the A.M.C. method for three of the five wings studied in the last section (g is the fictitious damping coefficient required for steady oscillation). Only the curve for the critical mode in each case is shown. Comparing first the curve in Fig. 6 for the ω_b = 69 cycle per min. wing with the critical α vs. U_0 curve from Fig. 1, it is seen that the latter indicates a much sharper onset of flutter than does the former. For the ω_b = 138 cycle per min. wing (see Figs. 3 and 6), a similar situation prevails; the approach to flutter is more severe in the natural mode study than in the U_0 vs. g curve. For this case it is interesting to note that the natural mode analysis indicates that the bending branch leads to flutter, whereas the A.M.C. method shows the torsion branch becoming unstable. Finally, for the ω_b = 207 cycle per min. wing (Figs. 4 and 6), the two analyses predict about equal severity in the flutter approach.*

Fig. 7 is taken from a flutter analysis of the ω_b = 138 cycles per min. wing, carried out by the Myklestad method. It shows the imaginary part of the generalized complex bending force required to sustain steady oscillations at various air speeds and at several values of the reduced speed; flutter is encountered at a reduced speed of 16.75. It is seen that the shaking force starts to drop toward the flutter value (zero) at a somewhat earlier relative air speed than does the critical mode damping data shown in Fig. 6.

These limited results tend to show that the use of the forced excitation method for flight-flutter testing will usually afford an earlier indication of the approach to flutter than will a study of the natural modes. Hence, the former method is to be preferred on the grounds of safety.

* It is to be noted that the flutter speeds indicated in Figs. 1–5 do not coincide exactly with those shown in Figs. 6 and 7. The data for the last two figures were calculated using the exact values of the flutter aerodynamic coefficients, whereas the Figs. 1–5 data are subject to the errors arising from the approximation used for $c(\lambda)$, see Eq. (13).

CONCLUSIONS

The present paper outlines the manner of arriving at the stability determinant for an aeroelastic system which permits the determination of the natural mode characteristics at any chosen flight speed. Although a wing bending vs. torsion system is specifically dealt with, extension of the analysis to other arrangements presents no theoretic difficulties.

Sample calculations for a series of wing systems subject to bending-torsion flutter show that the damping in the critical natural mode increases until at least 85 per cent of the flutter speed is attained; it then rapidly drops to the flutter value of zero as the critical air speed is approached. The maximum damping encountered in the critical mode decreases as the ratio of the normal bending and torsion frequencies in the system approaches unity.

For the noncritical mode, a sharp increase in damping is indicated as the air speed comes in close proximity to the critical speed. For systems with a ratio of normal bending to torsion frequencies less than one, the frequency of the bending branch mode does not change markedly as flutter is approached; however, that of the torsion branch mode drops so that both modes have frequencies close to each other.

Comparing the behavior of the natural modes near flutter with the system response induced by forced excitation, it appears that the forced response usually gives the earliest indication of an approach to a critical

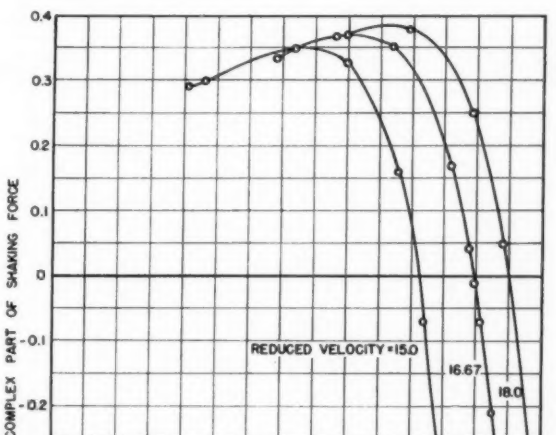

FIG. 7. Complex part of shaking force required to sustain steady oscillations, plotted vs. air speed and for several values of reduced speed, as calculated by the Myklestad method for the wing bending-torsion system with ω_b = 138 cycles per min. and ω_t = 304 cycles per min. (Flutter is at a reduced velocity of 16.75.)

state. Hence, for flight-flutter testing of bending-torsion configurations, the method of forced excitation usually affords greater safety than a study of the natural modes.

References

[1] Burow, H., and Roos, H., *Flight-Vibration Tests*, available from U.S. Air Force, Intelligence Department, Air Materiel Command, Wright-Patterson Air Force Base, Dayton, Ohio, as Report No. F-TS-765-RE, released February, 1948.

[2] Myklestad, N. O., *Vibration Analysis*, Section VI-6; McGraw-Hill Book Company, Inc., New York, 1944.

[3] Smilg, B., and Wasserman, L. S., *Application of Three-Dimensional Flutter Theory to Aircraft Structures*, U.S. Army Air Forces, Technical Report No. 4798, Air Materiel Command, Dayton, Ohio, July, 1942.

[4] Wagner, H., *Über die Enstehung des dynamischen Auftriebes von Tragelflügeln*, Z.A.M.M., Vol. 5, February, 1925.

[5] von Kármán, T., and Sears, W. R., *Airfoil Theory for Non-Uniform Motion*, Journal of the Aeronautical Sciences, Vol. 5, No. 10, August, 1938.

[6] Jones, R. T., *Operational Treatment of the Non-Uniform Lift Theory in Airplane Dynamics*, N.A.C.A. T.N. No. 667, October, 1938.

[7] Carslaw, H. S., and Jaeger, J. C., *Operational Methods in Applied Mathematics*, Oxford University Press, London, England, 1941.

[8] Theodorsen, T., *General Theory of Aerodynamic Instability and the Mechanism of Flutter*, N.A.C.A. T.R. No. 496, 1935.

[9] Goland, M., and Luke, Y. L., *The Flutter of a Uniform Wing with Tip Weights*, Journal of Applied Mechanics, Vol. 15, No. 1, March, 1948.

Notice to Contributors

Manuscripts submitted for publication *must* be double- or triple-spaced originals. There should be wide margins on both sides of the sheets and triple spacing around formulas to allow for the marking of directions for the printer.

Original drawings (jet black India ink on white paper or tracing cloth) should accompany the manuscript. (*Blueprints are not acceptable.*) Photographs *must* be on glossy white paper.

Only the simplest formulas should be typewritten; all others should be carefully written in pen and ink. The difference between capital and lower-case letters and Greek symbols should be clearly distinguished.

See Inside Back Cover of this issue for further details.

The Flutter of Servo-Controlled Aircraft

JONATHAN WINSON*

Fairchild Engine and Airplane Corporation

SUMMARY

This paper considers the problem of the flutter of servo-controlled aircraft. The existence of flutter in such craft depends, in part, on the dynamic characteristics of the servomechanisms used for control. In classical flutter theory, the control surface is assumed to be part of a simple elastic system made up of inertia, spring, and damper components. With this representation, the equations of motion for control surface-wing motion are written. Their solution yields the flutter information required. In the servo-controlled aircraft, control surface motion under so-called locked stick conditions is an expression of the reaction of the highly complex servomechanism to external disturbance. The mechanism is usually nonlinear and difficult to treat mathematically.

In the present solution for the flutter of the servo-controlled craft, experimentally determined characteristics of the servo unit are used. A method is evolved wherein the impedance of the servo and related elastic structure, as obtained by test, is compared to a set of theoretical flutter boundary curves. The flutter boundary curves are functions of the aircraft parameters. The comparison yields a complete understanding of the flutter characteristics of the aircraft. The technique involved is general, embracing classical flutter as a special case. It is shown that the method is a revealing means of solving the classical flutter problem. A sample calculation is carried out for a particular ship with and without servo-control.

INTRODUCTION

SERVOMECHANISMS OF VARIOUS TYPES have achieved widespread use in the control of aircraft. Their use is universal in the intrinsically high-speed pilotless planes. With the development of servo-control has come the need to re-examine the concept of the flutter of an aircraft member in light of the contribution of the servomechanism to the flutter system.

As applied to conventional aircraft, flutter is a self-excited instability of a physical system involving a flexible wing (with or without a control surface) and the air through which the wing travels. To make possible the mathematical treatment of this system, it is assumed that the motion of the wing is compounded of a number of modes, each distinguished by mode shape and natural frequency. For example, a case of flutter may involve the interaction of three modes: one of wing bending, one of wing torsion, and one of control surface rotation. It is further assumed that the action in any one mode is that of a simple mechanical system containing mass or inertia (the wing or control surface), linear springing (the elastic structure), and damping proportional to the amplitude of motion (the internal damping of the structure). The particular components making up the control surface system are the surface itself and the structure connecting it to the command station. With the introduction of a servomechanism between the command station and the control surface, the mass-spring-damper idealization becomes untenable. The reaction of the servomechanism to excitation at its output end is a complex function of the frequency of excitation, a function that is best determined experimentally. In the present analysis, then, the idealization of the system governing control surface action is dropped. The system is allowed to have an arbitrary impedance (the vector division of sinusoidal exciting moment at the control surface by angular response of the surface). The conception of wing action in bending and torsion remains as in classical theory.

Under these conditions, the equations of wing-control surface motion are written. The method of solution consists in choosing specific values of flutter frequency and flight velocity and determining the unique impedance that will allow the neutrally stable flutter condition to exist. In the solution, the flutter frequency and frequency of servo-oscillation are necessarily equal. The field of frequency and velocity of practical interest in a given case is covered by systematic calculations of this sort. The values of the impedance required for flutter are plotted as a set of loci, each locus representing possible flutter at a given frequency carried from zero velocity to the top speed of the aircraft. The loci are termed flutter boundary curves. Comparison with the experimental frequency variation of impedance of the servo and control structure allows the flutter characteristics of the aircraft to be deduced.

The impedance of the classical control surface system is a theoretically defined quantity. Correlation with standard flutter theory is shown by consideration of this special case. The merits of the present method as applied to conventional (nonservo) aircraft are also discussed.

The technique that has been described is developed in detail below. Specifically, the work is divided into the following sections: (I) The Equations of Motion. (II) Specification of Flutter Boundary Curves: Case (a) Torsion-Bending-Control Surface Rotation; Case (b) Bending-Control Surface Rotation; Case (c) Torsion-Control Surface Rotation. (III) Sample Calculation.

NOMENCLATURE

Geometric Quantities

- a = distance from mid-chord to elastic axis in per cent of semichord, positive aft
- b = semichord
- c = distance from mid-chord to control surface leading edge in per cent of semichord, positive aft

Received February 23, 1949.

* In Charge of Dynamics, Pilotless Plane Division.

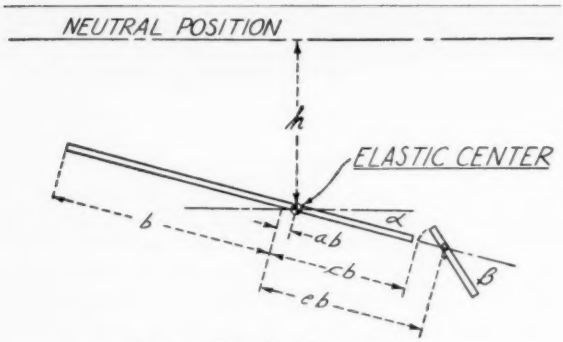

FIG. 1. The wing-aileron system.

e = distance from mid-chord to control surface hinge line in per cent of semichord, positive aft
h = vertical bending deflection, positive down
α = angular deflection in torsion of airfoil section, positive when trailing edge is depressed
β = angular deflection of control surface about the hinge line, positive when trailing edge is depressed

Aerodynamic Quantities

V = forward velocity of the aircraft
ρ = density of the air
M_α = aerodynamic moment of the airfoil about the elastic axis per unit length of span at any instant in a steady oscillatory motion
M_β = aerodynamic moment of the control surface about the hinge line per unit length of span at any instant in a steady oscillatory motion
P = aerodynamic lift force per unit length of span at any instant in a steady oscillatory motion
R_{rs} = that part of the aerodynamic force or moment coefficient produced in the rth degree of freedom by a unit displacement in steady oscillating motion in the sth degree of freedom that is in phase with the motion in the sth degree of freedom
I_{rs} = the counterpart of R_{rs} that is in phase with the velocity of motion in the sth degree of freedom

Dynamic Quantities

C_α = torsional stiffness of airfoil section per unit length of span
C_h = airfoil vertical bending stiffness per unit length of span
g_α = airfoil torsional damping coefficient
g_h = airfoil vertical bending damping coefficient
I_α = mass moment of inertia of airfoil about elastic axis per unit length of span
I_β = mass moment of inertia of control surface about the hinge line per unit length of span
M = mass of airfoil per unit length of span
S_α = mass static moment of the airfoil about the elastic axis per unit length of span
S_β = mass static moment of the control surface about the hinge line per unit length of span
ω_α = natural frequency of a mode of torsional vibration of airfoil section
ω_h = natural frequency of a mode of bending vibration of airfoil section
ω = frequency of flutter oscillation
k = flutter parameter, $\omega b/V$
t = time
$\dot{v}$ = dv/dt, where v is a time variable

(I) EQUATIONS OF MOTION

Fig. 1 schematically portrays a wing-aileron system in displaced position. A unit span is considered and the equations of motion for wing bending, torsion, and aileron rotation are written. The equations set down are not for an arbitrary motion but, as is customary, are for the specific condition of simple harmonic motion of all the variables. The condition is one of neutral stability, separating a region of stability from a region of self-excited instability or flutter. Consideration of the neutrally stable state allows the flutter boundary to be specified in terms of the parameters of the problem.

Summing the forces on the section:

$$\ddot{h}M + hC_h(1 + ig_h) = P - \ddot{\alpha}S_\alpha - \ddot{\beta}S_\beta \qquad (1)$$

Complex notation is used to distinguish vector components in phase and out of phase with the bending motion. Idealized structural damping is indicated, such damping being in phase with the velocity of bending and proportional to the amplitude. The damping constant is put in the form $C_h g_h$ as a matter of convenience.

Taking moments about the elastic center of the section:

$$\ddot{\alpha}I_\alpha + \alpha C_\alpha(1 + ig_\alpha) = M_\alpha - \ddot{h}S_\alpha - \ddot{\beta}[I_\beta + b(e - a)S_\beta] \qquad (2)$$

Lastly, taking moments on the aileron about its hinge line:

$$f(\beta) = M_\beta - \ddot{h}S_\beta - \ddot{\alpha}[I_\beta + b(e - a)S_\beta] \qquad (3)$$

where the left-hand side of the equation is an unknown function of β.

To formalize the condition of harmonic motion, let

$$\left.\begin{aligned} \alpha &= \alpha_0 e^{i\omega t} \\ \beta &= \beta_0 e^{i(\omega t + \theta_1)} \\ h &= h_0 e^{i(\omega t + \theta_2)} \end{aligned}\right\} \qquad (4)$$

Substituting Eqs. (4) in Eqs. (1) and (2) and recognizing that $\omega_\alpha = \sqrt{C_\alpha/I_\alpha}$ and $\omega_h = \sqrt{C_h/M}$, there are obtained

$$-\alpha S_\alpha - \beta S_\beta - hM\left[1 - \left(\frac{\omega_h}{\omega}\right)^2(1 + ig_h)\right] = \frac{P}{\omega^2} \qquad (5)$$

$$-\alpha I_\alpha\left[1 - \left(\frac{\omega_\alpha}{\omega}\right)^2(1 + ig_\alpha)\right] - \beta\left[I_\beta + b(e - a)S_\beta\right] - hS_\alpha = \frac{M_\alpha}{\omega^2} \qquad (6)$$

With the substitution of Eqs. (4) in the right-hand side of Eq. (3), the sinusoidal moment forcing the motion of the aileron system becomes

$$\text{Moment} = M_\beta + \alpha\omega^2[I_\beta + b(e - a)S_\beta] + h\omega^2 S_\beta \qquad (7)$$

M_β is harmonic and of the same frequency as β.[1]

The vector impedance of the aileron system may be defined in terms of its response to a sinusoidal forcing moment $\mathfrak{M}$. Thus,

$$\text{Impedance } \beta \equiv \mathfrak{M}/\beta \qquad (8)$$

The impedance depends on frequency and, for the nonlinear servomechanism, on the magnitudes of $\mathfrak{M}$ and

β. The latter dependence is discussed at a later point in the paper. Impedance β is expressed in real and imaginary parts as follows:

$$\text{Impedance } \beta \equiv g_1 + i\, g_2 \tag{9}$$

Then

$$\mathfrak{M} = \beta(g_1 + i\, g_2) \tag{10}$$

Substituting in Eq. (10) the moment given by Eq. (7), the equation for aileron motion becomes

$$-\alpha[I_\beta + b(e - a)S_\beta] + \frac{\beta}{\omega^2}(g_1 + i\, g_2) - hS_\beta = \frac{M_\beta}{\omega^2} \tag{11}$$

The aerodynamic moments and force are*

$$\left.\begin{aligned} M_\alpha &= -\pi\rho b^4\omega^2\left[(R_{ah} + iI_{ah})\frac{h}{b} + (R_{a\beta} + iI_{a\beta})\beta + (R_{a\alpha} + iI_{a\alpha})\alpha\right] \\ M_\beta &= -\pi\rho b^4\omega^2\left[(R_{bh} + iI_{bh})\frac{h}{b} + (R_{b\beta} + iI_{b\beta})\beta + (R_{b\alpha} + iI_{b\alpha})\alpha\right] \\ P &= -\pi\rho b^3\omega^2\left[(R_{ch} + iI_{ch})\frac{h}{b} + (R_{c\beta} + I_{c\beta})\beta + (R_{c\alpha} + iI_{c\alpha})\alpha\right] \end{aligned}\right\} \tag{12}$$

where R_{ah}, I_{ah}, etc., are functions of airfoil geometry and the parameter $V/\omega b$. R_{ah}, I_{ah}, etc., or their equivalents are available in both equation and tabular form.[1, 2]

Substituting Eqs. (12) in Eqs. (5), (6), and (11), the flutter equations reduce to the following set:

$$\alpha\left(-\frac{I_\alpha}{\pi\rho b^4}\left[1 - \left(\frac{\omega_\alpha}{\omega}\right)^2(1 + ig_\alpha)\right] + [R_{a\alpha} + iI_{a\alpha}]\right) + \beta\left(-\left[\frac{I_\beta + b(e - a)S_\beta}{\pi\rho b^4}\right] + [R_{a\beta} + iI_{a\beta}]\right) + \frac{h}{b}\left(-\frac{S_\alpha}{\pi\rho b^3} + [R_{ah} + iI_{ah}]\right) = 0 \tag{13}$$

$$\alpha\left(-\left[\frac{I_\beta + b(e - a)S_\beta}{\pi\rho b^4}\right] + [R_{b\alpha} + iI_{b\alpha}]\right) + \beta\left(\frac{g_1 + i\, g_2}{\omega^2\pi\rho b^4} + [R_{b\beta} + i\, I_{b\beta}]\right) + \frac{h}{b}\left(-\frac{S_\beta}{\pi\rho b^3} + [R_{bh} + iI_{bh}]\right) = 0 \tag{14}$$

$$\alpha\left(-\frac{S_\alpha}{\pi\rho b^3} + [R_{c\alpha} + iI_{c\alpha}]\right) + \beta\left(-\frac{S_\beta}{\pi\rho b^3} + [R_{c\beta} + iI_{c\beta}]\right) + \frac{h}{b}\left(-\frac{M}{\pi\rho b^2}\left[1 - \left(\frac{\omega_h}{\omega}\right)^2(1 + ig_h)\right] + [R_{ch} + iI_{ch}]\right) = 0 \tag{15}$$

* The aerodynamic notation is that of reference 2.

As derived, the equations relate to a wing section of unit span. Following methods of conventional two-dimensional flutter analysis,[4] a sample wing strip is considered, and its action is assumed to indicate the action of the wing. The quantities ω_α and ω_h take on the meaning of the natural frequencies of the pair of wing vibration modes that are being investigated for possible unstable combination with the aileron system. Extension to the more rigorous three-dimensional treatment can be accomplished by integration of the unit strip effects along the span.

Eqs. (13), (14), and (15) are now solved for the values of g_1 and g_2 required for flutter.

(II) Specification of Flutter Boundary Curves

Case (a) Torsion-Bending-Control Surface Rotation

To satisfy Eqs. (13), (14), and (15), it is necessary that the determinant of the coefficients of the variables vanish. The following notation is introduced:

$$\begin{aligned}
\Omega &= 1/\omega^2 \\
C_1 &= -(I_\alpha/\pi\rho b^4) + R_{a\alpha} \\
C_2 &= I_{a\alpha} \\
C_3 &= I_\alpha\,\omega_\alpha^2/\pi\rho b^4 \\
C_4 &= C_3 g_\alpha \\
C_5 &= -\{[I_\beta + b(e - a)S_\beta]/\pi\rho b^4\} + R_{a\beta} \\
C_6 &= I_{a\beta} \\
C_7 &= -(S_\alpha/\pi\rho b^3) + R_{ah} \\
C_8 &= I_{ah} \\
C_9 &= -\{[I_\beta + b(e - a)S_\beta]/\pi\rho b^4\} + R_{b\alpha} \\
C_{10} &= I_{b\alpha} \\
C_{11} &= R_{b\beta} \\
C_{12} &= I_{b\beta} \\
C_{13} &= -(S_\beta/\pi\rho b^3) + R_{bh} \\
C_{14} &= I_{bh} \\
C_{15} &= -(S_\alpha/\pi\rho b^3) + R_{c\alpha} \\
C_{16} &= I_{c\alpha}
\end{aligned}$$

$$C_{17} = -(S_\beta/\pi\rho b^3) + R_{c\beta} \qquad C_{20} = I_{ch}$$
$$C_{18} = I_{c\beta} \qquad C_{21} = M\omega_h^2/\pi\rho b^2$$
$$C_{19} = -(M/\pi\rho b^2) + R_{ch} \qquad C_{22} = C_{21}g_h$$

The equation in the determinant of the coefficients is then

$$\begin{vmatrix} [(C_1 + \Omega C_3) + i(C_2 + \Omega C_4)] & [C_5 + iC_6] & [C_7 + iC_8] \\ [C_9 + iC_{10}] & \left[\left(C_{11} + \frac{\Omega g_1}{\pi\rho b^4}\right) + i\left(C_{12} + \frac{\Omega g_2}{\pi\rho b^4}\right)\right] & [C_{13} + iC_{14}] \\ [C_{15} + iC_{16}] & [C_{17} + iC_{18}] & [(C_{19} + \Omega C_{21}) + i\,(C_{20} + \Omega C_{22})] \end{vmatrix} = 0 \quad (16)$$

It can be solved directly for g_1 and g_2 in terms of the constants C_n and Ω. Expanding and separating real and imaginary parts, the following solution is obtained:

$$g_1 = (\pi\rho b^4/\Omega)\{[(A_1A_2 + B_1B_2)/(A_1^2 + B_1^2)] - C_{11}\} \quad (17)$$

$$g_2 = (\pi\rho b^4/\Omega)\{[(A_1B_2 - A_2B_1)/(A_1^2 + B_1^2)] - C_{12}\} \quad (18)$$

where

$$A_1 = [C_1C_{19} - C_2C_{20} - C_7C_{15} + C_8C_{16}] + \Omega[C_1C_{21} - C_2C_{22} + C_3C_{19} - C_4C_{20}] + \Omega^2[C_3C_{21} - C_4C_{22}] \quad (19)$$

$$B_1 = [C_1C_{20} + C_2C_{19} - C_7C_{16} - C_8C_{15}] + \Omega[C_1C_{22} + C_2C_{21} + C_3C_{20} + C_4C_{19}] + \Omega^2[C_3C_{22} + C_4C_{21}] \quad (20)$$

$$A_2 = [C_1(C_{13}C_{17} - C_{14}C_{18}) - C_2(C_{13}C_{18} + C_{14}C_{17}) + C_9(C_5C_{19} - C_6C_{20} - C_7C_{17} + C_8C_{18}) + C_{10}(-C_5C_{20} - C_6C_{19} + C_7C_{18} + C_8C_{17}) + C_{15}(-C_5C_{13} + C_6C_{14}) + C_{16}(C_5C_{14} + C_6C_{13})] + \Omega[C_3(C_{13}C_{17} - C_{14}C_{18}) - C_4(C_{13}C_{18} + C_{14}C_{17}) + C_{21}(C_5C_9 - C_6C_{10}) - C_{22}(C_5C_{10} + C_6C_9)] \quad (21)$$

$$B_2 = [C_1(C_{13}C_{18} + C_{14}C_{17}) + C_2(C_{13}C_{17} - C_{14}C_{18}) + C_9(C_5C_{20} + C_6C_{19} - C_7C_{18} - C_8C_{17}) + C_{10}(C_5C_{19} - C_6C_{20} - C_7C_{17} + C_8C_{18}) - C_{15}(C_5C_{14} + C_6C_{13}) + C_{16}(-C_5C_{13} + C_6C_{14})] + \Omega[C_3(C_{13}C_{18} + C_{14}C_{17}) + C_4(C_{13}C_{17} - C_{14}C_{18}) + C_{21}(C_5C_{10} + C_6C_9) + C_{22}(C_5C_9 - C_6C_{10})] \quad (22)$$

Case (b) Bending-Control Surface Rotation

The torsional mode of vibration is eliminated by dropping the first row and column of the determinant in Eq. (16). The resulting impedance required for bending, control surface flutter is given by Eqs. (17) and (18), with the following simplified values of the quantities A_1, B_1, A_2 and B_2:

$$A_1 = C_{19} + \Omega C_{21} \quad (23)$$

$$B_1 = C_{20} + \Omega C_{22} \quad (24)$$

$$A_2 = C_{13}C_{17} - C_{14}C_{18} \quad (25)$$

$$B_2 = C_{13}C_{18} + C_{14}C_{17} \quad (26)$$

Case (c) Torsion-Control Surface Rotation

The last row and column of the determinant in Eq. (16) is dropped to eliminate the bending mode. The values of A_1, B_1, A_2, and B_2 pertaining to torsion-control surface flutter become

$$A_1 = C_1 + \Omega C_3 \quad (27)$$

$$B_1 = C_2 + \Omega C_4 \quad (28)$$

$$A_2 = C_5C_9 - C_6C_{10} \quad (29)$$

$$B_2 = C_5C_{10} + C_6C_9 \quad (30)$$

Eqs. (17) and (18) give the value of the impedance required for flutter in terms of the basic parameters ω and $V/\omega b$. The entire field of operation of the aircraft-servo combination is explored by calculating loci of flutter at constant frequency, each locus being carried from zero value of $V/\omega b$ to that value corresponding to the top speed of the aircraft. The frequency range is taken from zero to a value high enough to preclude the coincidence of servo impedance and the impedance required for flutter.

A modification is made in the impedance before plotting; the effect of the inertia of the control surface is removed. The impedance finally handled is that of a physical system identical to the true system but with an inertialess control surface. The inertia of the surface contributes an amount $-I_\beta/\Omega$ to g_1 and nothing to g_2. The real part of the inertialess impedance is then $g_1 + (I_\beta/\Omega)$. This procedure reduces the impedance of the conventional mass, spring, damper control system to a quantity invariant with frequency—that is, a point on the flutter boundary chart. Thus, consider the equation of motion of the aforementioned system:

$$I_\beta\ddot{\beta} + C_\beta g_\beta \frac{\dot{\beta}}{\omega} + C_\beta\,\beta = \mathfrak{M} \quad (31)$$

where

C_β = stiffness of the control surface in rotation
g_β = structural damping coefficient for control surface motion
$\mathfrak{M}$ = sinusoidal forcing moment

The solution of Eq. (31) yields

$$\mathfrak{M}/\beta = [(C_\beta - (I_\beta/\Omega)] + i\,(C_\beta g_\beta) \tag{32}$$

then,

$$\left.\begin{aligned} \vartheta_1 &= C_\beta - (I_\beta/\Omega) \\ \vartheta_2 &= C_\beta g_\beta \end{aligned}\right\} \tag{33}$$

or, modifying ϑ_1, the impedance components of the inertialess system become

$$\left.\begin{aligned} \vartheta_1 + (I_\beta/\Omega) &= C_\beta \\ \vartheta_2 &= C_\beta g_\beta \end{aligned}\right\} \tag{34}$$

Eqs. (34) describe a point on the impedance plane. This condition reduces the solution of the conventional flutter problem to a simple case of impedance matching. The present technique applied to conventional flutter has the attribute of allowing a small band of critical frequencies to be examined for flutter with the parameter $V/\omega b$ a secondary variable. It also makes immediately apparent, in a given example, the effects of varying control system spring and damping constants. This subject will be treated more fully in the section that follows.

One last specification is made with regard to plotting the impedance. It is most convenient to plot the logarithm of the impedance—that is, the logarithm of the magnitude versus phase angle. The two coordinates for the flutter boundary curve chart are then

$$\ln\sqrt{[\vartheta_1 + (I_\beta/\Omega)]^2 + \vartheta_2^2}$$

and

$$\tan^{-1}\{\vartheta_2/[\vartheta_1 + (I_\beta/\Omega)]\}$$

A sample problem is now used to expand and elucidate the foregoing theory.

(III) Sample Problem

Consider an aircraft with the following characteristics of a chosen wing section: chord, 4 ft.; distance from mid-chord to elastic axis, 0.67 ft. forward; distance from mid-chord to leading edge of aileron, 1.072 ft. aft; distance from mid-chord to hinge line of aileron, 1.200 ft. aft;

M = 1.447 slugs per ft.
S_α = 0.941 slug ft. per ft.
S_β = 0.0645 slug ft. per ft.
I_α = 2.25 slug ft.^{2} per ft.
I_β = 0.0394 slug ft.^{2} per ft.
C_α = 455,000 ft.lbs. per rad.
C_h = 77,900 lbs. per ft.
g_α = 0
g_h = 0

It is desired to inspect the aircraft for flutter at sea level. Its top speed is 700 ft. per sec. at this altitude. Control system specification is given at a later point. The flutter boundary chart is prepared according to the following procedure:

(1) The values of ω for which loci will be calculated are chosen. They are 5, 10, 15, 20, 25, 30, 33, 35, 35.5, 36.0, 40, 45, and 50 cycles per sec. Close spacing of the frequencies is taken in the region of the natural bending frequency. The range is terminated at 50 cycles. It becomes obvious, on plotting, that no flutter of practical interest occurs above this frequency with the particular servo and conventional control systems involved.

(2) The maximum value of $V/\omega b$ for each constant frequency locus is determined by fixing a speed beyond which analysis is of no value. This speed is 700 ft. per sec. for the present case. However, the loci are carried to much higher speeds (uniformly to a value of $V/\omega b$ of 8) in order to illustrate their mathematical behavior more clearly. The velocities involved in this extension invalidate the aerodynamic assumptions that have been made. These later portions of the loci, then, have no physical significance. In other examples, though, equivalent portions of the loci may occur in a valid speed range. The parts of the flutter boundary diagram of physical significance in this specific problem are differentiated on the diagram from the parts of mathematical interest only.

(3) From the tabular values of the aerodynamic coefficients of reference 2 and the data of steps 1 and 2, a sufficient number of values of the constants C_1 through C_{22} and A_1, B_1, A_2 and B_2 are calculated to define the flutter boundary curves. No compressibility correction is used.

(4) The curves themselves, loci at constant frequency of

$$\ln\sqrt{[\vartheta_1 + (I_\beta/\Omega)]^2 + \vartheta_2^2}$$

versus

$$\tan^{-1}\{\vartheta_2/[\vartheta_1 + (I_\beta/\Omega)]\}$$

are plotted.

$$\ln\sqrt{[\vartheta_1 + (I_\beta/\Omega)]^2 + \vartheta_2^2}$$

is represented by

$$\sqrt{[\vartheta_1 + (I_\beta/\Omega)]^2 + \vartheta_2^2}$$

plotted to a logarithmic scale.

The flutter boundary chart is shown in Figs. 2a and 2b. Fig. 2a deals with frequencies from 0 through 30 cycles per sec.; Fig. 2b, with all higher frequencies. The loci are carried to 700 ft. per sec. as solid lines. Their mathematical extension is shown dotted. The

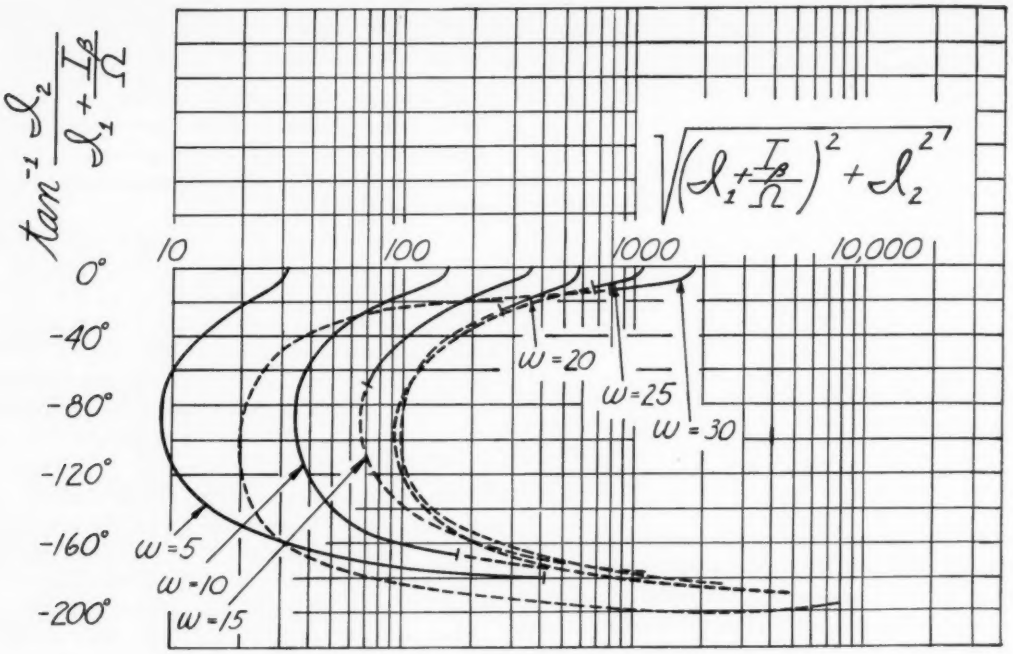

FIG. 2a. Flutter boundary chart, 0–30 cycles per sec.

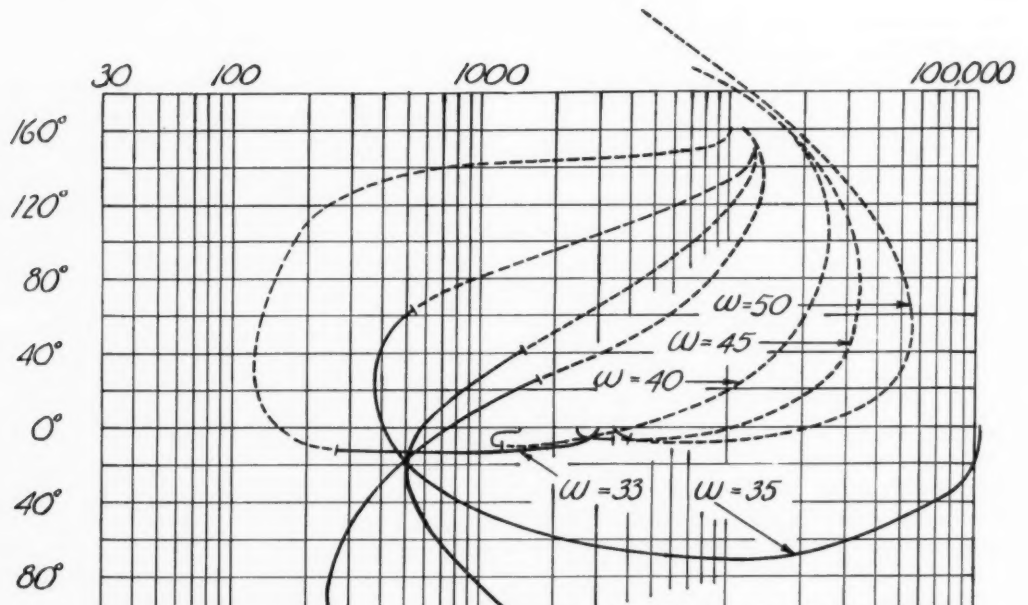

FIG. 2b. Flutter boundary chart, 30–50 cycles per sec.

locus at 5 cycles per sec. can be calculated to only 500 ft. per sec. because of the limit of $V/\omega b$ equal to 8 in the tabular listings of reference 2. It is extrapolated to 700 ft. per sec. The equations of reference 1 can be used to extend the aerodynamic tables if this is necessary.

As an aid in the interpretation of the flutter chart, the values of impedance required for flutter at zero velocity are plotted as a function of frequency in Fig. 3. The figure traces the starting points of the flutter boundary curves. The phase angle of the impedance for the zero velocity case (physically trivial) is either 0° or 180°, where the impedance is finite. Thus, referring to Figs. 2a and 2b, the flutter boundary curves begin on the horizontal lines 0° and −180°. The zero frequency curve is a point at zero, infinitely far to the left on the 0° line. As the frequency rises, the starting point moves to the right until, at a little above 35 cycles, it is infinitely far to the right. In this remote region, the point shifts to the −180° line and moves to the left with further increase in frequency. In the small range 35+ to 37+ cycles (approximately the natural bending frequency), the starting point sweeps the −180° line from plus infinity to minus infinity. This cycle then repeats itself, centering this time about a frequency somewhat above the natural frequency in torsion. The starting point of the infinite frequency locus is at plus infinity on the 0° line.

Fig. 2 in its entirety is complex. Consider its characteristics, first, from the point of view of conventional flutter. Allow the control system to take on definite values of C_β and g_β. The impedance of this system is then a point on Fig. 2. The point, ordinarily, is close to, and above, the 0° line. The phase angle of the impedance, $\tan^{-1} g_\beta$, is usually less than 12°. For the sake of argument let $g_\beta = 0$. The impedance is then a single point on the zero axis at a magnitude of C_β. For flutter to occur at some frequency, the flutter boundary curve at the frequency must coincide with C_β somewhere along its length. Regardless of the value of C_β, then, flutter can only occur when a locus crosses the zero axis at finite velocity or, in a limiting case, is tangent to the axis. There is no flutter, therefore, at frequencies up to approximately 31 cycles. There can be flutter at frequencies above 31 cycles at some velocity but only between 35- and 40-cycles within the speed range of the aircraft. The frequency range of flutter is now established. The mode involved is primarily bending, aileron. Each value of C_β has associated with it a definite flutter frequency and velocity. The velocity is available through the known spacing of the quantity $V/\omega b$ along each locus. Values of C_β from approximately 350 to 3,400 will cause flutter within the speed range of the aircraft. The complete flutter specification of the ship can be deduced from Fig. 2 and drawn. Figs. 4 and 5 give the variation of flutter frequency and velocity with the natural frequency of the control system. Final results may be stated as follows: the range of natural frequency of control system that will produce flutter within the speed of 700 ft. per sec. is 15 to 47 cycles per sec. The associated flutter frequency range is 34.5 to 39.5 cycles per

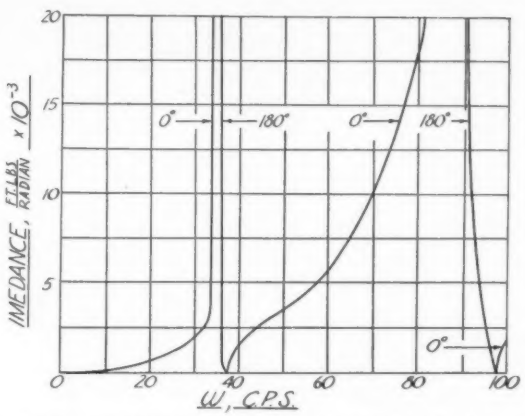

FIG. 3. Impedance required for flutter at zero velocity.

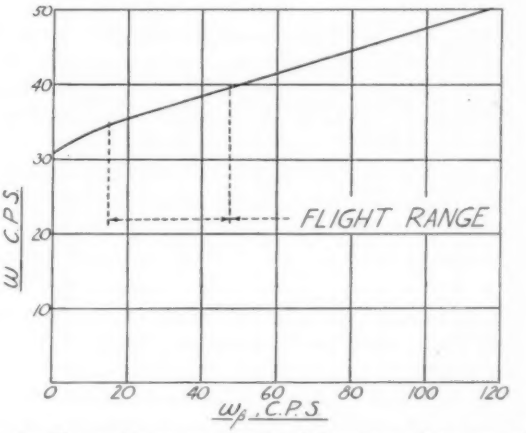

FIG. 4. Flutter frequency vs. natural frequency of the control system.

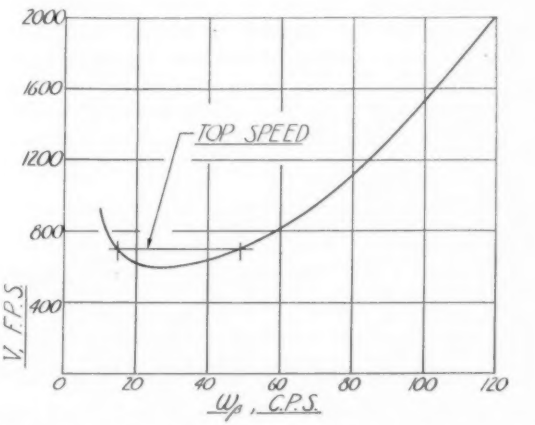

FIG. 5. Flutter velocity vs. natural frequency of the control system.

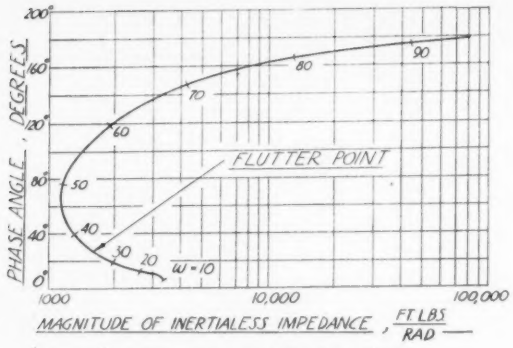

FIG. 6. Servomechanism impedance.

sec. The curves of Figs. 4 and 5 can be readily expanded into families for various amounts of damping.

The existence of a higher frequency flutter mode is shown by the action of higher frequency loci that cross the range of C_β under consideration. The crossings are of no practical significance, since they take place at extremely high speed, but they illustrate the means by which two modes of flutter may be associated with a single value of C_β.

To summarize the case of conventional flutter, it is seen that the technique of impedance plotting presents a rather powerful method of analysis. Where servo units are not involved, the loci may be computed only in the region of zero phase angle. Besides the evaluation of standard control systems, the flutter boundary plot can be used to investigate nonlinear spring and damping effects.

The criterion for flutter in the case of servo-control is that the point representing servo impedance at a given frequency coincide with the flutter boundary curve of that frequency somewhere along the length of the curve. The regions in which detailed flutter boundary curves are required depend on the servo impedance path. Critical frequency regions must be closely inspected. The flutter boundary curves that begin on the 180° axis, for example, although covering a frequency range of only 2 odd cycles, sweep a large portion of the impedance plane. This complication is less severe in the conventional control case, for the curves become regular at 0° phase.

Fig. 6 gives a response of a particular servomechanism with a quantity I_β/Ω added to its real part. With this characteristic, flutter will occur at approximate values of frequency and velocity of 36 cycles per sec. and 700 ft. per sec., respectively.

The servomechanism is a nonlinear device. Its response will be different for different amplitudes of aileron motion. Of primary interest is the response at small amplitudes. A response at some higher amplitude may indicate flutter. The flutter will occur, however, only if an aileron disturbance causes the system to pass this threshold amplitude. In addition to variation with amplitude, the servo response is usually a function of a number of electronic parameters. In a given case, it is necessary to decide on the responses required from the conditions of the flutter investigation and from the particular servomechanism behavior. An experimental means must then be devised to measure truthfully these responses. The problems involved are jointly electronic and dynamic and are beyond the scope of this discussion.

In summary, there has been presented a method of flutter analysis based on the concept of impedance mapping. It is hoped that broad usage will bring into proper perspective its relative merit with respect to other methods in the field.

REFERENCES

[1] Theodorsen, Theodore, *General Theory of Aerodynamic Instability and the Mechanism of Flutter*, N.A.C.A. T.R. No. 496, 1935.

[2] Benscoter, L. K., and Libby, P. A., *Tables for the Calculation of Aerodynamic Coefficients of an Oscillating Airfoil-Flap System in an Incompressible Fluid*, Navaer SM-30, June, 1947.

[3] Theodorsen, Theodore, and Garrick, I. E., *Mechanism of Flutter, A Theoretical and Experimental Investigation of the Flutter Problem*, N.A.C.A. T.R. No. 685, 1940.

[4] Myklestad, N. O., *Vibration Analysis:* McGraw-Hill Book Company, Inc., New York, 1944.

Changes of Address

Since the Post Office Department does not as a rule forward magazines to forwarding addresses it is important that the Institute be notified of changes in address 30 days in advance of publishing date to ensure receipt of every issue of the JOURNAL and REVIEW.

Notices should be sent directly to:

Institute of the Aeronautical Sciences, Inc.
2 East 64th Street, New York 21, New York

Theories of Plastic Buckling

S. B. BATDORF*

National Advisory Committee for Aeronautics

SUMMARY

The theory for the plastic buckling of columns, which appears finally to have achieved a satisfactory form, rests upon the well-established uniaxial stress-strain relation. The development of a correspondingly satisfactory theory for the plastic buckling of plates has been hampered by the nonexistence of an established polyaxial stress-strain relation in the plastic range.

Present theories for the polyaxial stress-strain relation beyond the elastic range can be divided into two types, often called flow and deformation theories. Theories of plastic buckling based on deformation theories are in better agreement with experiment than those based on flow theories. On the other hand, tests in which a material is compressed into the plastic range and then subjected to shear at constant compressive stress are in better agreement with flow than with deformation theories. Legitimate doubt therefore has existed as to the validity of any theory for the plastic buckling of plates.

As a result of studying these apparent contradictions, a new theory of plasticity has been developed which is of neither the flow nor the deformation type. It is based upon the concept of slip, and its formulation was guided more by physical, and less by mathematical, considerations than previous theories. Experimental evidence of limited scope but of crucial character is in better agreement with the new theory than with either flow or deformation theories. The new theory accounts for the apparent contradictions previously alluded to and justifies the use of deformation theory in the analysis of the plastic buckling of plates.

INTRODUCTION

THE THEORY FOR the plastic buckling of columns, which appears finally to have achieved a satisfactory form[1–3] rests upon the well-established uniaxial stress-strain relation. The recently established result that even a perfect column can buckle according to a tangent modulus law is rational and can be readily accepted on the basis of the following intuitive argument. The buckling stress of a column depends upon its stiffness against bending. In the elastic range, the stiffness is the product of E, the elastic modulus, and I, the moment of inertia of the cross section. Beyond the elastic range, the stiffness depends upon the stress and also on the rate of increase or decrease of compressive stress accompanying the bending. The effective modulus at a given stress may be anything between the elastic modulus (which applies if the relative rate of unloading and bending is such that all portions of the cross section are unloading) and the tangent modulus E_T (which applies if the relative rate of loading and bending is such that all portions of the cross section are loading). Since a structure always buckles in the mode associated with the lowest buckling stress and since the minimum buckling stress of the column is associated with the minimum bending stiffness, the effective modulus in plastic column buckling is the tangent modulus.

The development of a correspondingly satisfactory theory for the plastic buckling of plates has been hampered by the nonexistence of an established polyaxial stress-strain relation in the plastic range. It is not that no theory exists but rather that theories exist in great abundance.

PRESENT THEORIES OF PLASTICITY

Mathematical theories of plasticity take as their point of departure the stress-strain law for simple tension or compression. This is illustrated in Fig. 1. In the elastic range, the relation between the stress σ and the strain ϵ is essentially linear and is expressed by the equation

$$\sigma = E\,\epsilon \tag{1}$$

Beyond the elastic range, two methods of representation are used. In one, the finite relationship is retained between stress and strain, but the elastic modulus E is replaced by the so-called secant modulus E_S, which varies with the stress, so that Eq. (1) becomes

$$\sigma = E_S\,\epsilon \tag{2}$$

The other mode of representation is an incremental one employing the tangent modulus E_T, which also varies with the stress. The mathematical expression of this law is

$$d\sigma = E_T\,d\epsilon \tag{3}$$

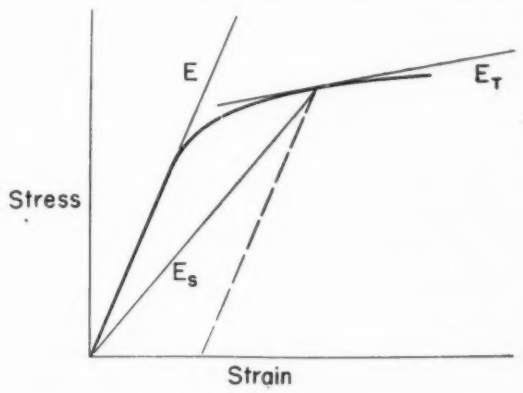

FIG. 1. Uniaxial stress-strain relation.

Presented at the Session on Structures—Static Loads, Seventeenth Annual Meeting, I.A.S., New York, January 24–27, 1949.

* Structures Research Division, Langley Aeronautical Laboratory.

Eqs. (2) and (3) apply as long as the loading continues to increase. Unloading, however, occurs elastically—that is, Eq. (3) applies with E_T replaced by the elastic modulus E, so that the relation between stress and strain during unloading is a straight line parallel to the elastic portion of the stress-strain curve.

The various theories of plasticity seek to generalize these results so as to formulate correctly stress-strain relations under complex loading conditions in the region beyond the elastic range. Those that have been proposed up until the present time can be classified into two types: One generalizes Eq. (2) and therefore involves relations of the finite type, while the other generalizes Eq. (3) and therefore involves incremental relationships. The theories involving finite laws are sometimes called deformation theories; those involving infinitesimal laws, flow theories. Both types of theory assume that the plastic law proposed applies during loading, while unloading occurs elastically. Whether the change in the stress state constitutes loading or unloading is supposed to depend upon whether the change increases or decreases a rotationally invariant function of the stresses. This function, which is sometimes termed the "stress intensity," is usually assumed to be proportional either to the maximum shear stress or to the so-called octahedral shear stress, which is related to the energy of distortion. In order to make a plasticity theory definite enough to be mathematically tractable, additional assumptions must be introduced, and these ordinarily include the assumption that the principal axes of stress coincide with the principal axes of the plastic part of the strain or its increment. (For a general survey of flow and deformation theories see reference 4.)

Theories for Plastic Buckling of Plates

It is only comparatively recently that attempts have been made to solve the problem of the plastic buckling of plates rigorously on the basis of one or another of the various mathematical theories of plasticity. A solution based on a flow theory was obtained by Handelman and Prager,[5] and a solution based on a deformation theory was obtained by Stowell.[6, 7] For the sake of simplicity, in the present paper attention will be limited to these two theories, which are reasonably representative of the types of plasticity theory on which they are based.

The discrepancy between the predictions of the two buckling theories is, in many cases, marked, and the available experimental data have been in decidedly better agreement with the buckling theory based on deformation theory.[8, 9] For example, Fig. 2, taken from reference 9, compares both theories with experimental data on the buckling of long simply supported plates. On the other hand, theoretical objections have been raised to deformation theories as a class, and experiments have been proposed to determine whether flow theories or deformation theories are in better

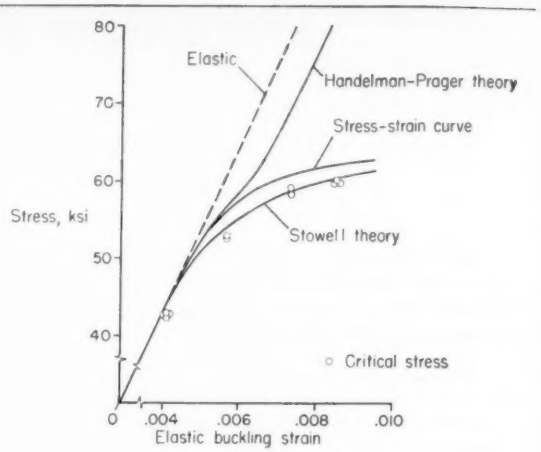

Fig. 2. Plastic buckling of long simply supported plates.

agreement with experiment.[10, 11] Some experiments for this purpose were carried out by Roger W. Peters and Norris F. Dow at the Langley Laboratory of the N.A.C.A. In the most directly applicable of these experiments, a cylinder was compressed into the plastic region and then, holding the compressive stress constant, was twisted. According to the deformation theory used by Stowell, which is closely related to the Nadai theory,[12] the initial effective shear modulus should have been $(E_s/E)G$, whereas according to flow theories it should have been the elastic value G. The experiment gave a value close to G in agreement with flow theories and in disagreement with the deformation theory. With suspicion thus raised against the foundation upon which is based the theory of plastic buckling in best agreement with experiment, there appeared to be grave doubts as to whether a satisfactory theory for the plastic buckling of plates could be said to exist at all.

In some cases the evidence was so conflicting as to appear paradoxical. For example, the theoretical buckling stress of an extremely long simply supported hinged flange in the elastic range can be shown to be given by the formula

$$\sigma = G(t/b)^2 \tag{4}$$

where t and b are the thickness and width of the flange, respectively. Since the modulus appearing in this equation is that for shear, which is to be expected since the flange buckles by twisting, the formula should evidently be amended in the plastic range by using the effective shear modulus of the material when subject to the compressive stress obtaining at the moment of buckling. This effective shear modulus was found in buckling experiments to be $(E_s/E)G$, in agreement with the predictions of the deformation theory (more precisely, deformation theory gives $(E_s/E)G$ times the nearly unit factor $2(1+\mu)/[3+(2\mu-1)(E_s/E)]$, where μ is the elastic value of Poisson's ratio; for simplicity,

this factor will be ignored throughout the present paper). On the other hand, the effective shear modulus determined directly by compressing and then twisting the cylinder, as just mentioned, was found to be the elastic value G in agreement with flow theory.

A New Theory of Plasticity

In delving into the reasons for this paradox, a new theory of plasticity was developed which is of neither the flow nor the deformation type.[13] This new theory assumes that all plastic deformation is due to slip, which occurs first along the plane of maximum shear stress in the direction of this stress at the moment the elastic limit for the material is exceeded. As the stress continues to increase, the slip along this plane also increases. In addition, slip commences along new planes slightly inclined to the plane of maximum shear as the shear stress on them also goes above the elastic limit. Moreover, as the shear stress on a given plane passes above the elastic limit, the number of directions in the plane in which the component of shear stress is large enough to cause slip increases. The theory assumes that slip occurs along every plane and in every direction in these planes in which the corresponding shear stress component is large enough to cause slip. The amount of slip in any direction along any plane is assumed to depend only on the prior history of the component in the direction of slip of the shear stress on this plane. Thus, strain hardening is anisotropic; it will take place only in those directions and planes along which slip has occurred.

The anisotropic character of strain hardening in the new theory is nicely illustrated in the example of a specimen subjected to a loading history in which pure tension is initially in a given direction after which the direction of the pure tension is rotated, keeping the stress magnitude constant. (Such an experiment was proposed for the purpose of assessing the relative merits of flow and deformation theories in reference 11.) According to flow theories, there is no loading during the rotation of the axes because there is no change in any stress invariant, and there will therefore be no additional plastic strain. According to deformation theories, the situation is ambiguous,[14, 15] since a finite rotation accompanied by an infinitesimal increase in stress magnitude would give a finite plastic strain, whereas the same rotation accompanied by an infinitesimal decrease in stress magnitude would give a zero plastic strain, since unloading occurs elastically. What is important for the present purpose, however, is that in the latter case both types of theory, and indeed any theory that defines loading in terms of the increase of a stress invariant, predict zero plastic strain during rotation. The new theory, on the other hand, predicts finite plastic strain, for during the rotation of axes new and unhardened planes will acquire shear stresses above the elastic limit and will therefore slip.

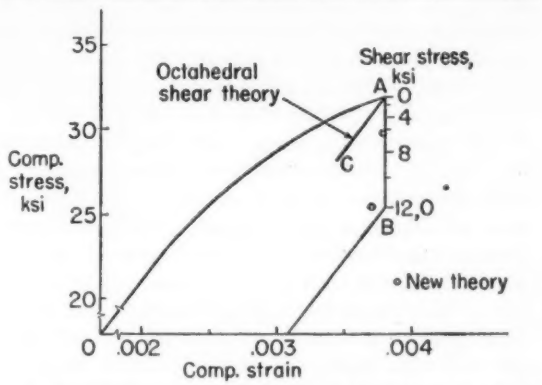

Fig. 3. Compressive stress-strain relations for cylinder subjected to compression and torsion.

An experiment somewhat like the one just described has been performed at Langley. A cylinder was compressed beyond the elastic range and was then twisted while holding the compressive strain constant. The essential data are given in Fig. 3. Throughout the twisting process (AB in the figure), the compressive stresses decreased while the shear stress increased. The compressive plastic strain continually increased. Simple calculations show, however, that during the early part of the twist both the octahedral shear stress and the maximum shear stress were decreasing. Compatibility with the known uniaxial behavior implies that, when the stress intensity decreases, plastic action stops and is not resumed until the stress intensity exceeds the highest previous value. If, as in most plasticity theories, the stress intensity is assumed to be proportional to the octahedral shear stress, the value at the beginning of twisting was not exceeded until the shear stress exceeded 8.6 ksi., and, according to these theories, the compressive stress and strain during twist should therefore have been related by the line AC. Maximum shear stress theories would predict the same relationship up to a shear stress equal to about 5 ksi. No attempt has been made to calculate the subsequent behavior on the basis of flow and deformation theories because there seems to be no general agreement as to how to apply these theories beyond the first loading and unloading. The predictions of the new theory as to the compressive strain associated with the applied stresses are in far better agreement with experiment (see Fig. 3).

Buckling on Basis of New Theory

The new theory affords an explanation to the paradox discussed earlier. An ideal long hinged flange loaded in compression remains straight until the moment of buckling, when it commences to twist. The twist may take place at constant compressive stress or may be accompanied by an increase in compressive stress (shown as type A and type B changes, respectively,

in Fig. 4). According to the deformation theory, the effective shear modulus is in both cases $(E_S/E)G$. According to flow theory, the effective shear modulus is in both cases G. The new theory, on the other hand, gives an effective shear modulus that depends upon the type of change under consideration. According to the new theory, many of the planes that were slipping when the applied stress was compressive commence to unload when shear is added in a type A change. Moreover, most of the planes that continue to slip are so oriented that they make only a small contribution to plastic shear deformation in the original system of coordinates. The effective shear modulus is therefore close to the elastic value G; just how close depends on the compressive stress prior to twisting. For a stress increment of type B approaching the vertical, on the other hand, practically all of the planes continue loading and suffer the same plastic deformation as though the final state had been reached by keeping the stress ratio fixed at the final value throughout the loading history. For loading conditions in which stress ratios are kept fixed, deformation and flow theories predict the same results, and, for the case in point, both give $(E_S/E)G$ for the effective shear modulus. Therefore, in the new theory, a type A change results in an effective shear modulus approximately G, and a type B change is close to the vertical results in an effective shear modulus approximately equal to $(E_S/E)G$. Since the twist experiment first discussed was a type A change and buckling is, according to the argument in the "Introduction" to this paper, a type B change, the new theory accounts for the apparent contradiction and also justifies the use of deformation theory in the analysis of the plastic buckling of plates.

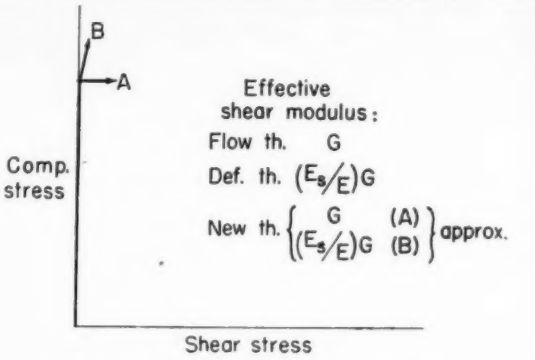

FIG. 4. Theories for effective shear modulus.

REFERENCES

[1] Shanley, F. R., *Inelastic Column Theory*, Journal of the Aeronautical Sciences, Vol. 14, No. 5, p. 261, May, 1947.

[2] von Kármán, Th., *Discussion*, Journal of the Aeronautical Sciences, Vol. 14, No. 5, p. 267, May, 1947.

[3] Wang, C. T., *Inelastic Column Theories and an Analysis of Experimental Observations*, Journal of the Aeronautical Sciences, Vol. 15, No. 5, p. 283, May, 1948.

[4] Prager, W., *The Stress Strain Laws of the Mathematical Theory of Plasticity—A Survey of Recent Progress*, Journal of Applied Mechanics, September, 1948.

[5] Handelman, G. H., and Prager, W., *Plastic Buckling of a Rectangular Plate Under Edge Thrusts*, N.A.C.A. T.N. No. 1530, August, 1948.

[6] Stowell, E. Z., *A Unified Theory of Plastic Buckling of Columns and Plates*, N.A.C.A. T.N. No. 1556, April, 1948.

[7] Stowell, E. Z., *Critical Shear Stress of an Infinitely Long Plate in the Plastic Region*, N.A.C.A. T.N. No. 1681, August, 1948.

[8] Pride, Richard A., and Heimerl, George J., *Plastic Buckling of Simply Supported Compressed Plates*, N.A.C.A. T.N. No. 1817, April, 1949.

[9] Prager, W., *Recent Developments in the Mathematical Theory of Plasticity*, paper presented at the Seventh International Congress for Applied Mechanics. London, September 5–11, 1948.

[10] Prager, W., *On the Interpretation of Combined Torsion and Tension Tests on Thin Walled Tubes*, N.A.C.A. T.N. No. 1501, January, 1948.

[11] Drucker, D. C., *Stress-Strain Relations for Strain-Hardening Materials—Discussion and Proposed Experiments*, to be published in Proceedings 1st Annual Symposium on Applied Mathematics, Brown University, August 2–4, 1947.

[12] Nadai, A., *Plasticity, a Mechanics of the Plastic State of Matter*, p. 75, McGraw-Hill Book Company, Inc., New York, 1931.

[13] Batdorf, S. B., and Budiansky, Bernard, *A Mathematical Theory of Plasticity Based on the Concept of Slip*, N.A.C.A. T.N. No. 1871, April, 1949.

[14] Handelman, G. H., Lin, C. C., and Prager, W., *On the Mechanical Behavior of Metals in the Strain Hardening Range*, Quarterly of Applied Mathematics, Vol. IV, No. 4, p. 397, January, 1947.

[15] Drucker, D. C., *A Shortcoming of All Theories of Plastic Deformation*, Brown University, Providence, R.I., Graduate Division of Applied Mathematics, A 11-7, November, 1947.

Note on the Relations Between Viscous and Structural Damping Coefficients

WALTER W. SOROKA*
University of California at Berkeley

SUMMARY

The use of the structural damping factor g in vibration problems implies that the damped free vibration frequency of the structure increases with damping. Relations are derived comparing the natural frequencies and logarithmic decrements for viscous and structural damping. For low values of damping (up to $g = 0.20$), the two concepts give nearly the same results when g is taken as twice the critical viscous damping ratio.

INTRODUCTION

THE MECHANISM whereby an oscillating system dissipates its energy of vibration is one of the most important properties of the system. Whether or not it is desirable, it is nonetheless present in all mechanical systems. It is certainly useful in those cases where it limits the resonant amplitudes of structures and drive systems; where it stabilizes instruments, servomechanisms, and automatic control systems; and where it reduces the danger of flutter. In such cases, controlled amounts of damping may be deliberately introduced when inherent damping is insufficient.

In general, analytical discussions of damping in vibrating systems are concerned with damping forces proportional to velocity—i.e., proportional to the product of frequency by amplitude. This has been particularly true of problems connected with engine and instrument isolation, torsional vibration of crankshafts, etc. More recently, there has been introduced the concept of a damping force proportional to amplitude[1, 2] but independent of frequency. Experience has indicated that, in structures such as aircraft wings and fuselages, the damping loss depends more closely on the latter relation. In both cases the damping force is in phase with the velocity of vibration.

Little has been written regarding the implications of this concept of damping in structures and how it compares fundamentally with the concept of viscous damping. It is the purpose of this note to compare the newer treatment with the classical method and to bring out the main points of difference and similarity.

FREQUENCIES OF THE TWO SYSTEMS

The classical treatment for the free vibrations of a single degree of freedom damped system sets up the differential equation of motion in the form

$$m\ddot{x} + c\dot{x} + kx = 0 \tag{1}$$

where m is the mass of the system, c is the viscous damping coefficient, and k is the spring stiffness.

The treatment propounded in reference 1 sets up the equation of motion in the form

$$m\ddot{x} + k(1 + ig)x = 0 \tag{2}$$

where g is the dimensionless structural damping coefficient and $i = \sqrt{-1}$. Here a complex stiffness, $k(1 + ig)$, serves to represent both components of the force proportional to displacement, x. One component, kx, is in phase with the amplitude; this is the usual spring force. The other component, $ikgx$, is in phase with the velocity (90° ahead of the displacement) by virtue of the unit vector i introduced into Eq. (2); this is the damping force.

The solution of Eq. (1) is presented in detail by Den Hartog.[3] This solution is

$$x = e^{-c/2m}(C_1 \cos \omega_n t + C_2 \sin \omega_n t) \tag{3}$$

wherein ω_n is the natural frequency of the damped motion and is given by

$$\omega_n = \sqrt{(k/m) - (c^2/4m^2)} \tag{4}$$

The damping coefficient may be put in dimensionless form as a ratio taken with respect to the critical damping coefficient, $c_c = 2\sqrt{mk}$. Thus, with

$$\lambda = c/c_c \tag{5}$$

$$\omega_n = \sqrt{k/m}\,\sqrt{1 - \lambda^2} \tag{6}$$

The damped natural frequency decreases, of course as the damping coefficient increases.

To solve Eq. (2), let

$$x = x_0 e^{st} \tag{7}$$

Substitution of Eq. (7) into Eq. (2) yields

$$ms^2 + k(1 + ig) = 0 \tag{8}$$

In Eq. (8) either g is zero or s must be complex to satisfy this relation. Since g is a property of the system, the latter situation must prevail. Therefore, let

$$s = a + ib \tag{9}$$

where a and b are to be determined so as to satisfy Eq. (8). Then,

$$m(a^2 + i2ab - b^2) + k(1 + ig) = 0$$

Received November 29, 1948.

* Associate Professor.

which splits into the two equations:

$$\left.\begin{aligned} 2\,abm + kg &= 0 \\ m(a^2 - b^2) + k &= 0 \end{aligned}\right\} \tag{10}$$

From Eqs. (10) we derive the fact that

$$a^2 = (k/2m)(-1 + \sqrt{1 + g^2}) \tag{11}$$

$$b^2 = (k/2m)(1 + \sqrt{1 + g^2}) \tag{12}$$

In Eq. (11), the negative value of a is to be taken, since this value represents a decay of the disturbance whereas a positive value of a represents increasing amplitude, which is a physical impossibility in a damped free oscillation.

Eq. (12) is an equation for the natural frequency of the damped free motion. We may rewrite it:

$$\omega_n = \sqrt{k/2m}\,\sqrt{1 + \sqrt{1 + g^2}} \tag{13}$$

A fundamental difference between the two assumptions of the character of the damping becomes evident from a comparison of Eqs. (6) and (13). Whereas the assumption of damping proportional to velocity implies a natural damped frequency that *decreases* with increase in damping, the assumption of damping proportional to amplitude implies a natural damped frequency that *increases* with increase in damping. The latter phenomenon is certainly not consistent with the usual conception of the effect of damping on a free vibration.

Logarithmic Decrement

The envelope of the free vibration amplitude is given by $e^{-\lambda\omega_0 t}$, where $\omega_0 = \sqrt{k/m}$ for the first case [see Eq. (1)]. For the second case, the corresponding expression is $e^{-g\omega_0^2 t/2\omega_n}$. A measure of the damping in a free vibration is afforded by the ratio of amplitudes at the beginning and end of a complete cycle. The time interval for a cycle is given by $2\pi/\omega_n$ sec. Thus, for the first case, the amplitude ratio, R, would be

$$R = \frac{e^{-\lambda\omega_0 t}}{e^{-\lambda\omega_0[t + (2\pi/\omega_n)]}} = e^{2\pi\lambda\omega_0/\omega_n} = e^{2\pi\lambda/\sqrt{1-\lambda^2}} \tag{14}$$

In the second case,

$$R = e^{\pi g\omega_0^2/\omega_n^2} = e^{2\pi g/(1 + \sqrt{1+g^2})} \tag{15}$$

The logarithmic decrement, δ, in each case is

$$\delta = 2\pi\lambda/\sqrt{1 - \lambda^2} \tag{16}$$

$$\delta = 2\pi g/(1 + \sqrt{1 + g^2}) \tag{17}$$

In general, λ is small in engineering structures, perhaps of the order of 0.02–0.04 or less, when no effort is made to introduce damping deliberately. This makes the quantity $\sqrt{1 - \lambda^2}$ little different from unity. Similarly, g is extremely small. In flutter analysis the value of g is rarely taken in excess of 0.05 and usually is appreciably less. Again, this makes the quantity $1 + \sqrt{1 + g^2}$ little different from the value 2. Consequently, for *small damping*, Eqs. (16) and (17) may be rewritten, approximately,

$$\delta = 2\pi\,\lambda \tag{16a}$$

$$\delta = \pi g \tag{17a}$$

Whatever assumptions are made for the damping effect in any given system, the rate of decay of a free vibration on test will be a physical property of the system irrespective of the assumptions. Consequently, the approximate relationship between λ and g for small damping from Eqs. (16a) and (17a) is given by

$$g = 2\lambda \tag{18}$$

Table 1 uses the relationship (18) to provide corresponding values of λ and g for comparing the logarithmic decrements and damped natural frequencies of a structure under the two assumptions of damping.

TABLE 1
Comparison of Logarithmic Decrements and Natural Frequencies

Viscous Damping			Solid Friction Damping		
λ	δ	ω_n/ω_0	$g(=2\lambda)$	δ	ω_n/ω_0
0.01	0.0628	1.00	0.02	0.0628	1.00
0.02	0.126	1.00	0.04	0.126	1.00
0.05	0.315	1.00	0.10	0.313	1.00
0.10	0.631	0.995	0.20	0.622	1.00
0.20	1.28	0.980	0.40	1.21	1.02
0.50	3.63	0.866	1.00	2.60	1.10
0.80	14.0	0.600	1.60	3.48	1.20

Hysteresis Loops

When a structure is subjected to steady-state vibration, the tip of the resultant restoring force vector (composed of the spring force and damping force) traces out an ellipse when plotted against displacement. This is true for either assumption as to the form of damping. The equations for the ellipses are given in parametric form by

$$\left.\begin{aligned} F &= x_0 k[\sin\omega t + (c\omega/k)\cos\omega t] \\ x &= x_0 \sin\omega t \end{aligned}\right\} \tag{19}$$

and

$$\left.\begin{aligned} F &= x_0 k(\sin\omega t + g\cos\omega t) \\ x &= x_0 \sin\omega t \end{aligned}\right\} \tag{20}$$

where ω is the steady-state forced frequency and x_0 is the amplitude of the motion.

The areas of the ellipses will be given by

$$A = \oint F\,dx = \pi c\omega x_0^2 \tag{21}$$

$$A = \pi k g\, x_0^2 \tag{22}$$

Eqs. (21) and (22) represent the amounts of energy dissipated per cycle under the two assumptions of damping. As the frequency ω goes to zero, the ellipse given by Eq. (19) gets progressively thinner, reaching zero at the same instant that ω reaches zero. In the

(*Continued on page 448*)

Interference Between Wing and Body at Supersonic Speeds—Analysis by the Method of Characteristics*

CARLO FERRARI†

Cornell Aeronautical Laboratory, Inc.

ABSTRACT

The problem of interference between wing and body which was investigated in the first report of this series (JOURNAL OF THE AERONAUTICAL SCIENCES, Vol. 15, No. 6, p. 317, June, 1948) is again examined, but now, in contrast to what was done there, the small perturbation condition is eliminated—i.e., it is no longer required that the perturbations produced by the body and the wing in the uniform flow field be small enough to permit the linearization of the differential equation of the fluid motion. It is still assumed, however, that a potential field exists—a condition less restrictive than the previous one—and the determination of the flow is carried out under the assumption that the very tip of the nose is conical.

Since the free-stream velocity is supersonic, the field in the region ahead of the wing does not depend upon the presence of this appendage, and thus this phase of the study warrants the use of the method already propounded by the author in a previous report, to which, however, substantial modification and simplification are now applied. As in the first report of this series, the wing is assumed to extend beyond the region perturbed by the body, or at least it is assumed that the wing plan form is such that the tip phenomena due to the finite aspect ratio of the wing remain unaltered in presence of the body.

The determination of the fluid motion is accomplished through use of the hodograph method in derivation of the field corresponding to the conical nose and through application of the method of characteristics in the remaining regions.

INTRODUCTION

ALTHOUGH THE EFFECT of interference between wing and body at supersonic speeds was treated with a satisfactory degree of precision in Part I of these reports, wherein the method of small perturbations was employed, the restrictions of that approach may not be tolerable except in cases where the results are required with a relatively small amount of labor and where accuracy and generality can be sacrificed to expediency.

A more exact solution to the problem is afforded by the method of characteristics, which is expounded in the present report so as to shape the details of this fundamental mathematical procedure to the specific three-dimensional problem requiring analysis. The report will thus have the nature of a stepwise procedural development of essentially simple relationships that are used repetitiously; consequently, the work will appear lengthy, while in fact there is little of a complex character involved. Most attention will be devoted to the working out of a systematic and thorough covering of every region of flow by a network of characteristic surfaces, from which the local flow conditions may then be ascertained.

Even this general and precise investigation of the problem of wing-body interference is, of course, based on several assumptions that may not agree rigidly with physical reality. An important restriction imposed on the present method is that the flow over the body is irrotational even in the presence of the shock wave emanating from the nose. It is believed that the discrepancy between physical reality and the present theory will be sufficiently small in most instances that it will not warrant the development of the more intricate solutions for which a potential does not exist.

Further restrictions to the method as applied here are artificial in that they can be removed or altered so as to fit any particular example that does not conform to the configuration being treated. Of course, the body has been assumed axially symmetric and also unyawed, although the angle of attack and wing incidence are arbitrary. The body contour, if not made up of jointed straight-line segments, is approximated thusly, so that the body is composed of a conical tip and a series of frustums of cones for the nose, while farther back a cylindrical portion is finally reached in the neighborhood of the wing-body juncture.

Because the flow is supersonic, the presence of the wing does not affect the fore part of the body, and, consequently, it is possible to begin the investigation of the entire flow field surrounding the body by means of standard procedures, which will be repeated here first of all for the sake of completeness.

LIST OF SYMBOLS

V_l	= limiting velocity of the stream (velocity attained upon adiabatic expansion of the flow to an absolute vacuum)
$\vec{V_0}$	= velocity of the undisturbed stream
C_0	= velocity of sound in the undisturbed stream
C	= local velocity of sound in the disturbed stream
$\vec{v_0}$	= V_0/V_l
c_0	= C_0/V_l
c	= C/V_l

Received August 30, 1948.

* Italian manuscript submitted to Cornell Aeronautical Laboratory, April 2, 1947. The translation was accomplished under Navy BuArd sponsorship.

† Member of C.A.L. consulting staff. Professor, Laboratorio di Aeronautica, Politecnico di Torino.

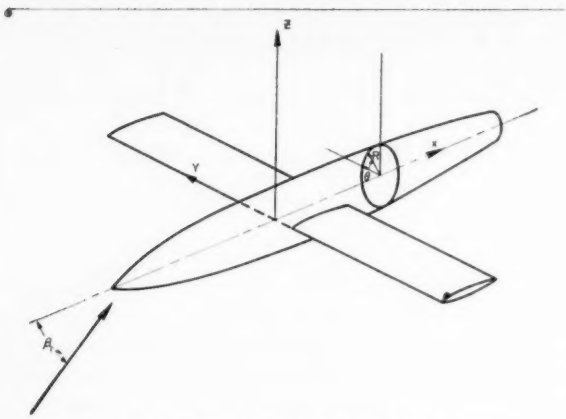

FIG. 1. Orientation of rectangular coordinate system.

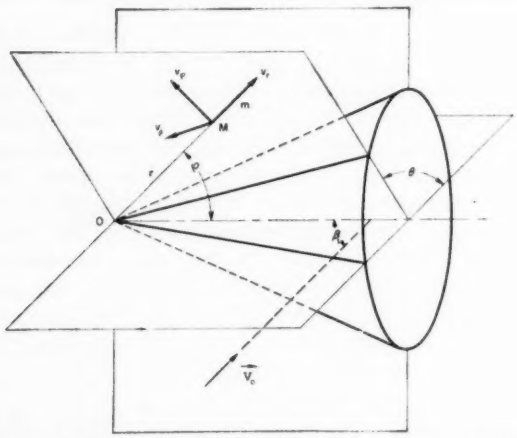

FIG. 2. Coordinate and vectorial orientation in the spherical coordinate system.

$\Phi_1 V_l$ = the potential of the field around the conical nose

$\Phi_2 V_l$ = the potential for the field that exists downstream of the initial characteristic surface from which perturbations are propagated into the fluid in consequence of deviations in the shape of the body from the conical form

$\Phi_3 V_l$ = the velocity potential in the region downstream of the initial characteristic surface (or shock wave) from which perturbations originate because of the presence of the wing

(x, Y, Z) = Cartesian coordinates with x along the axis of the body and oriented (Fig. 1) in the same sense as the undisturbed velocity $\vec{V}_0$; the Z-axis is normal to the x-axis and in the plane of symmetry, oriented in the sense of positive lift; the Y-axis is normal to the plane of symmetry and directed according to a right-handed system; the origin is located in such a way that the leading edge of the wing lies along the Y-axis

(x, y, θ) = cylindrical coordinates with x situated as for the Cartesian coordinates; the initial side of θ is the direction of the positive Y-axis; and y is perpendicular to x in any meridian plane and is positive in the direction of the terminal side of θ; the origin is at the tip of the conical nose (see Figs. 1 and 5)

(r, φ, θ) = spherical coordinates with origin at the apex of the conical tip of the nose; the initial side of the angle φ is in the direction of the positive x-axis (see Fig. 2)

(V_x, V_Y, V_Z) = velocity components along the Cartesian axes

(V_x, V_Y, V_θ) = velocity components based on the cylindrical coordinate system

$(V_r, V_\varphi, V_\theta)$ = velocity components based on the spherical coordinate system (Fig. 2)

The same letters in lower case refer to the ratios of the corresponding velocities to the limiting velocity V_l, while the use of primes or various subscripts will always denote velocity components at the points indicated in the text.

β_1 = angle of inclination of $\vec{V}_0$ with respect to the x-axis

p = pressure

ρ = density

k = adiabatic exponent (taken as 1.400 for air)

The meaning of the other symbols not listed here is indicated at appropriate points in the text.

(A) Determination of the Field Around the Conical Nose

(A-1) *Potential of the Conical Field*

(A-1-1) General Equations.—Let the potential of the conical field be expressed as

$$\Phi_1 V_l = V_l r F(\varphi, \theta) \tag{1}$$

in terms of the spherical coordinates (r, φ, θ). The velocity components v_r, v_φ, v_θ, along the radius r, in the direction normal to r and in the meridian plane, and in the direction normal to the meridian plane, respectively, are given by:

$$\left.\begin{aligned} v_r &= \frac{\partial \Phi_1}{\partial r} = F; \qquad v_\varphi = \frac{1}{r}\frac{\partial \Phi_1}{\partial \varphi} = \frac{\partial F}{\partial \varphi} \\ v_\theta &= \frac{1}{r \sin \varphi}\frac{\partial \Phi_1}{\partial \theta} = \frac{1}{\sin \varphi}\frac{\partial F}{\partial \theta} \end{aligned}\right\} \tag{2}$$

The differential equation defining Φ_1 is, consequently:[1]

$$\sin^2 \varphi \left(1 - \frac{v_\varphi^2}{c^2}\right)\frac{\partial^2 F}{\partial \varphi^2} - 2\frac{v_0 v_\varphi}{c^2}\frac{\partial^2 F}{\partial \theta \partial \varphi}\sin \varphi + \left(1 - \frac{v_0^2}{c^2}\right)\frac{\partial^2 F}{\partial \theta^2} + \sin^2 \varphi\, v_r \left(2 - \frac{v_\varphi^2 + v_\theta^2}{c^2}\right) + \frac{1}{2}\sin 2\varphi\, v_\varphi \left(1 + \frac{v_0^2}{c^2}\right) = 0 \tag{3}$$

while the local velocity of sound, c, is related to the velocity of sound in the undisturbed stream through the Bernoulli equation:

$$c^2 = c_0^2 + \frac{k-1}{2}(v_0^2 - v_r^2 - v_\varphi^2 - v_\theta^2)$$

(A-1-2) Determination of the Function F by the Hodograph Method.—If, in every meridian plane θ = con-

stant, the hodograph of the motion is drawn in terms of the components v_x, v_y of the velocity in the direction of the cylindrical coordinates x and y, it is evident that the velocity of the fluid for all points of the polar radius m, which is inclined to the x-axis by the angle φ (Fig. 3), is given by the tangent to the hodograph at the point M, and this tangent is perpendicular to the radius itself; also, the radius of curvature of the hodograph at M is:[2]

$$R = v_r + (\partial v_\varphi / \partial \varphi) \tag{4}$$

Because of Eq. (4) and taking into account Eqs. (2), it is possible to write Eq. (3) in the form:

$$\left(1 - \frac{v_\varphi^2}{c^2}\right) R = \frac{2}{\sin \varphi} \frac{v_\varphi v_\theta}{c^2} \left(\frac{\partial v_\varphi}{\partial \theta}\right) - \cot \varphi \times$$

$$\left[v_\varphi \left(1 + \frac{v_\theta^2}{c^2}\right)\right] - \left(1 - \frac{v_\theta^2}{c^2}\right)\left(v_r + \frac{1}{\sin \varphi} \frac{\partial v_\theta}{\partial \theta}\right) \tag{3'}$$

This equation permits the determination of the hodograph in all the meridian planes if the values of the velocity components v_r, v_φ, v_θ are known for all the points of a given surface S, which is assumed to be an arbitrary cone with apex at the origin.

Let the equation of this surface be:

$$\varphi = \varphi(\theta) \tag{5}$$

and let the known values of v_θ and v_φ on S be denoted by $v_\theta = v_\theta(\theta)$; $v_\varphi = v_\varphi(\theta)$; then

$$\left(\frac{dv_\theta}{d\theta}\right) = \frac{\partial v_\theta}{\partial \theta} + \frac{\partial v_\theta}{\partial \varphi} (\dot{\varphi})$$

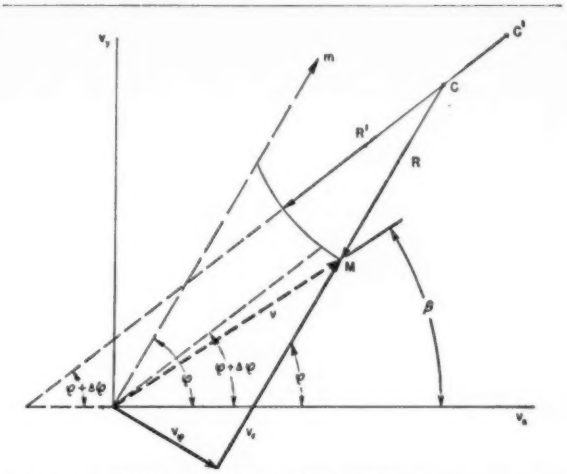

FIG. 3. Graphical extension of the hodograph to successive reference cones for flow over the conical nose.

where $\dot{\varphi}$ is the derivative with respect to θ of the function that is defined by Eq. (5).

But from Eq. (2):

$$\frac{\partial v_\theta}{\partial \varphi} = \frac{1}{\sin \varphi} \frac{\partial v_\varphi}{\partial \theta} - \cot \varphi \, (v_\theta)$$

and, hence,

$$\left(\frac{dv_\theta}{d\theta}\right)_S = \frac{\partial v_\theta}{\partial \theta} + \dot{\varphi}\left[\frac{1}{\sin \varphi} \frac{\partial v_\varphi}{\partial \theta} - \cot \varphi \, (v_\theta)\right]$$

Analogously,

$$\left(\frac{dv_\varphi}{d\theta}\right)_S = \frac{\partial v_\varphi}{\partial \varphi} (\dot{\varphi}) + \frac{\partial v_\varphi}{\partial \theta} = (R - v_r)\dot{\varphi} + \frac{\partial v_\varphi}{\partial \theta}$$

whence,

$$\partial v_\varphi / \partial \theta = (dv_\varphi / d\theta)_S - (R - v_r)\dot{\varphi}$$

$$\frac{\partial v_\theta}{\partial \theta} = \dot{\varphi}^2 \frac{R}{\sin \varphi} + \left(\frac{dv_\theta}{d\theta}\right)_S - \frac{\dot{\varphi}}{\sin \varphi}\left[\left(\frac{dv_\varphi}{d\theta}\right)_S + v_r\dot{\varphi} - \cos \varphi \, (v_\theta)\right]$$

and therefore, with aid of Eq. (3'):

$$\left\{1 - \frac{v_\varphi^2}{c^2} + \frac{2}{\sin \varphi} \frac{v_\varphi v_\theta}{c^2} \dot{\varphi} + \frac{[1 - (v_\theta^2/c^2)]}{\sin^2 \varphi} \dot{\varphi}^2\right\} R = \frac{2}{\sin \varphi} \frac{v_\varphi v_\theta}{c^2}\left[\left(\frac{dv_\varphi}{d\theta}\right)_S + v_r\dot{\varphi}\right] - \cot \varphi (v_\varphi)\left(1 + \frac{v_\theta^2}{c^2}\right) -$$

$$\left(1 - \frac{v_\theta^2}{c^2}\right)\left\{v_r + \frac{1}{\sin \varphi}\left(\frac{dv_\theta}{d\theta}\right)_S - \frac{\dot{\varphi}}{\sin^2 \varphi}\left[\left(\frac{dv_\varphi}{d\theta}\right)_S + v_r\dot{\varphi} - \cos \varphi \, (v_\theta)\right]\right\} \tag{6}$$

The second member of Eq. (6) is now known for all values of θ and for the value of φ which corresponds to the intersection m of the above-defined conical surface S with the meridian planes. Having located, for each meridian plane, the point M, which represents the velocity corresponding to the straight line m (Fig. 3), it is at once possible to locate the center of curvature, C, of the hodograph at M, since it lies on the parallel to m through M at a distance R, which may be calculated from Eq. (6).

Thus it is possible to draw, for all the hodograph planes relative to the various planes θ = constant, the arcs of circles that are osculatory to these hodographs, between the straight lines φ and $\varphi + \Delta\varphi$ (Fig. 3). Thus, the values of the velocity components v_r and v_φ are determined for all the straight lines m', inclined

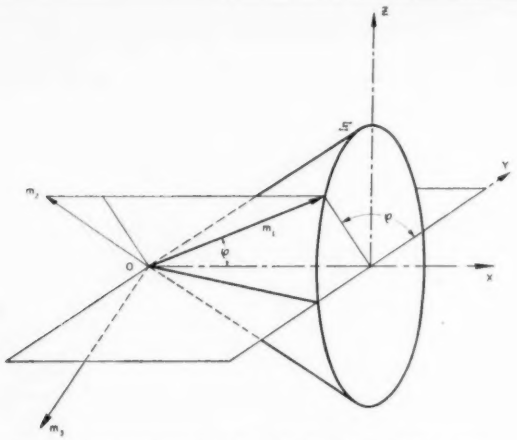

FIG. 4. Arrangement of the shock surface at the nose.

at the angle $\varphi + \Delta\varphi$, while the values of v_θ are obtained from the equation:

$$v_\theta = (v_\theta)_{\varphi=\varphi} + \left(\frac{\partial v_\theta}{\partial \varphi}\right)_{\varphi=\varphi} \Delta\varphi = (v_\theta)_{\varphi=\varphi}(1 - \cot\varphi\,\Delta\varphi) + \frac{1}{\sin\varphi}\left[\left(\frac{dv_\varphi}{d\theta}\right)_S - \dot{\varphi}(R - v_r)\right]_{\varphi=\varphi} \Delta\varphi \quad (7)$$

In this manner the values of v_r, v_θ, and v_φ, relative to a new conical surface S' defined by the equation $\varphi = \varphi + \Delta\varphi$, are obtained. The application of the above-described procedure can thus be repeated, and it is apparent that one can continue the drawing of the hodograph relative to all the meridian planes by proceeding step by step. If $\dot{\varphi}$ is extremely small for the surface S (i.e., if S closely approximates a right circular conic surface) and under the assumption that $\Delta\varphi$ is taken to be different from one meridian plane to the next, the problem reduces simply to that of a right circular conic surface as far as S' (or the successive S'') is concerned; this case makes possible an immediate simplification of Eq. (6).

(A-2) *Shock Wave on the Conical Nose*

(A-2-0) Alternative Points of View.—The problem of determining the velocity field around the conical nose is now reduced to that of establishing the initial data—that is, v_r, v_φ, and v_θ—on a conical surface S. Two procedures are available for this purpose. The first consists of assuming the data appertaining to the undisturbed stream—that is, the ratio V_0/V_l and the angle of attack β_1—and then in determining the shock waves that are compatible with such a stream and with a conical field of the sort dealt with in (A-1). The surface possessing the initial data is then the shock surface itself, while the form of the conical nose of the body is consequently determined as a result. The second procedure consists of assuming the conical shape of the body, a priori, and also the initial conditions of the stream over it; the surface possessing the initial data is then the surface of the body itself, and the arrangement of the shock wave, as well as the condition of the undisturbed stream, is consequently determined. The first procedure just mentioned is developed below in Sections (A-2-1) and (A-2-2) and is valid for a general conical shape of the nose of the body with the sole limitation that the surface be symmetrical with respect to the plane $\theta = \pi/2$. In contrast, in Section (A-2-3), the second procedure is dealt with, but there it will be necessary to restrict ourselves to the case in which the nose is part of a right circular cone with its axis coincident with the x-axis.

(A-2-1) Possible Conical Shock Waves in Uniform Flows.—Let

$$\varphi = f(\theta) \quad (8)$$

be the surface Ξ, which is the shock wave front. Let m_1, m_2, m_3 denote the straight lines that are, respectively, the intersection of Ξ with the general meridian plane θ = constant, the perpendicular to m_1 in the meridian plane, and the perpendicular to the meridian plane (Fig. 4). Then the components of the undisturbed velocity $\vec{v_0}$ along m_1, m_2, m_3 are:

For m_1: $v_0(\cos\beta_1\cos\varphi + \sin\beta_1\sin\varphi\sin\theta)$
For m_2: $v_0(-\cos\beta_1\sin\varphi + \sin\beta_1\cos\varphi\sin\theta)$
For m_3: $v_0\sin\beta_1\cos\theta$

while the analogous components of velocity after the shock are:

For m_1: F
For m_2: $\partial F/\partial\varphi$
For m_3: $(1/\sin\varphi)(\partial F/\partial\theta)$

Imposing the condition, therefore, that the change in velocity across Ξ be perpendicular to Ξ itself and knowing that the direction cosines of the normal, $\vec{n}$, to Ξ at a general arbitrary point are (with respect to m_1, m_2, and m_3 which you pass through the same point):

$$\cos(n, m_1) = 0$$
$$\cos(n, m_2) = \sin\varphi/\sqrt{\sin^2\varphi + \dot{f}^2}$$
$$\cos(n, m_3) = -\dot{f}/\sqrt{\sin^2\varphi + \dot{f}^2}$$

where $\dot{f} = df/d\theta$, then

$$\frac{v_0(\cos\beta_1\cos\varphi + \sin\beta_1\sin\varphi\sin\theta) - F}{0} =$$

$$\frac{v_0(-\cos\beta_1\sin\varphi + \sin\beta_1\sin\theta\cos\varphi) - (\partial F/\partial\varphi)}{\sin\varphi} =$$

$$\frac{v_0\sin\beta_1\cos\theta - (1/\sin\varphi)(\partial F/\partial\theta)}{-\dot{f}} = H$$

where H is the common value of the indicated ratios. Then on Ξ—that is, for $\varphi = f(\theta)$—it follows that:

$$\left.\begin{aligned} F &= v_0(\cos\beta_1\cos\varphi + \sin\beta_1\sin\varphi\sin\theta) \\ \partial F/\partial\varphi &= v_0(-\cos\beta_1\sin\varphi + \\ &\qquad \sin\beta_1\sin\theta\cos\varphi) - \mathrm{H}\sin\varphi \\ \partial F/\partial\theta &= v_0\sin\beta_1\cos\theta\sin\varphi + Hf\sin\varphi \end{aligned}\right\} \tag{9}$$

It can be verified directly that Eqs. (9) are compatible because the expression of F, $\partial F/\partial\theta$, and $\partial F/\partial\varphi$ by their equivalents from Eqs. (9) confirms that $dF/d\theta = (\partial F/\partial\theta) + (\partial F/\partial\varphi)(\dot{f})$.

On the other hand, the equation for the shock must be satisfied through Ξ. Let v_{n1} and v_{n2} be the velocity components (divided by V_l) along the normal to Ξ of the flow before and after the shock, respectively; and let v_t be the component (also divided by V_l) of the velocity which is tangent to the shock and which remains unaltered. Then the equation of the shock has the form:

$$v_{n1}v_{n2} = [(k-1)/(k+1)](1 - v_t^2) \tag{10}$$

Now

$$v_{n1} = v_0(-\cos\beta_1\sin\varphi + \sin\beta_1\sin\theta\cos\varphi)\frac{\sin\varphi}{\sqrt{\sin^2\varphi + \dot{f}^2}} - v_0\sin\beta_1\cos\theta\frac{\dot{f}}{\sqrt{\sin^2\varphi + \dot{f}^2}}$$

and

$$v_{n2} = \frac{\partial F}{\partial\varphi}\left(\frac{\sin\varphi}{\sqrt{\sin^2\varphi + \dot{f}^2}}\right) - \frac{1}{\sin\varphi}\frac{\partial F}{\partial\theta}\left(\frac{\dot{f}}{\sqrt{\sin^2\varphi + \dot{f}^2}}\right)$$

while

$$v_t^2 = v_0^2\left\{1 - \frac{[\sin\varphi\,(-\cos\beta_1\sin\varphi + \sin\beta_1\sin\theta\cos\varphi) - \dot{f}\sin\beta_1\cos\theta]^2}{\sin^2\varphi + \dot{f}^2}\right\}$$

In addition, let

$$a = \sin\varphi\,(\sin\beta_1\sin\theta\cos\varphi - \cos\beta_1\sin\varphi) - \sin\beta_1\dot{f}\cos\theta \tag{11}$$

Then, substituting these expressions for v_{n1}, v_{n2}, and v_t into Eq. (10), there evolves:

$$H = [2/(k-1)]\,[av_0/(\sin^2\varphi + \dot{f}^2)] - [(k-1)/(k+1)][(1 - v_0^2)/av_0] \tag{12}$$

which, together with Eqs. (9), defines all the postshock velocities that are permissible as a result of shock action (upon the uniform stream under consideration) by agency of the conical waves [Eq. (8)].

(A-2-2) Complete Determination of the Conical Field When the Configuration of the Conical Shock Wave Is Known.—Let f, which must be a periodic function of θ, take the form

$$f = \bar{\varphi} + \beta_1\sum_n b_n\sin n\theta \tag{8'}$$

where $\bar{\varphi}$ is independent of θ and n is odd because the flow phenomenon is symmetrical with respect to the plane $\theta = \pi/2$. Then the description of the flow on the surface Ξ is defined by Eqs. (9), having due regard for Eqs. (11) and (12), whenever v_0 and β_1 have been selected (that is, the condition of the undisturbed stream having been fixed), and, consequently, Ξ can be taken as the surface S, discussed in (A-1-2), for which the initial data are known.

The drawing of the hodographs of the motion in the various meridian planes must be continued up to the intersection of these planes with the contour surface of the body; such a trace is determined by the condition that upon reaching it the velocity of the fluid normal to the contour surface must be zero. If, therefore,

$$\varphi = \psi(\theta) \tag{13}$$

is the equation of the conical nose, then it is required that on this surface [Eq. (13)]:

$$\frac{\partial F}{\partial\varphi} - \frac{1}{\sin^2\varphi}\left(\frac{\partial F}{\partial\theta}\right)\dot{\psi} = 0 \tag{14}$$

Now in the semiplanes $\theta = \pm\pi/2$, the partial derivative $\partial F/\partial\theta$ is zero and so is $\dot{\psi}$, because of the symmetry of the motion and of the nose with respect to these semiplanes. Hence, for these planes,

$$\partial F/\partial\varphi = 0 \tag{15}$$

must hold.

Upon determination of the value of φ, by means of the hodograph in the semiplane $\theta = \pi/2$, such that Eq. (15) is satisfied, the intersection (generatrix) of the

nose with this semiplane is defined by the value of φ so obtained. Meanwhile, the other generatrices, which are intersections with the nose of the other semiplanes, are obtained more simply by proceeding step by step from relation (14). If $\varphi_i = \psi(\theta_i)$ is the value of φ which corresponds to the semiplane $\theta = \theta_i$, then in the semiplane $\theta = \theta_i + \Delta\theta$ the following is achieved:

$$\varphi_{i+1} = \varphi_i + \sin^2\varphi \frac{\left(\frac{\partial F}{\partial \varphi}\right)_{\substack{\varphi=\varphi_i \\ \theta=\theta_i}}}{\left(\frac{\partial F}{\partial \theta}\right)_{\substack{\varphi=\varphi_i \\ \theta=\theta_i}}} \Delta\theta \qquad (14')$$

Variation of φ and b_n and thus change in the shape of the shock wave generate shapes of nose. It must be noted that through this procedure $\partial F/\partial\varphi = 0$ must again occur, in the semiplane $\theta = 3\pi/2$, for the value of φ obtained by repeated application of Eq. (14'). This requirement will certainly be fulfilled if the deviation of the streamlines occasioned by the shock is small enough that the change of entropy from one streamline to another may be neglected; this change is of the order of magnitude of the product of the square of the average deviation by β_1. Under this condition the motion can indeed be regarded as irrotational, and no contradiction can exist between the assumptions and the results to which they have led.

(A-2-3) Determination of the Conical Field for a Given Nose.—If the configuration of the tip of the nose is given, and considering it to be a right circular cone, then the character of the stream at its surface may be assumed a priori, and this surface of the body may be taken as the one possessing the initial data, provided that the angle β_1 that V_0 makes with x is sufficiently small in order to make it legitimate to neglect v_θ^2/c^2 in comparison with unity in Eq. (3). Since $\partial^2 F/\partial\theta^2$ is already of the order of magnitude of β_1, the above-mentioned assumption leads to the suppression of terms of the order of magnitude of β_1^3. Indeed it is evident that with the above hypotheses it is possible to set

$$\sin^2\varphi\left(\frac{\partial^2 F}{\partial\varphi^2}\right) + (1/2)\sin 2\varphi\left(\frac{\partial F}{\partial\varphi}\right) + \frac{\partial^2 F}{\partial\theta^2} + 2\sin^2\varphi\,(F) = 0 \qquad (3'')$$

in the immediate vicinity of the body, since $v_\varphi = 0$ on it. But expression (3'') is the differential equation that defines the spherical harmonic functions of first order.[3] The general integral of this equation which satisfies the boundary conditions on the conical nose is:

$$F = A_0(\varphi) + A_1(\varphi)\sin\theta \qquad (16)$$

where A_0 and A_1 are a linear combination of the spherical harmonics of the first and second kind and of their associated functions, which need not be specified at present. Indeed, with proper selection of the constant coefficients of such a linear combination, it is possible to elicit the relations

$$dA_0/d\varphi = dA_1/d\varphi = 0$$

which hold for the value of φ corresponding to the conical nose, in order that the condition of tangency at the body, $v_\varphi = 0$, be fulfilled, while it is also true that

$$v_r = A_0 + A_1\sin\theta$$
$$v_\theta = (A_1/\sin\varphi)\cos\theta \qquad (17)$$

Now the coefficients A_0, A_1, and $\sin\varphi$ assume constant values on the surface of the cones, and, therefore, once the values of A_0 and A_1 are fixed, the values of the velocities on the conical contour of the body are consequently fixed also, and this surface can then be taken as the one possessing the initial data. The tracing of the hodographs in the various meridian planes must be carried out this time until the shock wave front is reached. The determination of the traces of the shock wave in the various meridian planes and of the flow conditions upstream of the shock can be accomplished by a process of successive approximations, which will now be set forth.

Consider first of all the semiplane $\theta = 0$. In it, as a first approximation, one may let

$$v_{n1} = -v_0\sin\varphi$$
$$v_{n2} = \frac{\partial F}{\partial\varphi} - \frac{1}{\sin\varphi}\frac{\partial F}{\partial\theta}\frac{\dot{f}}{\sin\varphi} \cong \frac{\partial F}{\partial\varphi}$$

(the approximation results because $(1/\sin\varphi)(\partial F/\partial\theta)$ is of the order of magnitude of β_1, and likewise so is $\dot{f}$) and

$$1 - v_t^2 = 1 - v_0^2 + v_0^2\sin^2\varphi = 1 - v_0^2\cos^2\varphi$$

Thus, through means of the equations of the shock [Eqs. (9) and (10)], there arise the expressions:

$$\left.\begin{aligned} -v_0\sin\varphi\,\frac{\partial F}{\partial\varphi} &= \frac{k-1}{k+1}(1 - v_0^2\cos^2\varphi) \\ F &= v_0\cos\varphi \end{aligned}\right\} \qquad (18)$$

Substituting

$$v_0 = F/\cos\varphi \qquad (19)$$

into the first part of relations (18), there is obtained:

$$-F(\tan\varphi)\frac{\partial F}{\partial\varphi} = \frac{k-1}{k+1}(1 - F^2) \qquad (20)$$

And since F and $\partial F/\partial\varphi$ are known, in consequence of the construction of the hodograph, for any value of φ, Eq. (20) affords the means of determining the value of φ, satisfying this equation and thus defining the generatrix (intersection) of the shock cone in the semiplane $\theta = 0$. The desired value of v_0 for this case is given directly by Eq. (19).

Now consider the semiplane $\theta = \pi/2$ (in which $\dot{f} = 0$). Since, in this plane,

$$v_{n1} = v_0 (-\sin\varphi + \sin\beta_1 \cos\varphi); \qquad v_{n2} = \partial F/\partial\varphi$$

and

$$1 - v_t^2 = 1 - v_0^2 \cos^2\varphi - v_0^2 \sin 2\varphi \sin\beta_1$$

it follows that

$$v_0(-\sin\varphi + \sin\beta_1\cos\varphi)\frac{\partial F}{\partial\varphi} = \frac{k-1}{k+1}(1 - v_0^2\cos^2\varphi - v_0^2\sin 2\varphi\sin\beta_1)$$

and

$$F = v_0(\cos\varphi + \sin\beta_1\sin\varphi) \tag{21}$$

From the second of the relations in Eqs. (21) one obtains

$$\sin\beta_1 = [(F/v_0) - \cos\varphi](1/\sin\varphi) \tag{22}$$

which, when substituted in the first of the relations (21), yields:

$$v_0(-\sin\varphi + \cot\varphi\frac{F}{v_0} - \cot\varphi\cos\varphi)\frac{\partial F}{\partial\varphi} = \frac{k-1}{k+1}\left(1 - v_0^2\cos^2\varphi - 2v_0^2\cos\varphi\frac{F}{v_0} + 2v_0^2\cos^2\varphi\right) = \frac{k-1}{k+1}(1 + v_0^2\cos^2\varphi - 2\cos\varphi\, v_0 F) \tag{23}$$

Now, since v_0 is known and since the hodograph gives the corresponding values of F and $\partial F/\partial\varphi$ for every φ, Eq. (23) affords the means of obtaining the value of φ, satisfying this equation and thus defining the generatrix trace of the shock wave in the plane under consideration. In the meantime, Eq. (22) permits the calculation of the value of β_1.

The generatrices of the wave, or intersections with the other semiplanes, are obtained through repeated application of Eq. (10), which may be rewritten in the form:

$$v_0(-\sin\varphi + \sin\beta_1\sin\theta\cos\varphi)\frac{\partial F}{\partial\varphi} = \frac{k-1}{k+1}\times (1 - v_0^2\cos^2\varphi - v_0^2\sin\beta_1\sin\theta\sin 2\varphi) \tag{10'}$$

Since v_0 and β_1 are known and since the hodograph furnishes the value of $\partial F/\partial\varphi$ corresponding to every φ, in the arbitrary general semiplane θ = const., Eq. (10′) affords the means of obtaining the value of φ, satisfying this equation and thus defining the generatrix for the general case. To check the degree of approximation (introduced through the use of the simplifying hypotheses), it is necessary to verify that the first of Eqs. (9) is also satisfied by the values of φ which are obtained from Eq. (10′).

The above-described procedure presents a first approximation for the case where the shock wave and the conditions of the flow upstream of the shock are to be determined. In general, the accuracy will be adequate if one stops at this first approximation, provided that the magnitude of the angle of attack, β_1, is sufficiently small. If a second approximation is desired, however, the values obtained thusly through use of the first approximation may be substituted into the equations of the shock, Eqs. (9) and (10), and the second approximation may then be carried out by means of a procedure that is quite analogous to the one pursued in obtaining the somewhat less exact first results.

(B) Determination of the Field Around that Portion of the Body which Lies Between the Conical Nose and the Wing

(*B-0*) *General Equations*

(*B-0-0*) *Equation of Motion and Associated Characteristic Surfaces.*—For the determination of the field around that part of the body which follows the nose and precedes the wing, the "method of characteristics" is applicable. The equation that defines the potential of the field corresponding to this region is, using the cylindrical coordinates (x, y, θ),

$$a_{11}\frac{\partial^2\Phi_2}{\partial x^2} + a_{22}\frac{\partial^2\Phi_2}{\partial y^2} + a_{33}\frac{1}{y^2}\frac{\partial^2\Phi_2}{\partial\theta^2} + 2a_{12}\frac{\partial^2\Phi_2}{\partial x\,\partial y} + 2a_{13}\frac{1}{y}\frac{\partial^2\Phi_2}{\partial\theta\,\partial x} + 2a_{23}\frac{1}{y}\frac{\partial^2\Phi_2}{\partial\theta\,\partial y} + \frac{v_y}{y} = 0 \tag{24}$$

where

$$\left.\begin{aligned} a_{11} &= 1 - \frac{v_x^2}{c^2}; & a_{12} &= -\frac{v_x v_y}{c^2}; & a_{22} &= 1 - \frac{v_y^2}{c^2} \\ a_{13} &= -\frac{v_x v_\theta}{c^2}; & a_{23} &= -\frac{v_y v_\theta}{c^2}; & a_{33} &= 1 - \frac{v_\theta^2}{c^2} \end{aligned}\right\} \tag{25}$$

First of all, the characteristic surfaces of Eq. (24) are sought. To this end, the equation of such surfaces is expressed in the form

$$W(x, y, \theta) = b \tag{26}$$

where b is a constant. Then W must consequently satisfy the equation:[4]

$$\sum a_{ik}\frac{\partial W}{\partial x_i}\frac{\partial W}{\partial x_k} = 0 \qquad (\text{for } i, k = 1, 2, 3) \tag{27}$$

in which we have set $dx_1 = dx$, $dx_2 = dy$, and $dx_3 = y\,d\theta$.

The discriminant of Eq. (27) is equal to

$$1 - [(v_x^2 + v_y^2 + v_\theta^2)/c^2]$$

and it is therefore negative everywhere; hence, the surfaces defined by Eq. (27) are real. Through solution of Eq. (26) for y and thus by transcription of the equation of the characteristics into the form

$$y = f(x, \theta, b) \tag{26'}$$

it follows that Eq. (27) may be expressed as:

$$a_{11}\dot{f}_x^2 - 2a_{12}\dot{f}_x + a_{22} + \frac{2a_{13}}{y}\dot{f}_x\dot{f}_\theta - \frac{2a_{23}}{y}\dot{f}_\theta + \frac{a_{33}}{y^2}\dot{f}_\theta^2 = 0 \tag{27'}$$

where $\dot{f}_x = \partial f/\partial x$ and $\dot{f}_\theta = \partial f/\partial\theta$.

Now the direction cosines, relative to the straight lines x_1, x_2, x_3, of the normal to a general arbitrary one of the surfaces [Eq. (27′)] (corresponding to an arbitrary value of the constant b) and erected at a given general point, are:

$$\dot{f}_x/\sqrt{1 + \dot{f}_x^2 + (\dot{f}_\theta^2/y^2)}$$
$$-1/\sqrt{1 + \dot{f}_x^2 + (\dot{f}_\theta^2/y^2)}$$
$$\dot{f}_\theta/y\sqrt{1 + \dot{f}_x^2 + (\dot{f}_\theta^2/y^2)}$$

where the lines x_1, x_2, and x_3 are directed, respectively, in this manner: x_1 along the x-axis, x_2 along the normal, y, to x in the given meridian plane, and x_3 along the normal to the meridian plane. Likewise, the direction cosines of the line of action of the fluid velocity in the same point and relative to the same lines x_1, x_2, x_3 are:

$$v_x/\sqrt{v_x^2 + v_y^2 + v_\theta^2}$$
$$v_y/\sqrt{v_x^2 + v_y^2 + v_\theta^2}$$
$$v_\theta/\sqrt{v_x^2 + v_y^2 + v_\theta^2}$$

Consequently, it is seen from Eq. (27′) that the normal, $\vec{n}$, to an arbitrary general characteristic surface is inclined to the direction of the velocity, $\vec{V}$, by an angle the magnitude of which is given as

$$\cos(\vec{n}, \vec{V}) = \pm C/V = \pm \sin\delta$$

if δ denotes the Mach angle. That is to say, the characteristic surfaces associated with Eq. (24) are the envelope surfaces of the Mach cones which propagate, from each point, the elemental disturbance created there. There are two sets of such characteristic surfaces; one of them (Σ) is characterized by the condition that the normals to the surfaces make the Mach angle δ with respect to $\vec{V}$, while the other one (Σ') is characterized by the condition that the normals to the surfaces make the angle $-\delta$ with respect to $\vec{V}$.

(B-0-1) Variation of the Velocities on the Characteristic Surfaces.—Consider any characteristic surface whatever of a set (for instance the set Σ), and designate by $d\sigma_1$ and $d\sigma_2$ the linear elements of the intersections of this surface (denoted by the symbol Σ) with an arbitrary general meridian plane, θ = const., and with a plane normal to the x-axis (x = const.), respectively (see Fig. 5).

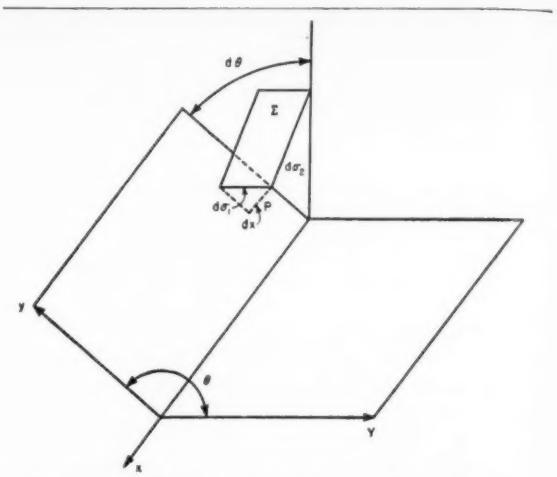

FIG. 5. Representative trace of a characteristic surface in a meridian plane and in a plane perpendicular to the x-axis.

The velocity changes—dv_x, dv_y, and $d(yv_\theta)$—which occur in traversing the distance $d\sigma_1$ (the projection of which upon x is denoted by dx), are given by:

$$\left.\begin{aligned} dv_x &= (p_{11} + p_{12}\dot{f}_x)dx \\ dv_y &= (p_{12} + p_{22}\dot{f}_x)dx \end{aligned}\right\} \tag{28}$$
$$d(yv_\theta) = (p_{13} + p_{23}\dot{f}_x)dx$$

where $p_{11} = \partial^2\Phi_2/\partial x^2$, $p_{12} = \partial^2\Phi_2/\partial x\,\partial y$, and $p_{13} = \partial^2\Phi_2/\partial x\partial\theta$, etc. From Eq. (28) it is evident that

$$p_{12} = (dv_y/dx) - p_{22}\dot{f}_x$$
$$p_{11} = (dv_x/dx) - \dot{f}_x(dv_y/dx) + p_{22}\dot{f}_x^2$$
$$p_{13} = (d(yv_\theta)/dx) - p_{23}\dot{f}_x$$

so that now, upon substitution of these expressions into Eq. (24), there evolves:

$$a_{11}\frac{dv_x}{dx} + \frac{dv_y}{dx}(a_{11}\dot{f}_x + 2a_{12}) + \frac{2a_{13}}{y}\frac{d(yv_\theta)}{dx} +$$
$$p_{22}(a_{11}\dot{f}_x^2 + a_{22} - 2a_{12}\dot{f}_x) + p_{23}\left(2\frac{a_{23}}{y} - 2\frac{a_{13}}{y}\dot{f}_x\right) +$$
$$a_{33}\frac{p_{33}}{y^2} + \frac{v_y}{y} = 0 \tag{29}$$

Analogously, the velocity changes that take place along $d\sigma_2$ are:

$$dv_x = (p_{12}\dot{f}_\theta + p_{13})d\theta$$
$$dv_y = (p_{22}\dot{f}_\theta + p_{23})d\theta$$
$$d(yv_\theta) = (p_{33} + p_{23}\dot{f}_\theta)d\theta$$

where $d\theta$ is the angle between the meridian planes within the confines of which the said element is contained. Whence it follows that

$$p_{23} = (dv_y/d\theta) - p_{22}\dot{f}_\theta$$
$$p_{33} = (d(yv_\theta)/d\theta) - \dot{f}_\theta(dv_y/d\theta) + p_{22}\dot{f}_\theta^2 \tag{28'}$$
$$p_{13} = (dv_x/d\theta) - p_{12}\dot{f}_\theta$$

Substitution of these values of p_{23} and p_{33} just found into Eq. (29) gives:

$$a_{11}\frac{dv_x}{dx} + (-a_{11}\hat{f}_x + 2a_{12})\frac{dv_y}{dx} + \frac{2a_{13}}{y}\frac{d(yv_\theta)}{dx} + \frac{a_{33}}{y^2}\frac{d(yv_\theta)}{d\theta} - \frac{a_{33}}{y^2}\hat{f}_\theta\frac{dv_y}{d\theta} + \frac{dv_y}{d\theta}\left(2\frac{a_{23}}{y} - 2\frac{a_{13}}{y}\hat{f}_x\right) + \frac{v_y}{y} + p_{22}\left(a_{11}\hat{f}_x^2 + a_{22} - 2a_{12}\hat{f}_x + \frac{a_{33}}{y^2}\hat{f}_\theta^2 - \frac{2a_{23}}{y}\hat{f}_\theta + \frac{2a_{13}}{y}\hat{f}_\theta\hat{f}_x\right) = 0$$

which, by aid of Eq. (27′), reduces to:

$$\left[a_{11}\frac{dv_x}{dx} + (-a_{11}\hat{f}_x + 2a_{12})\frac{dv_y}{dx} + 2\frac{a_{13}}{y}\frac{d(yv_\theta)}{dx}\right]_{\sigma_1} + \left[\frac{a_{33}}{y^2}\frac{d(yv_\theta)}{d\theta} + \left(-\frac{a_{33}}{y^2}\hat{f}_\theta + 2\frac{a_{23}}{y} - 2\frac{a_{13}}{y}\hat{f}_x\right)\frac{dv_y}{d\theta}\right]_{\sigma_2} + \frac{v_y}{y} = 0 \quad (30)$$

This is the relationship that correlates the changes in velocity which take place when proceeding along the two line-elements that are the intersections of a given characteristic surface with the two coordinate planes (θ = const., x = const.) passing through the same given point. Thus, Eq. (30) is the relation that corresponds to the one in two-dimensional motion that states the change in velocity along a characteristic element and is equivalent to that case in all respects with the mere substitution of the system of two orthogonal elements, shown in Fig. 5, for the single linear element with which one is concerned in the two-dimensional case. The element contained in the plane x = const. corresponds to the term indicated in Eq. (30) by means of the symbol $[]_{\sigma_1}$, which represents therein the influence upon the fluid motion of the fact that the flow is three-dimensional. When this relation is applied to the determination of the potential field, it is readily seen that this element does not introduce any greater complication than in the case of two-dimensional flow, at least from the standpoint of the concepts involved, because this element is upstream (with respect to the direction of motion) of the associated element belonging to the other orthogonal plane and therefore the conditions of flow on it are known independently of the conditions existing on the associated element.

If, now, Eqs. (28′) are substituted into Eq. (24), then by taking into account Eqs. (28), it follows that

$$\left[a_{11}\frac{dv_x}{dx} + \frac{dv_y}{dx}\left(2a_{12} - a_{11}\hat{f}_x - \frac{2a_{13}}{y}\hat{f}_\theta\right)\right]_{\sigma_1} + \left[\frac{2a_{13}}{y}\frac{dv_x}{d\theta} + \left(\frac{2a_{23}}{y} - \frac{a_{33}}{y^2}\hat{f}_\theta\right)\frac{dv_y}{d\theta} + \frac{a_{33}}{y^2}\frac{d(yv_\theta)}{d\theta}\right]_{\sigma_2} + \frac{v_y}{y} = 0 \quad (30')$$

So that from comparison of Eqs. (30′) and (30) it results that the following must be true:

$$\left[-\frac{dv_y}{dx}\hat{f}_\theta - \frac{d(yv_\theta)}{dx}\right]_{\sigma_1} + \left[\frac{dv_x}{d\theta} + \frac{dv_y}{d\theta}\hat{f}_x\right]_{\sigma_2} = 0 \quad (31)$$

This constitutes another relation between the velocity changes under consideration which take place along the two associated elements belonging to the two orthogonal planes, and it is substantially a necessary consequence of the irrotationality of the motion.

(*B-0-2*) *Fundamental Equations of the Characteristic Lines.*—Relations analogous to those of Eqs. (30) and (31) hold for the changes of velocity which occur along the elements $d\sigma_1'$ and $d\sigma_2'$, which are the intersections of a characteristic surface of the other set (Σ') with the planes θ = const. and x = const. In view of this, we now let $\hat{f}_\theta = \mu$ at an arbitrary general point and denote by λ_1 and λ_2 the two values of $\hat{f}_x$ which are obtained from Eq. (27′) when $\hat{f}_\theta = \mu$ is used therein (they are necessarily real if μ is sufficiently small, and this certainly happens in the case under consideration). Then the following fundamental equations hold for the characteristic lines (which is the name given to the intersections of the characteristic surfaces of the two sets with the planes θ = const. and x = const.):

(A) For the characteristic lines σ_1 and σ_2 belonging to the set of surfaces Σ:

$$\left.\begin{gathered}\hat{f}_\theta = \mu;\ \hat{f}_x = \lambda_1 \\ \left[a_{11}\left(\frac{dv_x}{dx} + \lambda_2\frac{dv_y}{dx}\right)\right]_{\sigma_1} + \left[2\frac{a_{13}}{y}\frac{dv_x}{d\theta} + \left(\frac{2a_{23}}{y} - a_{33}\frac{\mu}{y^2}\right)\frac{dv_y}{d\theta} + \frac{a_{33}}{y^2}\frac{d(yv_\theta)}{d\theta}\right]_{\sigma_2} + \frac{v_y}{y} = 0 \\ \left[-\frac{dv_y}{dx}\mu - \frac{d(yv_\theta)}{dx}\right]_{\sigma_1} + \left[\frac{dv_x}{d\theta} + \lambda_1\frac{dv_y}{d\theta}\right]_{\sigma_2} = 0\end{gathered}\right\} \quad (32)$$

where the third of these expressions is obtained from Eq. (30′) through utilization of the relation between the roots λ_1 and λ_2 of Eq. (27′). Now denote by τ_2 the tangent to σ_1' at the point P, which is considered to be in the neighborhood of the line-elements $d\sigma_1$ and $d\sigma_1'$ of the two characteristic lines lying in the plane θ = const.; then $\lambda_2 = \sin(\tau_2, x)/\cos(\tau_2, x)$. And upon letting

$$dv_\xi = dv_x\cos(\tau_2, x) + dv_y\sin(\tau_2, x)$$

further reflection shows that the third of Eqs. (32) yields:

$$\left[2\frac{a_{13}}{y}\frac{dv_x}{d\theta}+\left(2\frac{a_{23}}{y}-a_{33}\frac{\mu}{y^2}\right)\frac{dv_y}{d\theta}+\frac{a_{33}}{y^2}\frac{d(yv_\theta)}{d\theta}\right]_{\sigma_2}\cos(\tau_2,x)+\left(a_{11}\frac{dv_\xi}{dx}\right)_{\sigma_1}+\frac{v_y}{y}[\cos(\tau_2,x)]=0 \tag{32'}$$

It is easy to see that $(dv_\xi/dx)_{\sigma_1}$ defines the variation, along the element $d\sigma_1$, of the component of velocity that is parallel to the other element $d\sigma_1'$ passing through the same point P. Written in the form of Eq. (32'), this relation gives an even more precise appearance to the analogy between it and the relationship that holds for the case of two-dimensional flow, in which one has simply: $(dy_\xi/dx)_{\sigma_1}=0$.

(B) For the characteristic lines σ_1' and σ_2' belonging to the set of surfaces Σ':

$$\left.\begin{gathered}\dot{f}_\theta=\mu;\quad \dot{f}_x=\lambda_2\\ \left[a_{11}\left(\frac{dv_x}{dx}+\lambda_1\frac{dv_y}{dx}\right)\right]_{\sigma_1'}+\left[\frac{2a_{13}}{y}\frac{dv_x}{d\theta}+\left(\frac{2a_{23}}{y}-a_{33}\frac{\mu}{y^2}\right)\frac{dv_y}{d\theta}+\frac{a_{33}}{y^2}\frac{d(yv_\theta)}{d\theta}\right]_{\sigma_2'}+\frac{v_y}{y}=0\\ \left[-\frac{dv_y}{dx}\mu-\frac{d(yv_\theta)}{dx}\right]_{\sigma_1'}+\left[\frac{dv_x}{d\theta}+\lambda_2\frac{dv_y}{d\theta}\right]_{\sigma_2'}=0\end{gathered}\right\} \tag{33}$$

Again, denoting by τ_1 the tangent to σ_1 at the point P considered above, and then letting

$$\lambda_1=\sin(\tau_1,x)/\cos(\tau_1,x)$$

and

$$dv_\eta=dv_x\cos(\tau_1,x)+dv_y\sin(\tau_1,x)$$

it follows that the third of Eqs. (33) will yield:

$$\left[\frac{2a_{13}}{y}\frac{dv_x}{d\theta}+\left(2\frac{a_{23}}{y}-a_{33}\frac{\mu}{y^2}\right)\frac{dv_y}{d\theta}+\frac{a_{33}}{y^2}\frac{d(yv_\theta)}{d\theta}\right]_{\sigma_2'}\cos(\tau_1,x)+\left(a_{11}\frac{dv_\eta}{dx}\right)_{\sigma_1'}+\frac{v_y}{y}\cos(\tau_1,x)=0 \tag{33'}$$

It is apparent that $(dv_\eta/dx)_{\sigma_1'}$ defines the variation, along the element $d\sigma_1'$ of the component of velocity that is parallel to the other element $d\sigma_1$ through P.

Assume that the two line-elements $\overline{P_1P}$ and $\overline{P_1'P}$ of the characteristic lines σ_1 and σ_1', respectively, that pass through the point P, are given and represent on the hodograph plane (v_x, v_y), corresponding to the meridian plane under consideration, the two vectors defining the velocity components at P_1 and at P_1' which lie in this same plane. Then Eqs. (32') and (33') make it possible to determine immediately the analogous velocity component at P, provided the flow conditions are known on the characteristic surfaces Σ and Σ' to which the points P_1 and P_1' belong (or at least known in the neighborhoods of the surfaces that contain P_1 and P_1'). Under these conditions it is possible to calculate the values of dv_ξ and dv_η from Eqs. (32') and (33'), with the aid of which the graphical construction indicated in Fig. 6 is derived.

This construction is an obvious extension, to the problem of three-dimensional motion under consideration, of the procedure used for two-dimensional motion and suggested by R. Sauer[5] for the case of axially symmetric flow.

(*B-1*) *Field Corresponding to the Expansion Resulting from the Change in Direction of the Meridian Line*

(*B-1-2*) *Delineation of the Characteristic Surface at Which the Expansion Begins.*—The application of Eqs. (32) and (33) to the determination of the field of flow around that portion of the body that lies between the conical nose and the wing, when the field around the nose is known, is carried out by means of a step-by-step procedure that is entirely analogous to the one that is followed for the case of two-dimensional flow or for the case of axially symmetric motion.

Let AA be the circumference of the body (for a section normal to the body axis) where it adjoins the conical nose. Then the perturbation due to the change in direction of the meridian line begins to be propagated

FIGS. 6a–6b. Graphical construction for determining the velocity at the intersection of two characteristic surfaces when the velocity is known on them nearby.

within the fluid starting from a characteristic surface passing through AA. This surface is denoted by $\Sigma^{(0)}$, and it is determined on the basis of the results of the investigation discussed in Sections (A) and (B-0). Let the equation of this surface have the form

$$y = y_A + a_0^{(0)}(\theta)(x - x_A)$$

in the neighborhood of this parallel AA (the above-mentioned circumference); then $(\mu)_{x=x_A} = (\dot{f}_\theta)_{x=x_A} = 0$ for any θ, and $\lambda_1 = (\dot{f}_x)_{x=x_A} = a_0^{(0)}(\theta)$.

Upon substitution of these values into Eq. (27′), it is possible to calculate at once the values of $a_0^{(0)} = \lambda_1$, which correspond to the various meridian planes, in consequence of their being solutions of the second degree equation $a_{11}\lambda^2 - 2a_{12}\lambda + a_{22} = 0$. The coefficients of λ in this equation are known because the velocities are known. Let β denote the angle of inclination, with respect to x, of the component of velocity lying in the meridian plane, and let δ_1 be the local Mach angle corresponding to this component (or $\sin \delta_1 = c/\sqrt{v_x^2 + v_y^2}$); then it may be stated exactly that $\lambda_1 = \tan(\beta + \delta_1)$ and $\lambda_2 = \tan(\beta - \delta_1)$. Thus, it is possible to draw the tangents to the lines σ_1 (which lie in the various meridian planes) for the point at which $x = x_A$ and $y = y_A$. These tangents determine the tangent cone at AA for the surface $\Sigma^{(0)}$ under consideration. Upon cutting this cone with the plane $x = x_A + \Delta x$, therefore, the line with equation

$$\begin{aligned} x &= x_A + \Delta x = x_{A_1} \\ y &= y_A + a_0^{(0)}\Delta x = y_{A_1} \end{aligned}$$

is obtained for a sufficiently small value of Δx. In the neighborhood of this line, let the equation of the same surface be given in the form

$$y = y_{A_1} + a_1^{(0)}(\theta)(x - x_{A_1})$$

and therefore it follows that

$$(\mu)_{x=x_{A_1}} = (\dot{f}_\theta)_{x=x_{A_1}} = \dot{a}_0^{(0)}\Delta x$$

$$\lambda_1 = (\dot{f}_x)_{x=x_{A_1}} = a_1^{(0)}(\theta)$$

Consequently, when the values of $\dot{f}_\theta$ and $\dot{f}_x$ just determined are used in conjunction with Eq. (27′), it allows the determination of $a_1^{(0)}(\theta)$ for the surface $\Sigma^{(0)}$, and in this manner the whole shock front of $\Sigma^{(0)}$ is determined step by step.

The actual meridian line of the body is then replaced by a line of jointed segments inscribed in the original contour in such a way that the change in direction at each corner of this line is small enough to be propagated by only one characteristic surface of the set Σ. Letting $\Sigma^{(1)}$ be the surface of this set which propagates the perturbation originating at AA; then the equation of $\Sigma^{(1)}$, in the neighborhood of this parallel, is in the form:

$$y = y_A + a_1^{(1)}(\theta)(x - x_A)$$

whence again, $(\mu)_{x=x_A} = (\dot{f}_\theta)_{x=x_A} = 0$, for θ, and $\lambda_1 = (\dot{f}_x)_{x=x_A} = a_1^{(1)}(\theta)$.

In an arbitrary general meridian plane, consider the change of velocity along an element $\Delta\sigma_1'$ of characteristic line (belonging to set Σ') that passes through a general point $P_0^{(0)}$ of $\sigma_1^{(0)}$, which is the intersection of the meridian plane in question with the surface $\Sigma^{(0)}$.

This variation of velocity satisfies the third and fourth of Eqs. (33). If now Δv_x, Δv_y, and $\Delta(yv_\theta)$ denote the changes in the respective quantities between $P_0^{(0)}$ and the point $P_1^{(1)}$ where the element $\Delta\sigma_1'$ intersects $\sigma_1^{(1)}$ (Fig. 7), it follows that (here, for sake of simplicity of notation, the terms in the brackets $[]_{\sigma_1'}$, given in Eq. (33), have not been repeated):

$$\left.\begin{aligned} a_{11}(\Delta v_x + \lambda_1 \Delta v_y)_{\sigma_1'} + \Delta x[]_{\sigma_1'} + \Delta x(v_y/y) &= 0 \\ \Delta(yv_\theta)_{\sigma_1'} - \Delta x[]_{\sigma_1'} &= 0 \end{aligned}\right\} \quad (34)$$

in which a_{11}, v_y/y, and the coefficients of Δx must be calculated at $P_0^{(0)}$ and for the element of the characteristic line σ_2' which is normal to the meridian plane containing $P_0^{(0)}$ and $P_1^{(1)}$.

Now if we pass to the limit, as $\Delta x \to 0$, and therefore as $P_0^{(0)}$ and $P_1^{(1)}$ are made to tend to A along their respective characteristic lines (Fig. 7), Eq. (34) reduces to

$$\left.\begin{aligned} \lim_{\Delta x = 0}\left(\frac{\Delta v_x}{\Delta v_y}\right)_{\sigma_1'} = \frac{(\Delta v_x)_{lim}}{(\Delta v_y)_{lim}} &= -\lambda_1 \\ \Delta(yv_\theta)_{\sigma_1'} &= 0 \end{aligned}\right\} \quad (34')$$

The second relation of Eqs. (34′) states that component v_θ does not undergo any discontinuity in passing from $\Sigma^{(0)}$ to $\Sigma^{(1)}$ at the corner AA. The first of Eqs. (34′) expresses the important property that, in every meridian plane, the changes in the velocity components Δv_x and Δv_y at the parallel AA follow the same laws that hold for two-dimensional motion,[1] since $\mu = 0$, and therefore λ_1 is simply determined by

$$a_{11}\lambda^2 - 2a_{12}\lambda + a_{22} = 0$$

For the purpose of calculating these changes in velocity propagated by the wave $\Sigma^{(1)}$ and corresponding to a given change in direction $\Delta\beta$, one may use the formulas for two-dimensional motion:[6]

$$\left.\begin{aligned} (\Delta v_x)_{lim} &= \Delta\beta\left(\frac{-v_x^{(0)}}{\sqrt{M_0^2 - 1}} + v_y^{(0)}\right) \\ (\Delta v_y)_{lim} &= \Delta\beta\left(v_x^{(0)} - \frac{v_y^{(0)}}{\sqrt{M_0^2 - 1}}\right) \end{aligned}\right\} \quad (35)$$

where $v_x^{(0)}$ and $v_y^{(0)}$ are the velocity components at A on $\Sigma^{(0)}$ and M_0 is the local Mach Number at the same points, relative to the velocity component in the meridian plane only

$$\left\{M_0 = \sqrt{\frac{[v_x^{(0)}]^2 + [v_y^{(0)}]^2}{c^2}}\right\}$$

The first of Eqs. (34′), on the other hand, permits the

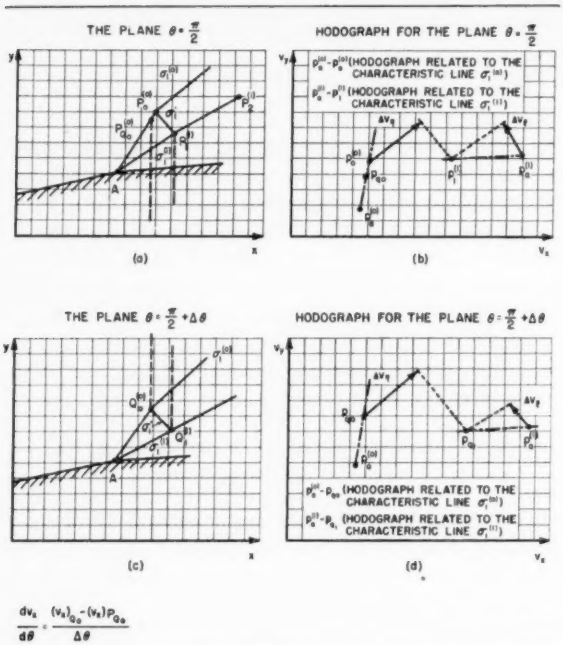
THE PLANE $\theta = \frac{\pi}{2}$
HODOGRAPH FOR THE PLANE $\theta = \frac{\pi}{2}$
(HODOGRAPH RELATED TO THE CHARACTERISTIC LINE $\sigma_1^{(0)}$)
(HODOGRAPH RELATED TO THE CHARACTERISTIC LINE $\sigma_1^{(1)}$)
(a)
(b)
THE PLANE $\theta = \frac{\pi}{2} + \Delta\theta$
HODOGRAPH FOR THE PLANE $\theta = \frac{\pi}{2} + \Delta\theta$
(HODOGRAPH RELATED TO THE CHARACTERISTIC LINE $\sigma_1^{(0)}$)
(HODOGRAPH RELATED TO THE CHARACTERISTIC LINE $\sigma_1^{(1)}$)
(c)
(d)
$\frac{dv_x}{d\theta} = \frac{(v_x)_{Q_0} - (v_x)_{P_{Q_0}}}{\Delta\theta}$

FIGS. 7a–7d. Extension of the hodograph from meridian plane to meridian plane for the expansion occurring at the base of the nose cone.

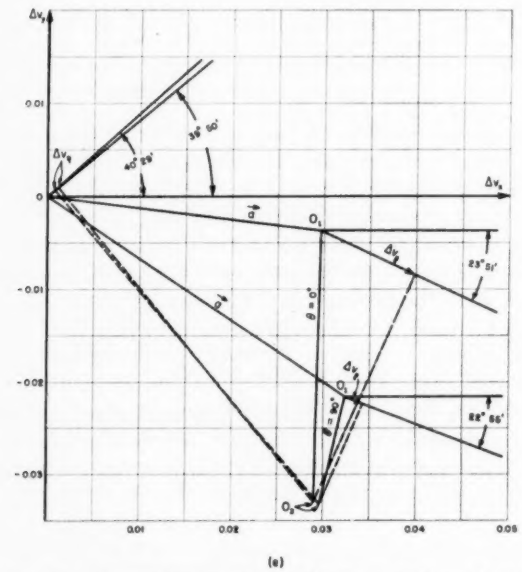

FIG. 7e. Determination of the velocity at $P_1^{(1)}$ and $Q_1^{(1)}$ by use of computed components of the increments that are directed along the characteristic lines σ_1' and $\sigma_1^{(1)}$.

calculation of λ_1, and therefore the determination of the tangents to the characteristic lines $\sigma_1^{(1)}$ in the various meridian planes.

(*B-1-2*) *Determination of the Characteristic Surface Marking the End of the First Expansion, As Well As Description of the Velocities Obtained As a Result of the Expansion.*—Now consider any point $P_1^{(1)}$ on the characteristic line $\sigma_1^{(1)}$ just determined, for the plane $\theta = \pi/2$; it also lies on a characteristic line σ_1', which passes through $P_0^{(0)}$ in the same plane, and it is close enough to A (Fig. 7) so that the arc $P_0^{(0)}P_1^{(1)}$ of σ_1' is indistinguishable from its tangent (which is known) at $P_0^{(0)}$. This is the situation considered in Section (B-0-2), and the velocity at $P_1^{(1)}$ can be obtained through application of the graphical construction that was described there (Fig. 7b). In consequence of the above, it is possible to find the tangent to $\sigma_1^{(1)}$ at $P_1^{(1)}$ by aid of Eq. (27′), with $\dot{f}_\theta = 0$ therein, and it may now be drawn in.

Then consider, in the meridian plane $\theta = (\pi/2) + \Delta\theta$, the intersection, $Q_1^{(1)}$, of the tangent to $\sigma_1^{(1)}$ at A (already drawn in, following what was explained above) with the plane $x = \text{const.} = x_{P_1}{}^{(1)}$, to which the point $P_1^{(1)}$ belongs (Fig. 7c), and let $Q_0^{(0)}$ be the point of the line $\sigma_1^{(0)}$, which belongs to the same characteristic line σ_1' that passes through $Q_1^{(1)}$. In turn, the Eqs. (32′) and (33′) make it possible to determine the velocity component at $Q_1^{(1)}$, lying in the plane $\theta = (\pi/2) + \Delta\theta$, while the fourth of Eqs. (32) [or the fourth of Eqs. (33)] allows the calculation of the difference between the values of (yv_θ) at the points $Q_1^{(1)}$ and A [or at the points $Q_1^{(1)}$ and $Q_0^{(0)}$] and therefore the determination of the value of the same component v_θ at $Q_1^{(1)}$ (see Fig. 7d; in the same Figs., 7a, 7b, and 7c, it is shown how the values of $(dv_x/d\theta)_{\sigma_2'}$, etc., corresponding to the linear elements of the characteristic σ_2', are obtained).

Writing the equation of $\Sigma^{(1)}$ in the form

$$y = y_A + [x_{P1}{}^{(1)} - x_A]a_1{}^{(1)}(\theta) + [x - x_{P1}{}^{(1)}]a_2{}^{(1)}(\theta)$$

in the neighborhood of the line that is the locus of points $P_1^{(1)}$, $Q_1^{(1)}$, etc., it follows that

$$(\mu)_x = x_{P_1}{}^{(1)} = (\dot{f}_\theta)_{x = xP_1}{}^{(1)} = (x_{P_1}{}^{(1)} - x_A)\dot{a}_1{}^{(1)}$$

which is known as a result of the preceding discussion. Then, knowing the velocity components at $Q_1^{(1)}$, it is possible to calculate the value of $\lambda_1 = a_2{}^{(1)}[(\pi/2) + \Delta\theta]$ at $Q_1^{(1)}$ by means of Eq. (27′), and thus it is possible to draw in the tangent to the characteristic line $\sigma_1^{(1)}$ at the same point $Q_1^{(1)}$.

Having calculated the velocity at the points $P_1^{(1)}$, $Q_1^{(1)}$, etc., and having determined the tangents to $\sigma_1^{(1)}$ at these points in all the meridian planes, one is again in a position to calculate the velocity at another $P_2^{(1)}$. In this manner, the repeated application of the procedure just explained makes it possible to obtain the whole $\Sigma^{(1)}$ and [through depiction in the hodographs related to the various $\sigma_1^{(1)}$] the velocity at all its points.

The following is a practical application of the method outlined above.

Table 1 lists the values of v_x, v_y, v_θ, $dv_x/d\theta$, $dv_y/d\theta$, and $dv_\theta/d\theta$ at such points as $P_0^{(0)}$, $Q_0^{(0)}$, etc., belonging to the various meridian semiplanes. Table 2 presents the same information for the points A belonging to $\sigma_1^{(1)}$ for the various meridian semiplanes.

TABLE 1

Values of the Velocity Components and Their Derivatives at Such Points as $P_0^{(0)}$, $Q_0^{(0)}$, etc., Belonging to the Various Meridian Semiplanes

θ	v_x	v_y	v_θ	$\frac{dv_x}{d\theta}$	$\frac{dv_y}{d\theta}$	$\frac{dv_\theta}{d\theta}$
90°	0.6385	0.09593	0	0	0	−0.04799
70°	0.6380	0.09480	0.01679	0.00252	0.00685	−0.04503
50°	0.6367	0.09154	0.03154	0.00470	0.01243	−0.03660
30°	0.6346	0.08658	0.04254	0.00634	0.01722	−0.02407
20°	0.6334	0.08360	0.04621	0.00696	0.01922	−0.01657
10°	0.6321	0.08034	0.04852	0.00709	0.02071	−0.00844
0°	0.6309	0.07692	0.04938	0.00701	0.02116	−0.00016

TABLE 2

Values of the Velocity Components and Their Derivatives at the Points A Belonging to $\sigma_1^{(1)}$ for the Various Meridian Semiplane

θ	v_x	v_y	v_θ	$\frac{dv_x}{d\theta}$	$\frac{dv_y}{d\theta}$	$\frac{dv_\theta}{d\theta}$
90°	0.6710	0.07447	0	0	0	−0.06266
70°	0.6703	0.07440	0.02143	0.00351	0.00039	−0.05888
50°	0.6685	0.07420	0.04028	0.00659	0.00073	−0.04800
30°	0.6657	0.07389	0.05426	0.00896	0.00102	−0.03133
20°	0.6641	0.07370	0.05888	0.00980	0.00112	−0.02143
10°	0.6623	0.07350	0.06171	0.01017	0.00113	−0.01088
0°	0.6605	0.07331	0.06266	0.01011	0.00112	0

On the semiplane $\theta = 90°$, the following values may be calculated at $P_0^{(0)}$:

$$a_{11} = -2.496; \quad a_{33} = 1.000; \quad \Delta x/y = 0.06699$$

assuming for y the average values between the ordinates of the points $P_0^{(0)}$ and $P_1^{(1)}$; $\cos(\tau_1, x) = 0.7607$; thus the equation that determines Δv_η is

$$(-0.04799)\,(0.06699)(0.7607) + (-2.496)\Delta v_\eta + (0.09593)(0.06699)\,(0.7607) = 0$$

whence $\Delta v_\eta = +0.00098$.

At the point A of the same semiplane belonging to $\sigma_1^{(1)}$, the following values may be obtained:

$$a_{11} = -3.136; \quad a_{33} = 1.000; \quad \Delta x/y = 0.5756$$

[along the segment $AP_1^{(1)}$ taking the average of the ordinates at A and $P_1^{(1)}$]; $\cos(\tau_2, x) = 0.9210$; thus the equation determining Δv_ξ becomes

$$-3.136\,\Delta v_\xi + (-0.06266)(0.5756)(0.9210) + (0.07447)\,(0.5756)(0.9210) = 0$$

whence, $\Delta v_\xi = +0.00200$.

Indicating the components of velocity at A with the subscript "1" and those at $P_0^{(0)}$ by the subscript "2", consider the vector $\vec{a}$ whose components in the meridian plane are $v_{1x} - v_{2x} = 0.6710 - 0.6385 = 0.03249$; $v_{1y} - v_{2y} = 0.07447 - 0.09593 = -0.02146$, respectively. This vector is represented in Fig. 7e by the directed segment $\overrightarrow{OO_1}$. Add to the vector $\vec{a}$ a vector of the same magnitude as Δv_ξ and parallel to the characteristic line σ_1' (through A) and draw through the end point of the vector sum the normal to the vector drawn parallel to σ_1'. Analogously, draw through the origin O of $\vec{a}$ a vector equal to Δv_η and parallel to the characteristic $\sigma_1^{(0)}$ through $P^{(0)}$. From the end point of this vector draw a line perpendicular to it [and therefore perpendicular to $\sigma_1^{(0)}$]. These two perpendicular lines intersect at a point O_2. The vector O_1O_2 is the change of velocity in passing from A (of $\sigma_1^{(1)}$) to $P_1^{(1)}$. From Fig. 7e it is seen that this velocity change has the components $\Delta v_x = -0.00282$ and $\Delta v_y = -0.01181$; thus the velocity components at $P_1^{(1)}$ are $v_x = 0.6710 - 0.0028 = 0.6682$ and $v_y = 0.07447 - 0.01181 = 0.06266$. The same procedure can be employed for $\theta = 0°$. At the point $Q_0^{(0)}$ in this plane, the following values may be obtained:

$$a_{11} = -2.352; \quad a_{13} = -0.2624; \quad a_{23} = -0.03199$$

$$a_{33} = 0.9795; \quad \frac{\mu}{y} = -0.01338; \quad \cos(\tau_1, x) = 0.7678$$

$$\frac{\Delta x}{y} = 0.06214; \quad \text{the term } []_{\sigma_1'} = -0.00551$$

so that $\Delta v_\eta = 0.00145$; at A:

$$a_{11} = -2.907; \quad a_{13} = -0.3706; \quad a_{23} = -0.041135$$

$$a_{33} = 0.9648; \quad \frac{\mu}{y} = 0; \quad \frac{1}{\lambda}\frac{dy}{d\theta} = -0.00105$$

$$\frac{\Delta x}{y} = 0.5490; \quad \cos(\tau_2, x) = 0.9146$$

whence $\Delta v_\xi = 0.01128$.

Repeating the graphical construction indicated above as shown in Fig. 7e, the following values are obtained:

$$\Delta v_x = -0.00051; \quad \Delta v_y = -0.02906$$

thus at $Q_1^{(1)}$ (for $\theta = 0°$),

$$v_x = 0.6605 - 0.00051 = 0.6600$$
$$v_y = 0.07331 - 0.02906 = 0.04425$$

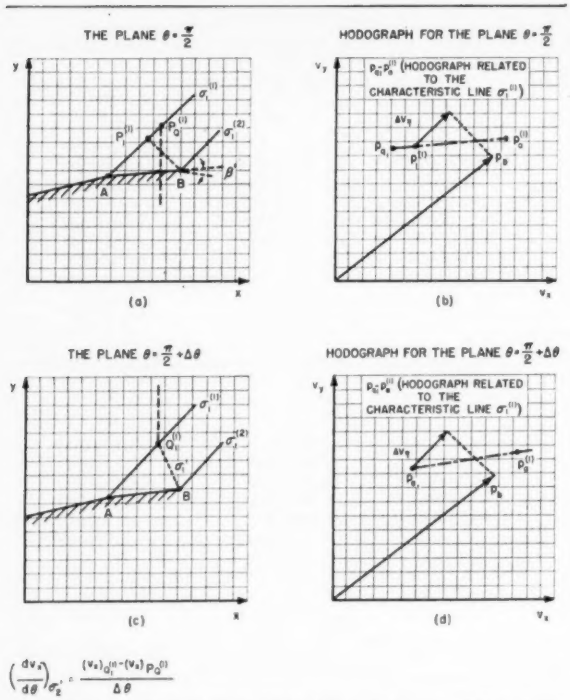
THE PLANE $\theta = \frac{\pi}{2}$
HODOGRAPH FOR THE PLANE $\theta = \frac{\pi}{2}$
$P_0^{(1)}P_0^{(2)}$ (HODOGRAPH RELATED TO THE CHARACTERISTIC LINE $\sigma_1^{(1)}$)
(a)
(b)
THE PLANE $\theta = \frac{\pi}{2} + \Delta\theta$
HODOGRAPH FOR THE PLANE $\theta = \frac{\pi}{2} + \Delta\theta$
$Q_0^{(1)}Q_0^{(2)}$ (HODOGRAPH RELATED TO THE CHARACTERISTIC LINE $\sigma_1^{(1)}$)
(c)
(d)
$\left(\frac{dv_x}{d\theta}\right)_{\sigma_2'} = \frac{(v_x)_{Q_1^{(1)}} - (v_x)_{P_0^{(1)}}}{\Delta\theta}$

FIGS. 8a–8d. Extension of the hodograph from meridian plane to meridian plane for the development along the straight-line portion of the first frustum.

In order to calculate v_θ at the point under consideration the fourth of Eqs. (33) may be used. This can be written in the form

$$\Delta v_\theta = \frac{\Delta x}{y}\left[\frac{dv_x}{d\theta} + \lambda_2\left(\frac{dv_y}{d\theta} - v_\theta\right)\right] - \Delta v_y \frac{\mu}{y}$$

dy/dx along σ_1' being equal to λ_2 and Δv_θ being the difference between v_θ at $Q_1^{(1)}$ and $Q_0^{(0)}$.

From the above values

$$\Delta v_\theta = 0.06214\,[0.00701 - 0.4830\,(0.02116 - 0.04938)] - (0.04425 - 0.07692)(-0.01338) = 0.00085$$

that is,

$$v_\theta = 0.04938 + 0.00085 = 0.05023$$

(B-2) *Field Corresponding to the Development Along the Straight-Line Portions of the Meridian Line*

Let BB be the parallel of the body that contains the vertices B of the line of jointed segments which is inscribed in the meridian line and which is assumed to be close enough to parallel AA that the portion of characteristic line σ_1' contained between B and $\Sigma^{(1)}$ can be replaced by its tangent, at the point of intersection of σ_1' with $\Sigma^{(1)}$ in every meridian plane. In the meridian plane $\theta = \pi/2$, if $P_1^{(1)}$ is this point of intersection, the changes in velocity along $P_1^{(1)}B$ satisfy Eq. (33′). Therefore, since the velocities on $\Sigma^{(1)}$ are known in consequence of what was found in Sections (B-1-1) and (B-1-2), this equation affords at once the means of calculating the component Δv_η [in the direction of $\sigma_1^{(1)}$ through $P_1^{(1)}$] of the vector difference between the velocities at B and at $P_1^{(1)}$.

On the other hand, the velocity at B has the imposed direction AB, and therefore the construction shown in Fig. 8 is evolved for the calculation of the velocity at B in the hodograph which is related to the plane $\theta = \pi/2$. Thus the tangent to $\sigma_1^{(2)}$ through B can also be traced in at once by use of Eq. (27′), because $\dot{f}_\theta = 0$ for $\theta = \pi/2$ and because the velocity components at B are now known.

In the meridian plane $\theta = (\pi/2) + \Delta\theta$, for the sake of simplicity of notation, again let $Q_1^{(1)}$ be the point where the line σ_1' (passing through the point B in the plane under consideration) intersects the plane $\Sigma^{(1)}$. Then a construction like that shown in Fig. 8b allows, in view of relation (33′), the determination of the velocity components, in the plane under consideration, at the point B. The construction is carried out in the hodograph that is related to this same plane, the velocity at $Q_1^{(1)}$ being known in consequence of the derivation presented in (B-1-2). (See Figs. 8c and 8d.)

Further, because of the irrotationality of the motion, it is necessary that

$$\frac{\Delta(yv_\theta)}{\Delta s} = \frac{\partial v_x}{\partial\theta}\cos\beta' + \frac{\partial v_y}{\partial\theta}\sin\beta' \qquad (36)$$

holds, where β' is the angle at which AB is inclined to x and where $\Delta(yv_\theta)$ is the difference between the values of (yv_θ) at B and at A and Δs is taken as the length of AB. Since, now,

$$\frac{\partial v_x}{\partial\theta} = \frac{(v_{x_B})_{\theta=(\pi/2)+\Delta\theta} - (v_{x_B})_{\theta=\pi/2}}{\Delta\theta}$$

and $\partial v_y/\partial\theta$ are known, the calculation of (yv_θ) at B, in the plane $\theta = (\pi/2) + \Delta\theta$, may be carried out by means of Eq. (36). Thus, in turn, the slope of the tangent to the $\sigma_1^{(2)}$ at B can be calculated by means of Eq. (27′), in which $(\dot{f}_\theta)_B$ must always be set equal to zero; this tangent can then be drawn in in the plane under consideration. Proceeding in a like manner from plane to plane and proceeding from point to point in the same plane, it is possible to complete the tracing of the $\Sigma^{(2)}$ which passes through the parallel BB and likewise the construction of the hodographs relative to its characteristic lines in the planes $\theta = \text{const.}$

The practical application of the method outlined above is made in a manner analogous to that indicated in Section (B-1-2); therefore, this application will not be repeated either in this section or in the following ones.

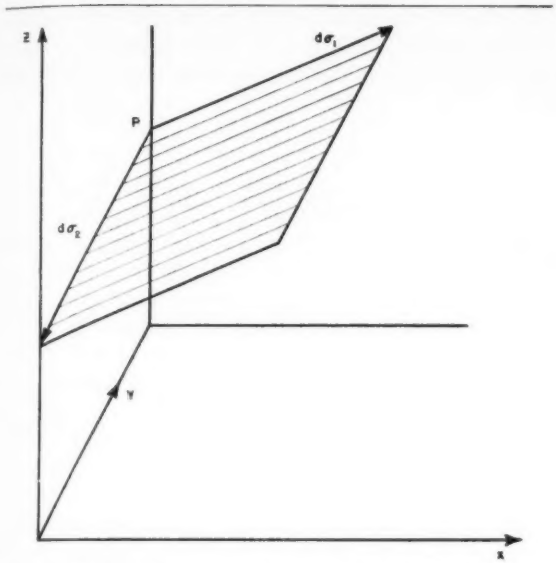

FIG. 9. Representative trace of a characteristic surface in planes which are normal to the Y-axis and the x-axis.

(C) DETERMINATION OF THE FIELD FOR THE REGION OF FLOW IN WHICH THE WING IS SITUATED

(C-0) *General Equations*

(C-0-0) Potential Motion in Cartesian Coordinates and the Corresponding Equation of the Characteristic Surfaces.—Let the potential in this region be $\Phi_3 V_1$. For the determination of the motion in the neighborhood of the wing it is convenient to make use of the Cartesian coordinates (x, Y, Z) and to take the plane of the wing as belonging to the coordinate plane (x, Y). For a study of the motion in proximity to the body, however, it is still convenient to use the cylindrical coordinates (x, y, θ).

By use of the Cartesian coordinates (x, Y, Z), the differential equation that defines Φ_3 is:

$$A_{11}\frac{\partial^2\Phi_3}{\partial x^2} + 2A_{12}\frac{\partial^2\Phi_3}{\partial x\,\partial Y} + A_{22}\frac{\partial^2\Phi_3}{\partial Y^2} + 2A_{13}\frac{\partial^2\Phi_3}{\partial x\,\partial Z} + 2A_{23}\frac{\partial^2\Phi_3}{\partial Y\,\partial Z} + A_{33}\frac{\partial^2\Phi_3}{\partial Z^2} = 0 \quad (37)$$

wherein

$$A_{11} = 1 - v_x^2/c^2 = a_{11}; \quad A_{12} = -v_xv_Y/c^2$$
$$A_{13} = -v_xv_Z/c^2; \quad A_{23} = -v_Yv_Z/c^2$$
$$A_{22} = 1 - (v_Y^2/c^2); \quad A_{33} = 1 - (v_Z^2/c^2)$$

Analogously to what was demonstrated in (B-0), it can be shown that Eq. (37) admits two sets of real characteristic surfaces. Letting the equations of these surfaces be of the form

$$x = f(Y, Z, b) \quad (38)$$

where b is again an arbitrary constant, the functions f must satisfy the equation:

$$A_{11} - 2A_{12}\dot{f}_Y - 2A_{13}\dot{f}_Z + A_{22}\dot{f}_Y^2 + 2A_{23}\dot{f}_Y\dot{f}_Z + A_{33}\dot{f}_Z^2 = 0 \quad (39)$$

from which it follows that the characteristic surfaces may be interpreted to be the envelope of the Mach cones that propagate the elemental perturbations, as has already been observed in (B-0).

(C-0-1) Variation of the Velocities Along the Characteristic Surfaces.—For any characteristic surface of a set (still denoted as Σ), let $d\sigma_1$ and $d\sigma_2$ again be the linear elements of the intersections of this surface with the planes $Y =$ const. and $Z =$ const., respectively (Fig. 9). As in (B-0-1) and (B-0-2), it is found that the increments of velocity, dv_x, dv_Y, and dv_Z, taking place along these linear elements, satisfy the equations:

$$\left[A_{22}\frac{dv_Y}{dY} + (-A_{22}\dot{f}_Y + 2A_{12})\frac{dv_x}{dY} + 2A_{23}\frac{dv_Z}{dY}\right]_{\sigma_2} + \left[A_{33}\frac{dv_Z}{dZ} + (-A_{22}\dot{f}_Z + 2A_{13} - 2A_{23}\dot{f}_Y)\frac{dv_x}{dZ}\right]_{\sigma_1} = 0 \quad (40)$$

which is analogous to Eq. (30′), and

$$\left[A_{22}\frac{dv_Y}{dY} + (2A_{12} - 2A_{23}\dot{f}_Z - A_{22}\dot{f}_Y)\frac{dv_x}{dY}\right]_{\sigma_2} + \left[2A_{23}\frac{dv_Y}{dZ} + (2A_{13} - A_{33}\dot{f}_Z)\frac{dv_x}{dZ} + A_{33}\frac{dv_Z}{dZ}\right]_{\sigma_1} = 0 \quad (40')$$

which is analogous to Eq. (30).

Here, dZ is the projection of the element $d\sigma_1$ upon the x-axis and dY is the projection of $d\sigma_2$ upon the Y-axis. From comparison of Eqs. (40) and (40′), it follows that

$$\left[-\dot{f}_Z\frac{dv_x}{dY} - \frac{dv_Z}{dY}\right]_{\sigma_2} + \left[\frac{dv_Y}{dZ} + \dot{f}_Y\frac{dv_x}{dZ}\right]_{\sigma_1} = 0 \quad (41)$$

which is analogous to Eq. (31).

(C-0-2) Fundamental Equations for the Characteristic Lines.—Relations that are analogous to those of Eqs. (40), (40′), and (41) exist for the changes in velocity along the elements $d\sigma_1'$ and $d\sigma_2'$, which are the intersections of the planes $Y =$ const. and $Z =$ const. with the characteristic surfaces of the other set (Σ').

Let $\dot{f}_Y = \mu$, and let λ_1 and λ_2 denote the two roots of Eq. (39) when $\dot{f}_Y$ is set equal to μ in it (these roots are necessarily real if μ is small enough, as certainly happens in the problem under consideration); then the following equations hold for the characteristic lines σ_1 and σ_2, which are the intersections of the characteristic surface of the set Σ with the planes Y = const. and Z = const.:

$$\left.\begin{gathered} \dot{f}_Y = \mu;\ \dot{f}_Z = \lambda_1 \\ \left[A_{33}\left(\frac{dv_Z}{dZ} + \lambda_2 \frac{dv_x}{dZ}\right)\right]_{\sigma_1} + \left[A_{22}\frac{dv_Y}{dY} + (-A_{22}\mu + 2A_{12})\frac{dv_x}{dY} + 2A_{23}\frac{dv_Z}{dY}\right]_{\sigma_2} = 0 \\ \left[-\lambda_1 \frac{dv_x}{dY} - \frac{dv_Z}{dY}\right]_{\sigma_2} + \left[\frac{dv_Y}{dZ} + \mu \frac{dv_x}{dZ}\right]_{\sigma_1} = 0 \end{gathered}\right\} \tag{42}$$

For the characteristic lines σ_1' and σ_2' belonging to the set of surfaces Σ', one has, analogously, that

$$\left.\begin{gathered} \dot{f}_Y = \mu;\ \dot{f}_Z = \lambda_2 \\ \left[A_{33}\left(\frac{dv_Z}{dZ} + \lambda_1 \frac{dv_x}{dZ}\right)\right]_{\sigma_1'} + \left[A_{22}\frac{dv_Y}{dY} + (-A_{22}\mu + 2A_{12})\frac{dv_x}{dY} + 2A_{23}\frac{dv_Z}{dY}\right]_{\sigma_2'} = 0 \\ \left[-\lambda_2 \frac{dv_x}{dY} - \frac{dv_Z}{dY}\right]_{\sigma_2'} + \left[\frac{dv_Y}{dZ} + \mu \frac{dv_x}{dZ}\right]_{\sigma_1'} = 0 \end{gathered}\right\} \tag{43}$$

Denote by τ_2 the tangent to the σ_1' at an arbitrary general point P on it, and let

$$dv_\xi = dv_x \cos(\tau_2, x) + dv_Z \sin(\tau_2, x)$$

then since $\lambda_2 = \cos(\tau_2, x)/\sin(\tau_2, x)$, the third relation of Eqs. (42) produces

$$[A_{33}(dv_\xi/dZ)]_{\sigma_1} + [\,]_{\sigma_2} \sin(\tau_2, x) = 0 \qquad (42')$$

and, as in Section (B-0-2), it is evident that $(dv_\xi/dZ)_{\sigma_1}$ defines the change along the linear element $d\sigma_1$ of the velocity component parallel to the other element $d\sigma_1'$, which passes through the same point P.

Likewise, denote by τ_1 the tangent to the σ_1 at P, and let

$$dv_\eta = dv_x \cos(\tau_1, x) + dv_Z \sin(\tau_1, x)$$

then, since

$$\lambda_1 = \cos(\tau_1, x)/\sin(\tau_1, x)$$

the third of Eqs. (43) gives

$$[A_{33}(dv_\eta/dZ)]_{\sigma_1'} + [\,]_{\sigma_2'} \sin(\tau_1, x) = 0 \qquad (43')$$

where $(dv_\eta/dZ)_{\sigma_1'}$ defines the change along the linear element $d\sigma_1'$ of the velocity component parallel to the other element $d\sigma_1$ which passes through the same point P.

Therefore the construction described in (B-0-2) is again valid for the determination of the velocity component at P and which lies in the plane Y = const., provided the two segments P_1P and $P_1'P$ of the characteristic lines σ_1 and σ_2', passing through P, are given and provided further that the conditions of flow in the neighborhood of the points P_1 and P_1' on the characteristic surfaces Σ and Σ', to which they belong, are known.

It must also be noted that, if there were no interference effect of the body upon the wing, then the term within the empty bracket in Eqs. (42′) and (43′) would be zero, and these Eqs. (42′) and (43′) would reduce to the relations $dv_\xi/dZ = 0$ and $dv_\eta/dZ = 0$, which are the equations of two-dimensional flow. The construction just described would then reduce to the well-known construction based on the reciprocal relationship between the bounding net of the Mach lines in the plane of motion and the limiting (principal) net of the analogous characteristic lines in the hodograph plane.[7] These same terms, which go into the empty brackets, therefore describe the effect of interference on the local changes of velocity at the various points of the velocity field.

(*C-1*) *Description of the Field Existing on the Top Surface of the Wing*

(*C-1-1*) *Expansion Field Around the Leading Edge.*— The application of the formulas (42), (43), (42′), and (43′) to the determination of the field of flow on the upper surface of the wing is performed by means of a procedure that is analogous to the one expounded in Section (B). The wing is taken to be a flat plate that lies in the plane $Z = 0$. Without loss of generality in application of the procedure, it is permissible to assume that the fluid stream suffers an expansion on the upper surface of the wing; indeed, it will become clear as a result of the considerations to follow what the procedure should be in case a compression rather than an expansion occurs, or in case the wing, instead of being in the form of a flat plate, has any contour whatsoever (provided that it is compatible with a stream that is everywhere supersonic).

Also, for the sake of simplicity in explanation of the procedure and in the related formulas, it is herewith assumed that the body is cylindrical, at least over that portion of the body which is affected by the wing; it is assumed that the radius of this cylinder is R, and the plane $Y = R$ can be regarded as the plane of symmetry

as far as the study of the flow over the wing is concerned. This hypothesis makes it possible to determine the flow on the wing and body separately, for each of which it is convenient to apply a different reference system, and yet it is not likely to alter the results of the investigation in any appreciable way.

(*C-1-1-1*) *Delimitation of the characteristic surface at which the expansion begins:* The perturbation produced by the wing is propagated into the stream flowing over the upper surface beginning with the characteristic surface arising at the leading edge of the said wing. This surface is still indicated here as $\Sigma^{(0)}$, since there is no danger of ambiguity; it is possible to obtain its description at once, in view of the investigation presented in (B).

If the equation of $\Sigma^{(0)}$ is written in the form

$$x = ZA_0^{(0)}(Y) \tag{44}$$

for the neighborhood in proximity to the leading edge, then it follows that

$$(\dot{f}_Z)_{Z=0} = A_0^{(0)}(Y) = \lambda_1; \quad (\dot{f}_Y)_{Z=0} = 0$$

and if these relationships are substituted into Eq. (39) there is obtained:

$$A_{11} - 2A_{13}\lambda + A_{33}\lambda^2 = 0$$

Thus it is possible to arrive at the value of λ_1 through the utilization in A_{ik} of the known values of the velocity components on the edge of the wing and upstream of the surfaces $\Sigma^{(0)}$.

It is deduced that $\lambda_1 = \cot(\beta + \delta_1)$, where β now denotes the angle of inclination, with respect to the x-axis, of the component of velocity in the plane $Y =$ const. and δ_1 stands for the local Mach angle corresponding to this component

$$(\sin \delta_1 = c/\sqrt{v_x^2 + v_Z^2})$$

In the various planes $Y =$ const., it is thus possible to draw in the tangents to the lines $\sigma_1^{(0)}$, which are the intersections of the surface $\Sigma^{(0)}$ with these planes and which constitute a ruled surface that is tangent to the characteristic surface $\Sigma^{(0)}$ at the edge of the wing. Then pass the plane $Z = A_0$ through this ruled surface, and the line with equation

$$\begin{cases} x = \Delta_0 A_0^{(0)}(Y) = x_1 \\ Z = \Delta_0 \end{cases}$$

is produced.

Let the equation of $\Sigma^{(0)}$ in the neighborhood of this line be expressed in the form

$$x = x_1 + (Z - \Delta_0)A_1^{(0)}(Y) \tag{45}$$

then it follows that

$$(\dot{f}_Z)_{Z=\Delta_0} = A_1^{(0)}(Y) = \lambda_1$$
$$(\dot{f}_Y)_{Z=\Delta_0} = \Delta_0 \dot{A}_0^{(0)}(Y)$$

When the values of $\dot{f}_Z$ and $\dot{f}_Y$ just determined are substituted into Eq. (39), it affords the means of getting $\lambda_1 = A_1^{(0)}(Y)$ and therefore of continuing the tracing of the $\sigma_1^{(0)}$ in the planes $Y =$ const. Thus the entire surface $\Sigma^{(0)}$ is determined by proceeding step by step.

(*C-1-1-2*) *Determination of the characteristic surface constituting the boundary between the first and second of the n expansions used to align the flow with the wing surface at the leading edge:* The total change of direction, $\beta(Y)$, that the streamlines must undergo at the leading edge, in every plane $Y =$ const., in order to align themselves with the plane of the wing, is assumed to be propagated through means of n characteristic surfaces of the set Σ, in such a way that each one of these surfaces propagates the change $\Delta\beta(Y) = \beta(Y)/n$.

The equation of $\Sigma^{(1)}$ in the vicinity of $x = 0$ and $Z = 0$ may be written in the form $x = ZA_1^{(1)}(Y)$, with the consequence that

$$(\dot{f}_Z)_{Z=0} = \lambda_1 = A_1^{(1)}(Y)$$
$$(\dot{f}_Y)_{Z=0} = \mu = 0$$

In the arbitrary general plane $Y =$ const., the velocity changes, along an element $\Delta\sigma_1'$ of the characteristic line (belonging to the set Σ') passing through an arbitrary general point $P_0^{(0)}$ of $\sigma_1^{(0)}$ just obtained above, satisfy the third and fourth relations of Eqs. (43). Consequently, if Δv_x, Δv_Y, and Δv_Z denote the changes in the components of velocity between $P_0^{(0)}$ and $P_0^{(1)}$,

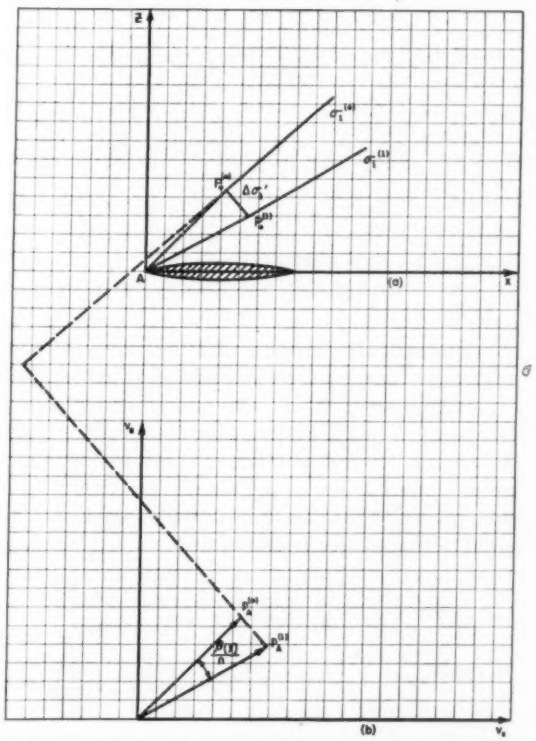

FIG. 10. Relation between hodograph and characteristic surfaces for velocity changes through shock at wing leading edge.

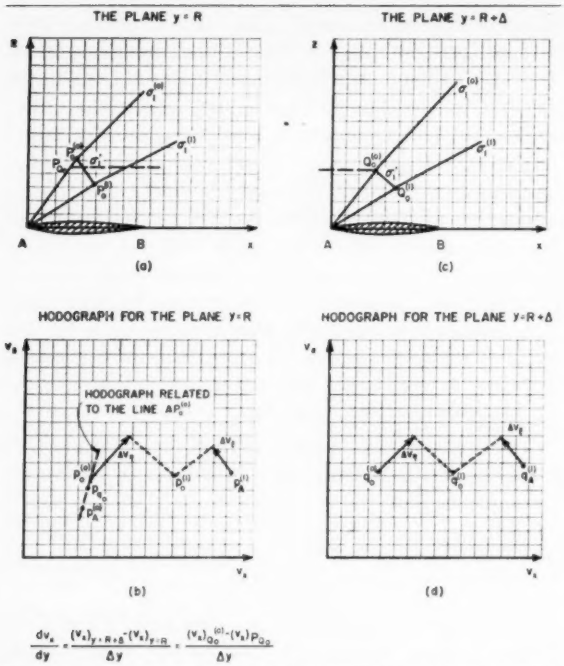

$$\frac{dv_x}{dy} = \frac{(v_x)_{y=R+\Delta} - (v_x)_{y=R}}{\Delta y} = \frac{(v_x)_{Q_0^{(0)}} - (v_x)_{P_{Q_0}}}{\Delta y}$$

FIGS. 11a–11d. Extension of the hodograph out along the wing span.

then we have

$$\left.\begin{aligned} [A_{33}(\Delta v_Z + \lambda_1 \Delta v_x)]_{\sigma_1'} + \Delta Z[\ ]_{\sigma_1'} = 0 \\ [\Delta v_Y]_{\sigma_1'} - \Delta Z[\ ]_{\sigma_1'} = 0 \end{aligned}\right\} \qquad (46)$$

Of course $P_0^{(1)}$ is the intersection of the straight-line element $\Delta\sigma_1'$ with the line $\sigma_1^{(1)}$ (Fig. 10).

Now, therefore, if we pass to the limit, as $\Delta Z \to 0$, and thus for $P_0^{(0)}$ and $P_0^{(1)}$ approaching the leading edge of the wing along their respective characteristic lines, Eqs. (46) reduce to

$$\left.\begin{aligned} \lim_{\Delta Z = 0} \left(\frac{\Delta v_Z}{\Delta v_x}\right)_{\Delta Z = 0} = \frac{(\Delta v_Z)_{lim}}{(\Delta v_x)_{lim}} = -\lambda_1 \\ (\Delta v_Y)_{lim} = 0 \end{aligned}\right\} \qquad (47)$$

The interpretation of Eqs. (47) is entirely identical to that pointed out in Section (B-1-1)—namely, that the velocity component v_Y does not suffer any discontinuity across Σ at the leading edge of the wing. Meanwhile, at $x = 0$ and $Z = 0$ the changes in the components v_x and v_Z, lying in any plane $Y = \text{const.}$, follow the same laws that are valid for two-dimensional motion. Therefore there is evolved:

$$\left.\begin{aligned} (\Delta v_x)_{lim} = \frac{\beta(Y)}{n}\left(\frac{v_x^{(0)}}{\sqrt{M_0^2 - 1}} + v_Z^{(0)}\right) \\ (\Delta v_Z)_{lim} = \frac{\beta(Y)}{n}\left(-v_x^{(0)} + \frac{v_Z^{(0)}}{\sqrt{M_0^2 - 1}}\right) \end{aligned}\right\} \qquad (48)$$

where $v_x^{(0)}$ and $v_Z^{(0)}$ are now the velocity components at the leading edge of the wing and ahead of $\Sigma^{(1)}$, while M_0 is the Mach Number at the same locations and is defined as

$$M_0 = \sqrt{\{[v_x^{(0)}]^2 + [v_Z^{(0)}]^2\}/c^2}$$

The value of λ_1 may then be computed at once by means of Eq. (39) [or by Eq. (47)], and therefore the tangents to the characteristic lines $\sigma_1^{(1)}$ belonging to $\Sigma^{(1)}$ and lying in the various planes $Y = \text{const.}$ may be determined. The evaluation of $(\Delta v_x)_{lim}$ and of $(\Delta v_Z)_{lim}$ can thus be carried out graphically by interpreting Eq. (48) in the way noted in Fig. 10b. The value of λ_1 is then obtained directly from Eq. (47).

(C-1-1-3) Description of the velocities obtained after the expansion at the leading edge takes place: Now consider any point $P_0^{(1)}$ whatsoever, belonging to the characteristic line $\sigma_1^{(1)}$ just determined and lying in the plane $Y = R$ and also belonging to the characteristic line $\sigma_1^{(1)}$ passing through point $P_0^{(0)}$ of the same plane; it is considered to be close enough to the leading edge to make the arc $P_0^{(0)}P_0^{(1)}$ of the line σ_1' indistinguishable from its tangent at $P_0^{(0)}$. This is the same situation already met with in Section (B-1-2), and the velocity at $P_0^{(1)}$ can be obtained by means of the construction therein described (Figs. 11a and 11b).

Since it is legitimate to set $\dot{f}_Y = 0$ in the plane under consideration because of the assumption made at the beginning of Section (C-1-1), then knowing the velocity at $P_0^{(1)}$ makes it possible to calculate λ_1 by aid of Eq. (39), and therefore the tangent to $\sigma_1^{(1)}$ at $P_0^{(1)}$ may be drawn in.

In the plane $Y = R + \Delta$, consider the point of intersection $Q_0^{(1)}$ that is formed when the tangent to $\sigma_1^{(1)}$ at the leading edge, and already drawn in [see Section (C-1-2)], meets the plane $Z = \text{const.}$ passing through the point $P_0^{(1)}$. Let $Q_0^{(0)}$ be the point of $\sigma_1^{(0)}$ which lies on the same characteristic line σ_1' that passes through $Q_0^{(1)}$. Then the velocity components at $Q_0^{(1)}$ and in the plane $Y = R + \Delta$ may be determined by means of Eqs. (42′) and (43′). Meanwhile, the difference between the values of v_Y at the points $Q_1^{(1)}$ and at the leading edge A [or at the points $Q_0^{(1)}$ and $Q_0^{(0)}$] may be computed through use of the fourth of Eqs. (42), or the fourth of Eqs. (43); consequently, the value of v_Y at $Q_0^{(1)}$ is determined.

Let the equation of the surface $\Sigma^{(1)}$ in the neighborhood of the plane $Z = Z_{P_0^{(1)}}$ be written in the form

$$x = Z_{P_0^{(1)}} A_1^{(1)}(Y) + (Z - Z_{P_0^{(1)}}) A_2^{(1)}(Y)$$

then there exist the relationships

$$(\dot{f}_Z)_{Z = Z_{P_0^{(1)}}} = \lambda_1 = A_2^{(1)}(Y)$$

and

$$(\dot{f}_Y)_{Z = Z_{P_0^{(1)}}} = Z_{P_0^{(1)}} \dot{A}_1^{(1)}(Y)$$

Now, since $A_1^{(1)}(Y)$ is known, substitution of this value in Eq. (39) allows the calculation of λ_1 from it

without ado, and then the tangent to $\sigma_1^{(1)}$ at $Q_0^{(1)}$ may be traced in.

Thus the repeated application of this procedure produces the entire surface $\Sigma^{(1)}$ and the velocities at its various points. The determination of the $\Sigma^{(2)}$ in the plane $Y = R$ is then undertaken, but this does not require anything other than the repetition of the method just described.

(C-1-2) Determination of the Field Along the Top Surface of the Wing.—In the plane $Y = R$, let D be the point at which the characteristic line σ_1', passing through $P_0^{(n)}$ of the line $\sigma_1^{(n)}$ and also sufficiently close to the leading edge, intersects the plane of the wing (Fig. 12a). The change in velocity along the element $P_0^{(n)}D$ satisfies Eq. (43′); on the other hand, the velocity at D has a known direction, and on this account the graphical construction, shown in Fig. 12b, is evolved for determination of the velocity. It is thus possible in this way to draw in the tangent to the characteristic line σ_1 passing through D by letting $(\bar{f}_Y)_{Y=R} = 0$ in Eq. (39) and by using the values just obtained for v_x and v_Z.

In the plane $Y = R + \Delta$, let D' be the point on the wing which lies in this plane and has the same abscissa as D, and let $Q_0^{(n)}$ be the point of the line $\sigma_1^{(n)}$ which belongs to the same characteristic line σ_1' passing through D'. Since the velocity at $Q_0^{(n)}$ is known (or can be determined immediately by interpolation between the values of the velocities computed along $\sigma_1^{(n)}$ by means of the above-mentioned procedure) and since at the same time the direction at D' of the velocity component in the plane under consideration is known, then the magnitude of this component can be determined by the usual graphical construction (Figs. 12c and 12d). Furthermore, because of the irrotationality of the motion, we know $\partial v_Y/\partial x = \partial v_x/\partial Y$, and, therefore, if A denotes the leading edge of the wing, it follows that

$$\frac{(v_Y)_{D'} - (v_Y)_A}{x_{D'}} = \frac{(v_x)_{D'} - (v_x)_D}{\Delta}$$

The value of $(v_Y)_D$ may be obtained easily from this relation.

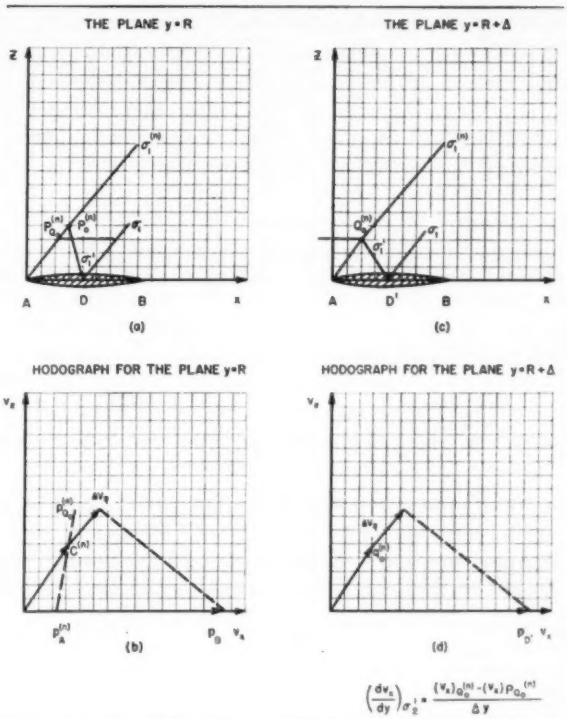

FIGS. 12a–12d. Extension out along the wing span of the hodograph for the field over the upper surface of the wing.

Eq. (39) gives the value of λ_1 if one assumes for the velocity components the values just determined at D' and also sets $(\bar{f}_Y)_{Z=0} = 0$ and $(\bar{f}_Z)_{Z=0} = \lambda_1$ therein. The calculation of this quantity thus makes it possible to draw in the tangent to σ_1 at D'.

In this way one may obtain the velocities at all the points in the plane of the wing which belong to the plane $x = x_D$, and proceeding in the usual way one may also determine the entire characteristic surface Σ which intersects the wing along the straight line $Z = 0$, $x = x_D$, and one may calculate the velocities at the points of this surface.

Therefore the complete determination of the flow over the upper surface requires but the repeated application of the procedure just described.

(C-2) *Description of the Field Existing on the Bottom Surface of the Wing*

(C-2-1) Determination of the Shock Wave for the Flow Field in Contact with the Lower Surface.—The compression in the fluid stream which touches the lower surface is propagated by means of a shock wave that originates at the leading edge of the wing. Let the equation of the shock wave, in the neighborhood of the leading edge, be expressed in the form:

$$x = Zg(Y) \tag{49}$$

Since the direction cosines of the normal, $\vec{n}$, to the wave surface are, for $x = Z = 0$:

$$\cos(n, x) = \frac{1}{\sqrt{1+g^2}}; \quad \cos(n, Y) = 0; \quad \cos(n, Z) = \frac{-g}{\sqrt{1+g^2}}$$

then the condition that the velocity be normal to the wave front leads us to write

$$\frac{v_x^{(0)} - \bar{v}_x}{1} = \frac{v_Y^{(0)} - \bar{v}_Y}{0} = \frac{v_Z^{(0)} - \bar{v}_Z}{-g} = H$$

where we again let $v_x^{(0)}$, $v_Y^{(0)}$, $v_Z^{(0)}$ denote the values of the velocity components before the shock and $\bar{v}_x$, $\bar{v}_Y$, $\bar{v}_Z$ denote the values of the same components after the shock. From this set of equalities we may write

$$\bar{v}_Y = v_Y^{(0)}; \quad \bar{v}_x = v_x^{(0)} - H; \quad \bar{v}_Z = v_Z^{(0)} + gH$$

After the shock the stream must be tangent to the wing, and therefore it must be true that $\bar{v}_Z = 0$; consequently, $H = -v_Z^{(0)}/g$. Consider, in addition, that the velocity components normal to the wave are

$$[v_x^{(0)}/\sqrt{1 + g^2}] - [v_Z^{(0)}(g)/\sqrt{1 + g^2}]$$

before the shock and

$$[v_x^{(0)}/\sqrt{1 + g^2}] - [H/\sqrt{1 + g^2}]$$

behind the shock, while the tangential component is expressed as

$$v_t^2 = \{[v_x^{(0)}]^2 + [v_Y^{(0)}]^2 + [v_Z^{(0)}]^2\} \sin^2 \gamma = [v_Y^{(0)}]^2 + \frac{[v_x^{(0)}]^2 g^2 + [v_Z^{(0)}]^2 + 2v_x^{(0)} v_Z^{(0)} g}{1 + g^2}$$

provided γ denotes the angle between the normal, $\vec{n}$, to the shock and the direction of the upstream velocity. Then, by utilization of the equation of the shock, it follows that

$$\left[\frac{v_x^{(0)}}{\sqrt{1 + g^2}} - \frac{v_Z^{(0)} g}{\sqrt{1 + g^2}}\right]\left[\frac{v_x^{(0)}}{\sqrt{1 + g^2}} + \frac{v_Z^{(0)}}{g\sqrt{1 + g^2}}\right] = \frac{k - 1}{k + 1}\left\{1 - [x_Y^{(0)}]^2 - \frac{[v_x^{(0)}]^2 g^2 + [v_Z^{(0)}]^2 + 2v_x^{(0)} v_Z^{(0)} g}{1 + g^2}\right\}$$

that is,

$$\frac{[v_x^{(0)} - v_Z^{(0)} g][v_x^{(0)} g + v_Z^{(0)}]}{g\{1 - [v_Y^{(0)}]^2\}} = \frac{k - 1}{k + 1}\left(1 - \frac{[v_x^{(0)}]^2 g^2 + [v_Z^{(0)}]^2 + 2v_x^{(0)} v_Z^{(0)} g}{\{1 - [v_Y^{(0)}]^2\}(1 + g^2)}\right) \tag{50}$$

This relationship is equivalent to the equation defining g for a two-dimensional stream that has, ahead of the shock, the components

$$v_x^{(0)}/\sqrt{1 - [v_Y^{(0)}]^2} \text{ and } v_Z^{(0)}/\sqrt{1 - [v_Y^{(0)}]^2}$$

Remember now that

$$v_x^{(0)} = V_x^{(0)}/V_i \text{ and } v_Z^{(0)} = V_Z^{(0)}/V_i$$

and set

$$V_i^{*2} = V_i^2 - [V_Y^{(0)}]^2 \tag{51}$$

so that

$$\frac{v_x^{(0)}}{\sqrt{1 - [v_Y^{(0)}]^2}} = \frac{V_x^{(0)}}{V_i^*} \text{ and } \frac{v_Z^{(0)}}{\sqrt{1 - [v_Y^{(0)}]^2}} = \frac{V_Z^{(0)}}{V_i^*}$$

It is apparent then that, in any plane Y = const., the trace of the shock wave at the leading edge can be determined as though the upstream flow were two-dimensional and with components equal to the actual components $V_x^{(0)}$ and $V_Z^{(0)}$ but with the limiting velocity of the stream less than the real one by the amount indicated in Eq. (51).

(C-2-2) Determination of the Field Along the Lower Surface.—(C-2-2-1) Construction of the series of characteristic surfaces that emanate from spanwise lines aft of the leading edge: In the plane $Y = R$, let $S_0^{(0)}$ be a point on the trace of the shock wave and situated so close to the leading edge that it is legitimate to consider $S_0^{(0)}$ as belonging to the tangent to this trace, which was described in Section (C-2-1). Now consider the characteristic line σ_1', passing through $S_0^{(0)}$; its slope can be determined by means of Eq. (39) because $f_Y = 0$ and the velocity at $S_0^{(0)}$ is known. Let D_f denote the intersection of σ_1 with the plane of the wing (Fig. 13a). Then the velocity change along $S_0^{(0)} D_f$ satisfies Eq. (43′), and since v_Z must also be zero at D_f,

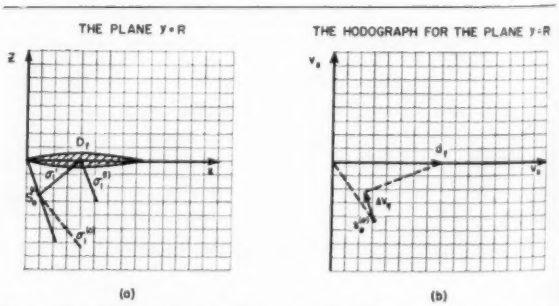

FIGS. 13a–13b. Determination of velocity on lower surface of wing behind the compression shock.

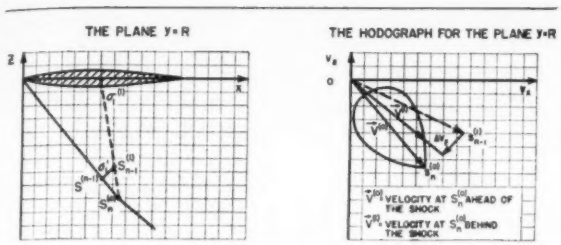

FIGS. 14a–14b. Determination of velocity on the shock front for lower surface of wing.

the velocity at D_f is found with little difficulty by means of the construction given in Fig. 13b, for example.

Now that the value of the velocity is known at D_f, it is possible to compute the value of $\dot{f}_Z = \lambda_1$ by means of Eq. (39), wherein $\dot{f}_Y = 0$ is still to be employed; consequently, it is possible to draw in the tangent to $\sigma_1^{(1)}$ through the point D_f.

In the plane $Y = R + \Delta$ (and in the other planes, Y = const.), the same procedure as described above is followed in order to obtain the velocity at the points D_f', which lie on the same straight line, $x = x_{Df}$, in the plane of the wing. At these points the tangent to $\sigma_1^{(1)}$ which passes through them is traced in for each one of the planes. Proceeding along the line $\sigma_1^{(1)}$, it is possible to calculate the values of the velocity in each plane Y = const. by means of the repeated application of the procedure already fully described, until finally the intersection of the surface $\Sigma^{(1)}$ with the shock wave is reached.

(*C-2-2-2*) *Determination of the velocities at the intersections of the characteristic surfaces which begin on the wing surface and meet the shock wave from the leading edge:* Let $S_n^{(0)}$ denote the intersection of the line $\sigma_1^{(1)}$, lying in the plane $Y = R$, with the trace of the shock wave. The determination of the velocity at $S_n^{(0)}$ and of the tangent to the trace of the shock wave at $S_n^{(0)}$ comes about as a result of the following considerations. Along the arc $S_{n-1}^{(1)}S_n^{(0)}$ of σ_1' (Fig. 14) the velocity change satisfies Eq. (42′). Since the velocities are known at all points of $\sigma_1^{(1)}$ which correspond to the $S_{n-1}^{(1)}$, lying in the various planes Y = const., this Eq. (42′) furnishes the means of computing the velocity component $\Delta v_{\bar{t}}$ in the direction of σ_1' and through $S_{n-1}^{(1)}$. This component must be added, together with its normal component, to the velocity at $S_{n-1}^{(1)}$ in order to obtain the velocity at $S_n^{(0)}$. On the other hand, at $S_n^{(0)}$, downstream of the shock, the velocity change produced by the shock must satisfy the equation of the shock wave itself. If the vector defining the velocity ahead of the shock, at $S_n^{(0)}$, is drawn in in the hodograph plane, together with the corresponding shock polar, then the construction shown in Fig. 14b is readily available for determination of the velocity behind the shock at $S_n^{(0)}$.

In the plane $Y = R + \Delta$, let $T_n^{(0)}$ be the intersection of the line $\sigma_1^{(1)}$ with the trace of the shock wave. The points $S_n^{(0)}$, $T_n^{(0)}$, etc., which are obtained in the various planes Y = const., constitute the locus of a line. Starting at this line, the equation of the shock wave may be expressed in the form

$$x = \Delta'(Y)g(Y) + (Z - \Delta')g_1(Y) \tag{52}$$

wherein $\Delta'(Y)$ is the coordinate relative to the Z-axis of the points $S_n^{(0)}$, $T_n^{(0)}$, etc. The direction parameters for the normal to the shock surface at the points indicated become:

$$\begin{matrix} & & & & \text{APP.} \\ 1; & -\dot{\Delta}'g - \Delta'\dot{g} + \dot{\Delta}'g_1 = -\Delta'\dot{g}; & -g_1 \end{matrix}$$

respectively, provided it is assumed that $\dot{\Delta}'(g - g_1)$ may be neglected on the basis that it is of second order in magnitude in comparison with $\Delta'\dot{g}$.

In each plane Y = const., assume, in addition, that the x-axis is the straight line parallel to the velocity component at $T_n^{(0)}$ ahead of the shock (this point of view is convenient in order to reduce the formal complication of the computation; because of this, the values of Δ' and of g will be modified in an obvious way with respect to their corresponding values in the system of axes which has been used until now). Then, employing the same notation as adopted in Section (C-2-1) and with the understanding that the velocity components are now referred to the system of axes which was just described, it must be true that, as a result of the condition that the velocity change produced by the shock has to be perpendicular to the wave,

$$\frac{v_x^{(0)} - \bar{v}_x}{1} = \frac{v_Y^{(0)} - \bar{v}_Y}{-\Delta'\dot{g}} = \frac{\bar{v}_Z}{g_1} = H$$

from which we obtain

$$\bar{v}_x = v_x^{(0)} - H; \quad \bar{v}_Y = v_Y^{(0)} + \Delta' g H; \quad \bar{v}_Z = g_1 H \tag{53}$$

If such terms as $\Delta'^2\dot{g}^2H$ and $[v_Y^{(0)}]^2\Delta'^2\dot{g}^2$ are neglected, then use of the shock equation produces the relation:

$$\left[\frac{v_x^{(0)}}{\sqrt{1+g_1^2}} - \frac{v_Y^{(0)}\Delta'\dot{g}}{\sqrt{1+g_1^2}}\right]\left[\frac{\bar{v}_x}{\sqrt{1+g_1^2}} - \frac{v_Y^{(0)}\Delta'\dot{g}}{\sqrt{1+g_1^2}} - \frac{\bar{v}_Z g_1}{\sqrt{1+g_1^2}}\right] =$$

$$\frac{k-1}{k+1}\left\{1 - [v_Y^{(0)}]^2 - \frac{g_1^2[v_x^{(0)}]^2 + 2v_x^{(0)}v_Y^{(0)}\Delta'\dot{g}}{1+g_1^2}\right\} \tag{54}$$

If the velocities are referred to the reduced limiting velocity defined by Eq. (51) instead of being referred to the actual limiting velocity, so that we therefore let

$$\frac{v_x^{(0)}}{\sqrt{1 - [v_Y^{(0)}]^2}} = v_x^*; \quad \frac{v_Z^{(0)}}{\sqrt{1 - [v_Y^{(0)}]^2}} = v_Z^*; \text{ etc.}$$

then Eq. (54) becomes

$$v_x^* \bar{v}_x^* - v_x^* g_1 \bar{v}_Z^* = (1 + g_1^2) \frac{k-1}{k+1} - \frac{k-1}{k+1} (v_x^*)^2 g_1^2 + 2 v_x^* v_Y^* \Delta' \dot{g} \left(\frac{1}{k+1}\right)$$

wherein the term $\bar{v}_Z^* v_Y^* \Delta' \dot{g}$ has now been neglected and we have let

$$v_x^* v_Y^* \Delta' \dot{g} = \bar{v}_x^* v_Y^* \Delta' \dot{g}$$

But from Eq. (53) we have

$$g_1 = \bar{v}_Z / H = \bar{v}_Z / [v_x^{(0)} - \bar{v}_x] = \bar{v}_Z^* / (v_x^* - \bar{v}_x^*)$$

so that, upon solving for $\bar{v}_Z^{*2}$, it is found that

$$\bar{v}_Z^{*2} = (v_x^* - \bar{v}_x^*)^2 \left\{ \left[\frac{k-1}{k+1} - v_x^* \bar{v}_x^* + 2 v_x^* v_Y^* \frac{\Delta'}{k+1} (\dot{g}) \right] \Big/ \left[\bar{v}_x^* v_x^* - \frac{v_x^{*2}}{k+1} - \frac{k-1}{k+1} \right] \right\} \tag{55}$$

Substitution of the value $v_Y^* = 0$ (or of $\dot{g} = 0$) into this equation reduces it to the well-known relationship that defines the shock strophoid.

Eq. (55) describes the new shock polar in the arbitrary general plane $Y = \text{const.}$ Once this polar has been drawn in in the respective hodograph it permits the determination of the velocities at the points $T_n^{(0)}$, and of the traces of the shock wave at these points, by means of a procedure similar to that discussed in the case of the hodograph for the plane $Y = R$. In this way the complete determination of the flow along the bottom surface requires only the repeated application of the procedure described in the preceding sections.

(D) Determination of the Field for the Portion of the Body That Is Affected by the Wing

(D-0) General Equations

In order to study the flow near the fuselage in the region where the disturbances produced by the wing are felt, it is still convenient to refer the velocity potential of the field to a system of cylindrical coordinates, as was done in Section (B). Now solve the equation of the characteristic surfaces for x, and write the equation so obtained in the form $x = f(y, \theta, b)$ through use of such a cylindrical reference system, so that then

$$a_{11} - 2a_{12} f_y - 2a_{13} \left(\frac{1}{y}\right) f_\theta + 2a_{23} \left(\frac{1}{y}\right) f_y f_\theta + a_{33} \left(\frac{1}{y^2}\right) f_\theta^2 + a_{22} f_y^2 = 0 \tag{56}$$

The intersections of the set of characteristic surfaces Σ with the cylinders $y = \text{const.}$ and with the planes $\theta = \text{const.}$ produce the characteristic lines that are still to be denoted by σ_1 and σ_2. The fundamental equations that define the law of variation of the velocity along these characteristic lines now become

$$\left.\begin{gathered} f_y = \lambda; \quad f_\theta = \mu_1 \\ \left[\frac{a_{33}}{y^2}\left(\frac{d(yv_\theta)}{d\theta} + \mu_2 \frac{dv_x}{d\theta}\right)\right]_{\sigma_1} + \left[\frac{dv_x}{dy}(2a_{12} - a_{22}\lambda) + a_{22}\frac{dv_y}{dy} + 2a_{23}\frac{1}{y}\frac{d(yv_\theta)}{dy}\right]_{\sigma_2} + \frac{v_y}{y} = 0 \\ \left[\frac{d(yv_\theta)}{dy} + \mu_1 \frac{dv_x}{dy}\right]_{\sigma_1} = \left(\frac{dv_y}{d\theta} + \lambda \frac{dv_x}{d\theta}\right)_{\sigma_2} \end{gathered}\right\} \tag{57}$$

At the same time, the intersections of the set of characteristic surfaces Σ' with the cylinders $y = \text{const.}$ and with the planes $\theta = \text{const.}$ produce the characteristic lines denoted by σ_1' and σ_2', and for these lines, the following hold:

$$\left.\begin{gathered} f_y = \lambda; \quad f_\theta = \mu_2 \\ \left[\frac{a_{33}}{y^2}\left(\frac{d(yv_\theta)}{d\theta} + \mu_1 \frac{dv_x}{d\theta}\right)\right]_{\sigma_1'} + \left[\frac{dv_x}{dy}(2a_{12} - a_{22}\lambda) + a_{22}\frac{dv_y}{dy} + 2a_{23}\left(\frac{1}{y}\right)\frac{d(yv_\theta)}{dy}\right]_{\sigma_2'} + \frac{v_y}{y} = 0 \\ \left[\frac{d(yv_\theta)}{dy} + \mu_2 \frac{dv_x}{dy}\right]_{\sigma_1'} = \left(\frac{dv_y}{d\theta} + \lambda \frac{dv_x}{d\theta}\right)_{\sigma_2'} \end{gathered}\right\} \tag{58}$$

The quantities μ_1 and μ_2 in Eqs. (57) and (58) are the two roots of Eq. (56) which result when $\dot{f}_y$ is set equal to λ and the equation is solved for $\dot{f}_\theta$. Eqs. (57) and (58) are valid over the whole region that corresponds, through Eq. (56), to the case where the two values of $\dot{f}_\theta$, obtained for a given value λ of $\dot{f}_y$, are real and distinct; this certainly happens in the neighborhood of the plane $\theta = 0$ (or $\theta = \pi$).

Analogously to what was done in Sections (B-0-2) and (C-0-2), the third of Eqs. (57) and (58) may be replaced by:

$$\left[\frac{a_{33}}{y}\left(\frac{dv_\xi}{d\theta}\right)\right]_{\sigma_1} + \left[\ \right]_{\sigma_2} \sin(\tau_2, x) + \left(\frac{v_y}{y}\right)\sin(\tau_2, x) = 0 \tag{57'}$$

$$\left[\frac{a_{33}}{y}\left(\frac{dv_\eta}{d\theta}\right)\right]_{\sigma_1'} + \left[\ \right]_{\sigma_2'} \sin(\tau_1, x) + \left(\frac{v_y}{y}\right)\sin(\tau_1, x) = 0 \tag{58'}$$

Here τ_1 and τ_2 are, respectively, the tangents to σ_1 and σ_1' at the point P, in the neighborhood of which the Eqs. (57′) and (58′) are being considered. In addition, $dv_\xi/yd\theta$ defines the change along σ_1 of the component of velocity in the direction of the tangent to σ_1'; likewise, $dv_\eta/yd\theta$ defines the change along σ_1' of the component of velocity in the direction of the tangent to σ_1.

(D-1) *Disturbed Flow over the Body Emanating from the Upper Side of the Wing*

The perturbations produced by the wing will first be felt starting at the characteristic surface $\Sigma^{(0)}$; just as was done in Section (C-1-1-1), this surface is determined first of all. In the neighborhood of the leading edge of the wing and therefore in the neighborhood of $\theta = 0$, let the equation of $\Sigma^{(0)}$ be expressed in the form

$$x = \theta h_0^{(0)}(y) \tag{59}$$

Then we have

$$\lambda = (\dot{f}_y)_{\theta=0} = 0; \quad \mu_1 = (\dot{f}_\theta)_{\theta=0} = h_0^{(0)}(y)$$

which, when substituted into Eq. (56), leads to the determination of $h_0^{(0)}(y)$. It is readily perceived that the quantity $h_0^{(0)}(y)$ coincides with $A_0^{(0)}(Y)$ as defined in Section (C-1-1-1). Now consider the various cylindrical surfaces $y = \text{const.}$ (in particular, the one $y = R$), or, even better, let us give our attention to the planes into which these cylindrical surfaces can be developed. Then, in view of the above, the tangents to the lines $\sigma_1^{(0)}$ can be drawn, where $\sigma_1^{(0)}$ are the intersection of these planes with the surface $\Sigma^{(0)}$.

The surface [Eq. (59)] is then cut by the plane $\theta = \Delta$. In the neighborhood of the line of intersection $x = \Delta h_0^{(0)}(y)$, $\theta = \Delta$, it is assumed that the equation of $\Sigma^{(0)}$ is given by:

$$x = \Delta h_0^{(0)}(y) + (\theta - \Delta)h_1^{(0)}(y)$$

from which it now follows that

$$\lambda = (\dot{f}_y)_{\theta=\Delta} = \Delta\dot{h}_0^{(0)}$$
$$\mu_1 = (\dot{f}_\theta)_{\theta=\Delta} = h_1^{(0)}(y)$$

Thus Eq. (56) affords the means of obtaining $h_1^{(0)}(y)$ when the values just given for $\dot{f}_y$ and $\dot{f}_\theta$ are substituted in it. Then it is possible to trace in all the $\sigma_1^{(0)}$ by proceeding step by step over the cylindrical surfaces or, better, upon the planes into which the latter are developed.

With respect to what was done in Section (C-1), therefore, no modification arises in the procedure used in application of Eqs. (57) and (58) and Eqs. (57′) and (58′) to the determination of the characteristic lines σ_1 and σ_1' and σ_2 and σ_2', as well as of the related hodographs. The procedure is now carried out on the planes into which the cylindrical surfaces $y = \text{const.}$ are developed in the same way as was done in Section (C) for the planes $Y = \text{const.}$; likewise, the planes $\theta = \text{const.}$ now correspond to the planes $Z = \text{const.}$

Because of the considerations evolved in Section (C), it is indeed sufficient to consider the flow only in the neighborhood of the cylindrical surface $y = R$. When one restricts himself therefore to so consider the motion, the equations can be simplified, in actual calculation, because $v_y = 0$ for $y = R$; so we may neglect the term v_y/y, and may let $a_{22} = 1$ and $a_{23} = a_{13} = 0$ therein. One must then consider a set of cylindrical surfaces, $y = \text{const.}$, which are close to one another in order that such simplifications would be legitimate for them. Moreover, they must be of sufficient number to allow the determination of the flow over the entire portion of the body which is of interest.

(D-2) *Disturbed Flow over the Body Emanating from the Under Side of the Wing*

Observe that on the cylinder $y = R$, which is a stream surface, the shock wave is normal thereto because the shock must not produce any change of the velocity component v_y. Therefore, in the neighborhood of this surface the equation of the shock front may be expressed as

$$x = g_0(\theta) + g_1(\theta)[(y - R)^2] \tag{60}$$

The following conditions serve to determine $g_0(\theta)$ and $g_1(\theta)$: The shock wave has an intersection (trace) on the cylinder $y = \text{const.}$ The tangent to this trace

at the plane $\theta = 0$ is found easily and directly by means of the deductions made in Section (C-2).

Consequently, one proceeds, in the manner that was there described, by working in the planes into which these cylinders have been developed; and through utilization of Eqs. (57) and (58) and of Eqs. (57′) and (58′), the velocity at the points D_f is calculated. The points D_f belong to the plane of the wing and, of course, are close to the leading edge.

Now, as long as the characteristics σ_1 that originate at these points D_f do not intersect the trace of the shock wave on the respective cylinders (that is, on the related developed planes), the velocity component pertaining to each of these cylinders has the direction of the x-axis, downstream of the shock front. Then, because the velocity upstream of the shock is known, the change in direction that the shock must produce is consequently also known.

It is possible, therefore, to determine the trace of the shock which is capable of producing the required change through evaluation of the shock polar (which coincides with the shock polar based on the local velocity, because v_y is zero or negligible, in the region of the field under consideration). The characteristics σ_1, through the points D_f of the wing contour, intersect the traces of the shock which were just described. Again, through employing the method developed in (C-2-2-2), the velocities at these points of intersection are calculated (for the case where the cylinders are developed into planes). One may assume that the shock polar is the strophoid that corresponds to the local velocity, in view of the fact that v_y is negligible; thus the above-mentioned method is simplified.

References

[1] Ferrari, C., *Determination della Pressione sopra Solidi di Rivoluzione a Prora Acuminata Disposti in Deriva in Corrente di Fluido Compressible a Velocità Ipersonora,* Atti della Reale Accademia delle Scienze di Torino, Vol. 72, pp. 140–163, November–December, 1936. Also in Report No. 94, Laboratorio di Aeronautica, University of Turin, November, 1936. See British R.T.P. Translation No. 1105, *Determination of the Pressure Exerted on Solid Bodies of Revolution with Pointed Noses Placed Obliquely in a Stream of Compressible Fluid at Supersonic Velocity,* War Office Translation No. M.I.1. (T) 9238.

[2] Cicala, P., *Seconda Relazione sul Quesito della Resistenza dei Proietti al Movimento dell' Aria,* La Ricerca Scientifica, Anno V, Vol. II, No. 3-4, Rome, 1933; or Busemann, A., *Drücke auf Kelgelförmige Spitzen bei Bewegung mit Ueberschallgeschwindigkeit,* Zeitschrift für angewandte Mathematik und Mechanik, Vol. 9, p. 496, Berlin, 1929.

[3] Lamb, H., *Hydrodynamics,* 6th Ed., p. 112; Cambridge University Press, London, 1932.

[4] Goursat, E., *Cours d'Analyse Mathématique,* Vol. III, p. 92; Gauthier-Villars, Paris, 1933.

[5] Sauer, R., *Theoretische Einführung in die Gasdynamik,* p. 141; Springer, Berlin, 1943. Hill-Alpher translation: *Theoretical Gas Dynamics,* p. 214; J. W. Edwards, Ann Arbor, 1947.

[6] Ibid., p. 56; in the Hill-Alpher translation, p. 87.

[7] Ibid., p. 109; in the Hill-Alpher translation, p. 169.

Erratum

The title of the article by Adolf Busemann in the June, 1949, issue of the JOURNAL (Vol. 16, No. 6, p. 337) was incorrectly stated. The correct title is:

"The Problem of Drag at High Subsonic Speeds"

Performance Analysis of Centrifugal Compressors

SHAO-PAN LIANG*

Chekiang University, Hangchow, China

ABSTRACT

Elementary analysis of centrifugal compressors indicates that the energy received by each unit weight of gas compressed is merely a function of impeller tip speed. This, as shown by experimental results, is far from true. The pressure of delivery falls off with the increase of quantity of discharge, and the efficiency of compression is also affected. It is the purpose of this paper to point out that, based on force and energy calculations, performance can be predicted with reasonable accuracy.

INTRODUCTION

THE DEVELOPMENTS OF POWER GAS TURBINES and jet engines have opened a new field of application for compressors of the centrifugal type. Following Moss's analysis, the energy input per unit weight of gas is

$$W = SU^2/g \tag{1}$$

where U is the tip speed of the impeller; g, the gravitational acceleration; and S, the ratio of tangential velocity of the gas leaving the impeller to the impeller tip speed. The discharge pressure depends on S and η and the efficiency of compression and has not been theoretically surveyed. In this analysis, the author has followed the conventional method of momentum and energy considerations. Such relations alone, however, do not yield fruitful results. The friction loss in the impeller is an unknown factor, which makes the process deviate from the isentropic one. By treating the process as a combination of losing energy and adding heat, an extra equation is obtained.

ENERGY RECEIVED BY AND FORCES ACTING ON AN ELEMENTARY MASS OF AIR

Consider an elementary mass of air between two adjacent blades and at radius r on an impeller (Fig. 1). The angular momentum about the axis of the impeller is $Sr^2\omega\rho A\, dr/g$, where ω is the angular velocity of the impeller, ρ is the density of the air in question, and A is the cross-sectional area of airflow. Since the angular momentum of the air is zero before entering the impeller, this change of momentum is associated with an increase of energy, which can be easily seen to be $Sr^2\omega^2/g$ per unit weight of air. This energy may take either the form of sensible heat or stored as mechanical energy, and the total sum is

$$\frac{Sr^2\omega^2}{g} = \frac{(Sr\omega)^2}{2g} + \frac{v^2}{2g} + C_p(T - T_0) \tag{2}$$

in which v is the relative radial velocity of air in the impeller; C_p is the specific heat of air at constant pressure, expressed in mechanical units; T is the absolute temperature of air in the impeller; and T_0 is the absolute temperature of atmospheric air.

The forces acting on the elementary mass of air are: (a) the pressure of the neighboring air and of the impeller blades, and (b) the friction forces exerted by the impeller.

Taking the above-mentioned air as a free body, the summation of forces along radial direction is

$$-A\, dp - f\frac{\rho v^2}{2g}\, l\, dr = \frac{\rho A\, dr}{g}\, a_r \tag{3}$$

where f is the coefficient of friction of the impeller, l is the length of circumference of the area concerned, and a_r is the acceleration of air in radial direction.

As the motion of the air is composed of a circular motion with tangential velocity $Sr\omega$ and a radial motion with velocity v, the radial component of acceleration is

$$a_r = v(dv/dr) - S^2r\omega^2 \tag{4}$$

Hence,

$$-A\, dp - f\frac{\rho v^2}{2g}\, l\, dr = \frac{pA\, dr}{gRT}\left(v\frac{dv}{dr} - S^2r\omega^2\right) \tag{5}$$

in which R is the gas constant of air.

Since the frictional force is, in general, extremely small compared with the pressure gradient, the equation can be further simplified by omitting the friction term, with the result

$$-\frac{R}{p}\frac{dP}{dR} = \frac{1}{gT}\left(v\frac{dv}{dr} - S^2r\omega^2\right) \tag{6}$$

Eliminating v between Eqs. (2) and (6), we have

$$-\frac{R}{p}\frac{dp}{dr} = \frac{1}{2gT}\left\{\frac{d}{dr}\left[2Sr^2\omega^2 - S^2r^2\omega^2 - 2gC_p(T - T_0)\right] - 2S^2r\omega^2\right\} \tag{7}$$

By assuming that S is independent of r, the equation may be simplified to

$$-\frac{R}{p}\frac{dp}{dr} = \frac{1}{gT}\left[2S(1 - S)r\omega^2 - gC_p\frac{dT}{dr}\right] \tag{8}$$

Received October 13, 1948.

* Professor, Department of Aeronautical Engineering.

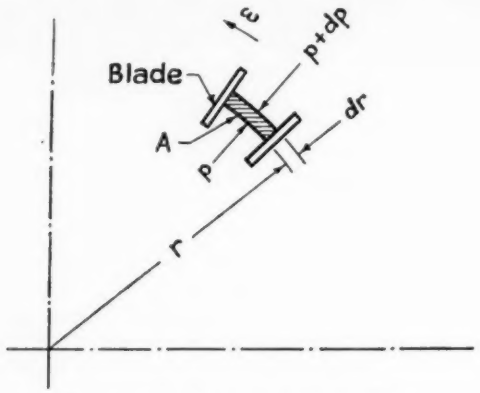

FIG. 1. Forces acting on air at radius r.

This gives the relation between pressure and temperature at different radii, and another equation is required to obtain a solution.

THE TRANSFORMATION OF ENERGY DUE TO FRICTION

In order to determine the pressure variation, we must consider the effect of friction loss. With the assumption of no heat transfer from outside, any loss of energy due to friction will again be absorbed by the gas. Therefore the process is practically a transformation of mechanical energy into heat energy, with the total amount unchanged.

Since the cross-sectional area of airflow is roughly of a rectangular shape, the length of circumference may be expressed as

$$l = 2[(2\pi r/n) + (nA/2\pi r)] \tag{9}$$

in which n is the total number of blades.

The energy loss per unit weight of gas is directly proportional to the velocity head (relative velocity) and lateral area, while inversely proportional to the cross-sectional area of flow, so the loss due to impeller friction may be expressed as

$$f\frac{v^2 + (1 - S)^2r^2\omega^2}{2g}\left[2\left(\frac{2\pi r}{n} + \frac{nA}{2\pi r}\right)dr/A\right]$$

The friction due to the compressor casing, being less in magnitude for normal rate of flow, may be neglected. Thus, the entropy increase due to this energy transformation is, from gas laws,

$$C_p\frac{dT}{T} - R\frac{dp}{p} = \frac{2f}{T}\frac{v^2 + (1 - S)^2r^2\omega^2}{2g} \times \left(\frac{2\pi r}{nA} + \frac{n}{2\pi r}\right)dr \tag{10}$$

This relationship between friction and change of state helps in determining the effectiveness of compression. As can be readily seen, the less the magnitude of f, the nearer will be the process to the isentropic one.

Eliminating v between Eqs. (2) and (10), we have

$$\frac{C_p}{T}\frac{dT}{dr} - \frac{R}{p}\frac{dp}{dr} = \frac{2f}{T}\left[\frac{r^2\omega^2}{2g} - C_p(T - T_0)\right] \times \left(\frac{2\pi r}{nA} + \frac{n}{2\pi r}\right) \tag{11}$$

Substitution of Eq. (8) into Eq. (11) results in

$$\frac{S(1 - S)r\omega^2}{g} = f\left[\frac{r^2\omega^2}{2g} - C_p(T - T_0)\right] \times \left(\frac{2\pi r}{nA} + \frac{n}{2\pi r}\right) \tag{12}$$

which gives the absolute temperature at different radii. With this known, the pressure of gas can be found from Eq. (8), while the radial velocity v is found from the combination of Eqs. (4) and (12)—namely,

$$\frac{S(1 - S)r\omega^2}{g} = f\left[\frac{v^2 + (1 - s^2)r^2\omega^2}{2g}\right] \times \left(\frac{2\pi r}{nA} + \frac{n}{2\pi r}\right) \tag{13}$$

After the computation of pressure and temperature, the quantity of discharge becomes extremely simple as indicated by the equation of continuity

$$q = \rho vnA \tag{14}$$

where q is the weight of discharge per unit time.

SIMPLIFICATION OF RESULTS

The above equations, while based on theoretical analysis, are rather complicated in actual computations. They can be further simplified if the number of impeller blades is small. In such case, the term $n/2\pi r$ is small in comparison to the term $2\pi r/nA$ and may be dropped out. Thus we have the approximate equations

$$\frac{S(1 - S)\omega^2}{g} = f\left[\frac{r^2\omega^2}{2g} - C_p(T - T_0)\right]\frac{2\pi}{nA} \tag{15}$$

and

$$S(1 - S)\omega^2 = (f\pi/nA)[v^2 + (1 - S)^2r^2\omega^2] \tag{16}$$

instead of Eqs. (12) and (13).

Since A is practically constant, we have $dA/dr = 0$, so that differentiation of Eq. (15) gives

$$C_p(dT/dr) = r\omega^2/g \tag{17}$$

Combining with Eq. (8) gives

$$R(dp/p) = ZC_p(dT/T) \tag{18}$$

in which $Z^2 = S^2 + (1 - S)^2$. This holds good for the entire path through the impeller.

For the complete compressor, detailed information regarding the entry and diffuser section is required to obtain a definite solution. By assuming a constant temperature-pressure relationship throughout the unit.

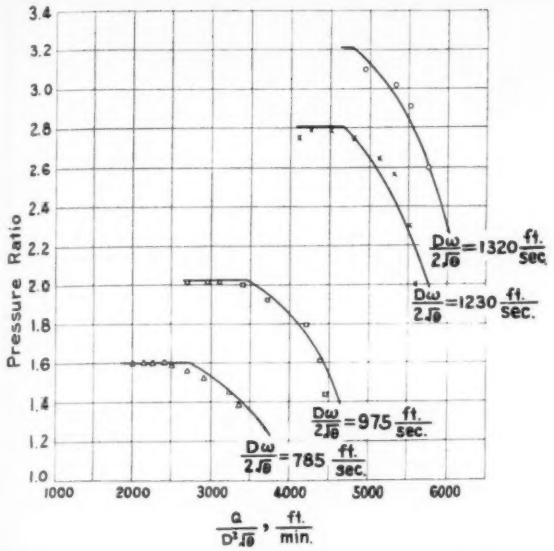

FIG. 2. Comparison of experimental data and theoretical results. ($f = 0.40$ for all theoretical curves.)

the problem can be further simplified. Thus, the equation

$$p_3/p_0 = (T_3/T_0)^{\gamma Z/(\gamma - 1)} \tag{19}$$

gives the pressure ratio and the expression

$$\eta = [(T_3/T_0)^Z - 1]/[(T_3/T_0) - 1] \tag{20}$$

gives the adiabatic efficiency of compression. (The symbol γ denotes the ratio of specific heats of air.) The final temperature T_3 may be determined from the law of conservation of energy as

$$T_3 = T_0 + (SU^2/gC_p) \tag{21}$$

From the above statements, the density ratio at radius r_1 is

$$\frac{\rho_1}{\rho_0} = \left\{1 + \frac{\gamma - 1}{2}\left(\frac{r_1\omega}{c_0}\right)^2 \times \left[1 - \frac{S(1 - S)(1 - h^2)}{f}\right]\right\}^{Z/(\gamma - 1)} \tag{22}$$

in which ρ_1 is the density of air at radius r_1, ρ_0 is the atmospheric density, r_1 is the radius of impeller eye, h is the ratio of diameters of impeller hub and impeller eye, and c_0 is the sonic velocity in the atmospheric air. The rate of flow is

$$q = \rho_1\omega\pi r_1^3(1 - h^2) \times \left[\frac{S(1 - S)(1 - h^2)}{f} - (1 - S)^2\right]^{1/2} \tag{23}$$

The specific volume-rate-of-flow, as commonly used in American practice is

$$\frac{Q}{D^2\sqrt{\theta}} = \frac{\pi}{\sqrt{\theta}}\frac{\rho_1}{\rho_0}\frac{r_1^3\omega}{D^2}(1 - h^2) \times \left[\frac{S(1 - S)(1 - h^2)}{f} - (1 - S)^2\right]^{1/2} \tag{24}$$

in which Q is the total volume of airflow per unit time, D is the impeller tip diameter, and θ is the ratio of T_0 to the assigned reference temperature. (519°F. is commonly used.)

Empirical Limit of Application

From the above equations, it is evident that S is determined for given values of Q and f, at any speed. The pressure ratio, as shown in Eq. (19), is also fixed under such conditions. With the value of f properly chosen, theoretical results will check fairly well with the experimental ones. In Fig. 2, the data of Campbell and Talbert[2] are taken for comparison. The equation loses its validity when maximum pressure is attained, and this happens in the neighborhood of $S = 0.9$ for all speeds. Further reduction of quantity would theoretically give still higher pressures, while experimental data show otherwise. The explanation for such discrepancy is that friction due to impeller casing was neglected in the above derivations. When the quantity of flow is small, the heat generated becomes greater and greater for each unit weight of air. Consequently, the temperature rises higher and higher and efficiency is lowered. The quick fall of efficiency in this range leads to the phenomenon of surge, as may be seen in practice. By assuming that S is constant after reaching 0.9, sufficiently close results can be obtained up to the surge point. Since operation in this range is not stable, only the right portions of the curves are of practical interest.

References

[1] Pye, D. R., *Internal Combustion Engines, Vol. II, Aero-Engines.*

[2] Campbell, K., and Talbert, J. E., *Some Advantages and Limitations of Centrifugal and Axial Compressors*, S.A.E. Transactions, Vol. 53, pp. 607–620, 1945.

Services of the Libraries of the Institute of the Aeronautical Sciences

The services of the Libraries are available to all members of the Institute, to Corporate Members, to advertisers in the AERONAUTICAL ENGINEERING REVIEW and AERONAUTICAL ENGINEERING CATALOG, and, under usual library limitations, to the public. Four specialized services are available.

The Paul Kollsman Lending Library

This lending library service makes available, *without charge*, the latest and more important aeronautical books.

Members may request the loan of any aeronautical or technical book they wish to borrow. Through an exchange agreement with the Engineering Societies Library, any book on general engineering may be borrowed from its great collection of over 160,000 volumes.

A photostating service is available at usual library rates.

Applications for membership in the library and further information will be sent on request.

The W. A. M. Burden Reference Library

This reference library contains over 12,000 aeronautical books, magazines, pamphlets, and reports gathered from world-wide sources and is one of the most complete aeronautical libraries in the world. Material from this library is not available for loan but may be used for reference purposes.

The Pacific Aeronautical Library

7660 Beverly Boulevard
Los Angeles 36, California

Established in cooperation with the aircraft companies the library serves. The leading aircraft companies in or near Los Angeles participate in its support and operation.

This service library for aeronautical research is available to the public for reading privileges. Source material includes aerodynamic and structural research reports, as well as books on drafting, production methods, history, and allied sciences. It furnishes books, periodicals, and pamphlet material to the participating aircraft companies to supplement their engineering libraries.

Technical Information Service

This service has experienced personnel under the supervision of trained aeronautical engineers to compile any information desired. The services range from listing specialized reference books to the preparation of exhaustive bibliographies, digesting of reports, and general surveys of any aeronautical subject. Some of the available services are:

Bibliographies on any aeronautical subject.
Reports on any aeronautical subject.
Digests of aeronautical books, papers, periodicals, and references.
Translations.
Engineering investigations of special aeronautical subjects.
Biographies of individuals engaged in aeronautics.
Photostats of any aeronautical or general engineering material.
Microfilms made on special order.
Photographs made from the Institute's photographic collection.
Drawings and tracings made.

In addition to the services mentioned any commission which comes within the scope of the Service will be accepted. Special arrangements may be made for work requiring several weeks or months.

Translators are available for accurate transcriptions of all foreign language data. Translations are carefully edited by trained engineers.

Reproductions of any material in the collections of the Institute may be ordered at standard photostat rates.

INSTITUTE OF THE AERONAUTICAL SCIENCES, INC.
2 EAST 64th STREET, NEW YORK 21, N.Y.

Readers' Forum

BRIEF REPORTS of important findings in aeronautical sciences and discussions of papers published in the JOURNAL *will be presented in this special department. The publication will be completed 6 to 8 weeks after receipt of the material. No proof will be sent to the authors. The Editorial Committee does not hold itself responsible for the opinions expressed by the correspondents. Contributions should not exceed 800 words in length.*

Transient Phenomena at Sonic Speed

N. Rott
Institute for Aerodynamics, Swiss Federal Institute of Technology, Zürich
March 21, 1949

BY APPLICATION of the linearized theory to the calculation of transient loads of an airfoil of infinite span and of zero thickness, finite results are obtained even at sonic speed, as in the case of harmonic oscillations.[1] With the latter solution as a starting point, the same methods may be applied as in the supersonic case.[2] (Further references are given in reference 2.) As an example, the response of an airfoil to a sharp-edged gust will be calculated for $M = 1$.

If the velocity distribution along the airfoil in the plane $y = 0$, leading edge at $x = 0$, is given by a wave proceeding with the sonic velocity a,

$$v_0 = -\bar{v}e^{ik(at-x)} \tag{1}$$

the corresponding pressure (on the upper side of the airfoil) at sonic speed may be calculated from Eq. (5) of reference 1:

$$p_0 = -\rho a\bar{v}(2\pi iKx)^{-1/2}e^{ik[at-(x/2)]} \tag{2}$$

To represent boundary conditions for an airfoil in a sharp gust with constant upward velocity $\bar{v}$, the step-function is obtained from Eq. (1) by the following operation:[3]

$$v_G = \frac{1}{2\pi}\lim_{\beta=0}\int_{-\infty}^{+\infty}\frac{v_0\,dK}{\beta+iK} = -\bar{v}, \quad x < at \tag{3a}$$

$$= 0, \quad x < at \tag{3b}$$

The corresponding pressure is given by

$$p_G = (1/2\pi)\lim_{\beta=0}\int_{-\infty}^{+\infty} p_0 dK/(\beta+iK)$$

or introducing p_0 from Eq. (2)

$$p_G = -\frac{\rho a\bar{v}}{\sqrt{2\pi x}}\frac{1}{2\pi}\lim_{\beta=0}\int_{-\infty}^{+\infty}\frac{e^{ik[at-(x/2)]}}{(\beta+iK)\sqrt{iK}}\,dK \tag{4}$$

If

$$A(s) = (1/2\pi)\lim_{\beta=0}\int_{-\infty}^{+\infty} e^{iKs}\,dK/(\beta+iK)\sqrt{iK}$$

then the inverse (or Carson's) integral equation for $A(s)$ is[3]

$$1/\sqrt{K} = K\int_0^\infty e^{-ks}A(s)\,ds$$

which is satisfied by

$$A(s) = (2/\sqrt{\pi})\sqrt{s}$$

Applied to Eq. (4), the pressure becomes

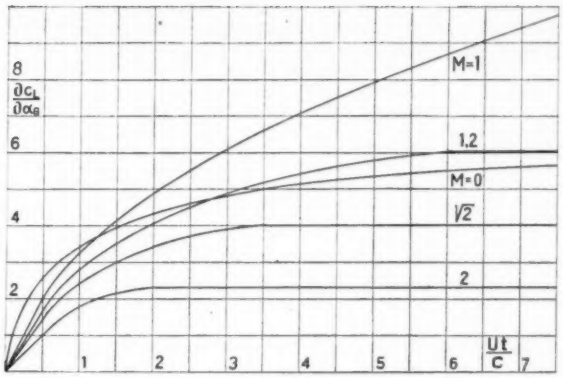

FIG. 1. $\partial C_L/\partial\alpha_G$ vs. Ut/C.

$$p_G = (pa\bar{v}/\pi)\sqrt{(2at/x)-1}, \quad x < 2at \tag{5a}$$

$$= 0, \quad x > 2at \tag{5b}$$

The same result appears also as the limiting case of the supersonic solution.[2] According to Eq. (16) of reference 2, the pressure p_G in a stream of velocity $U = Ma$ $(M > 1)$ is

$$p_G = -\rho a\bar{v}\frac{M}{\sqrt{M^2-1}}, \quad x < (M-1)at \tag{6a}$$

$$= -\rho a\bar{v}\frac{M}{\sqrt{M^2-1}}\frac{\psi}{\pi}, \ (M-1)at < x < (M+1)at \tag{6b}$$

$$= 0, \quad x > (M+1)at \tag{6c}$$

where

$$\cos\psi = M - (M^2-1)at/x \tag{6d}$$

For $M \to 1$, $\cos\psi \to 1$; then ψ must be small so that $\cos\psi \approx 1 - (\psi^2/2)$ or from Eq. (6d)

$$\psi = \sqrt{2(M-1)[(M+1)(at/x)-1]}$$

Introducing this limiting value in Eq. (6b), Eq. (5a) follows for $M = 1$.

For the lift coefficient of an airfoil, with chord c, due to a gust at sonic speed, the following expressions are obtained from Eq. (5) (introducing $\alpha_G = \bar{v}/a$):

$$\partial c_L/\partial\alpha_G = 4at/c, \ at < c/2 \tag{7a}$$

$$= \frac{4at}{c}\frac{\sigma+\sin\sigma}{\pi}, \quad at > c/2 \tag{7b}$$

where

$$\cos\sigma = 1 - (c/at) \tag{7c}$$

For large values of at/c,

$$\partial c_L/\partial\alpha_G \approx (8/\pi)\sqrt{2at/c} \tag{7d}$$

In Fig. 1, $\partial c_L/\alpha_G$ is plotted, together with the corresponding supersonic values given by Miles[2] and the solution of Küssner and von Kármán-Sears for $M = 0$.

The distance d of the center of pressure from the leading edge is given by

$$d/c = at/2c, \quad at < c/2 \tag{8a}$$

$$= (at/2c)\frac{\sigma-\sin\sigma\cos\sigma}{\sigma+\sin\sigma}, \quad at > c/2 \tag{8b}$$

For $at/c \to \infty$, $d/c \to 1/3$.

Sudden changes of the angle of attack may be investigated at sonic speed by the same methods. If the disturbance remains stationary after the sudden change, it is characteristic for all solutions that the pressure grows finally with $\sqrt{t}$. Naturally,

the validity of the results of linearized theory is at least doubtful for $M = 1$, but these finite solutions may suggest again the importance of nonstationary phenomena.

REFERENCES

[1] Rott, N., *Oscillating Airfoils at Mach Number One*, Readers' Forum, Journal of the Aeronautical Sciences, Vol. 16, No. 6, p. 380, June, 1949.

[2] Miles, J. W., *Transient Loading of Airfoils at Supersonic Speeds*, Journal of the Aeronautical Sciences, Vol. 15, No. 10, pp. 592–598, October, 1948.

[3] von Kármán and Biot, *Mathematical Methods in Engineering*; McGraw-Hill Book Company, Inc., New York, 1940.

Quasi-Stationary Thin Airfoil Theory

John W. Miles

Department of Engineering, University of California at Los Angeles

March 17, 1949

THE AERODYNAMIC DERIVATIVES for use in dynamic stability calculations are frequently calculated on the basis of steady flow, the argument being advanced that the motion is small so that nonstationary aerodynamic effects are negligible. This line of reasoning overlooks the fact that the damping forces are first order in frequency, and the quantities neglected may therefore be of the same order of magnitude as these forces. In particular, if ϕ is the velocity potential, the pressure is given by Newton's law as

$$p = -\rho \frac{D\phi}{Dt} = -\rho U \frac{\partial \phi}{\partial x} - \rho \frac{\partial \phi}{\partial t} \tag{1}$$

The first term in this equation is the only one entering stationary airfoil theory, but the second is evidently first order in frequency.

The correct lift and moment coefficients for quasi-stationary (i.e., correct to first order terms in frequency) motion of a two-dimensional thin airfoil may be obtained as limiting cases of the flutter results.[1] In the case of incompressible flow the results are

$$c_l = 2\int_0^\pi \left\{\left[\left(1 - \frac{\pi k}{2}\right) + ik\left(\gamma - \ln\frac{2}{k}\right)\right] \times (1 - \cos\varphi) + ik\sin^2\varphi\right\} \frac{w(-\cos\varphi)}{U}\, d\varphi + 0(k^2 \ln k) \tag{2}$$

$$c_{m_{1/4}} = (1/2)\int_0^\pi [(\cos\varphi - \cos 2\varphi) - ik(1 - \cos\varphi) \times \sin^2\varphi][w(-\cos\varphi)/U]d\varphi + 0\,(k^2 \ln k) \tag{3}$$

$$k = \omega c/2U \tag{4}$$

where γ is Euler's constant ($= 0.577216$), ω is the angular frequency, c is the chord, U is the free stream velocity, $\varphi = 0(\pi)$ specifies the leading (trailing) edge of the airfoil, and w is the local down-wash. If the displacement at a point $x = -(c/2)\cos\varphi$ is $z(x)\exp(i\omega t)$, positive down,

$$w(2x/c) = U(\partial z/\partial x) + i\omega z \tag{5}$$

If k is set equal to zero in Eqs. (2) and (3), they reduce to the well-known Munk formulas.[2] For the case of a simple plunging motion of the airfoil (i.e., $z(x) \equiv 1$), $w(x)$ is of order k, so that the Munk formulas are correct to order $k^2 \ln k$, but in the case of pitching about the quarter chord $\{z = [x + (c/4)]\alpha\}$, Eqs. (2) and (3) yield

$$\frac{\partial c_l}{\partial \alpha} = 2\pi\left\{\left(1 - \frac{\pi k}{2}\right) + ik\left[\frac{3}{2} + \gamma - \ln\left(\frac{2}{k}\right)\right]\right\} + 0(k^2 \ln k) \tag{6}$$

$$\partial c_m/\partial\alpha = -(\pi/2)ik \tag{7}$$

whereas the results given by the Munk formula are

$$\partial c_l/\partial\alpha = 2\pi(1 + ik) \tag{6'}$$

$$\partial c_m/\partial\alpha = -(\pi/4)ik \tag{7'}$$

Since k will generally be quite small (<0.1), the failure of Eq. (6′) to include the logarithmic term is a matter of some importance, for the sign of the imaginary part of $(\partial c_l/\partial\alpha)$ is reversed. While most of the damping in rotary motions of conventional aircraft arises from the plunging motion of the aerodynamic center, an appreciable part is due to rotation about this center—i.e., to the imaginary part of $(\partial c_l/\partial\alpha)$. If the distance from the airplane center of gravity to tail aerodynamic center is five times the mean tail chord, the decrease in total damping calculated on the basis of Eqs. (6) and (7) over that predicted by Eqs. (6′) and (7′) is approximately 38 per cent for $k = 0.01$. For smaller c.g.-tail chord ratios the decrease is, of course, greater. Similarly, the damping in pitch of a swept wing is reduced. The effect of this error in calculating stability derivatives would appear to be most severe in the case of fin damping of small, high-speed aircraft. Thus, most modern jet aircraft tend to "snake," probably due to reduced (damping) effectiveness of the fin. (This problem was evidently not so serious for lower speed aircraft for a number of reasons.)

In conclusion, it should be remarked that compressibility effects in nonstationary flow are not correctly accounted for by simply introducing the Prandtl-Glauert factor $(1 - M^2)^{-1/2}$, since compressibility introduces additional phase lags. The writer has obtained a closed form solution for the Possio integral equation,[3] correct to terms of order $k^2 \ln k$, and hopes to publish the results soon. The quasi-stationary problem for linearized, supersonic flow has been discussed previously.[4]

REFERENCES

[1] Schwarz, L., *Berechnung der Druckverteilung einer harmonisch sich verformenden Tragflache in ebener Stromung*, Luftfahrtforschung, Vol. 17, pp. 379–386, 1940.

[2] Munk, M., *General Theory of Thin Wing Sections*, N.A.C.A. T.R. No. 142, 1922.

[3] Possio, C., *L'Azione Aerodinamica sul Profilo Oscillante in un Fluido Compressibile a Velocita Posonora*, L'Aerotecnica, Vol. 18, pp. 441–458, 1938.

[4] Miles, J. W., *On Harmonic Motion at Supersonic Speeds*, Readers' Forum, Journal of the Aeronautical Sciences, Vol. 16, No. 6, p. 378, June, 1949.

Maneuvering Horizontal Tail Loads

Innes Bouton

McDonnell Aircraft Corporation, St. Louis, Mo.

March 30, 1949

A SEMIRATIONAL EXPRESSION has been derived for use in determining the maneuvering horizontal tail loads for an airplane. This expression has the essential simplicity of the empirical methods now in use but includes in a rational fashion all the factors that vary between different designs. It is derived from consideration of rational methods involving the airplane motion resulting from a given elevator deflection variation with time but eliminates the complicated calculations based on an elevator deflection function that in itself is empirical.

The net maneuvering tail load, P_t, is defined as follows:

$$P_t = \frac{C_{M_{c.g.}} S_W q \bar{c}}{l_t} + \frac{\bar{\theta} I_y}{l_t} \tag{1}$$

where $C_{M_{c.g.}}$ is the airplane pitching moment coefficient about the c.g. at the load factor in question, SB is the wing area, q is the dynamic pressure, $\bar{c}$ is the wing mean aerodynamic chord, l_t is the length from c.g. to tail center of pressure, $\bar{\theta}$ is the maximum or minimum angular acceleration of the airplane in pitch at the load factor associated with $C_{M_{c.g.}}$ used, and I_Y is the airplane

moment of inertia in pitch. The first term in the expression is what is often called the balancing tail load, while the second term is the incremental tail load needed to produce the angular acceleration, $\ddot{\theta}$.

The evaluation of the first term is straightforward, although it is often difficult to determine $C_{M_{c.g.}}$ accurately. It is in the determination of the second term that current methods have a fundamental disagreement.

Methods that specify an arbitrary value of $\ddot{\theta}$ become irrational when statistical data, based on past configurations that were all geometrically and aerodynamically similar, are applied to radically different configurations. For instance, there is a general trend in high-performance airplanes toward sweptback tails with relatively short chord elevators, which results in lower elevator effectiveness. Also the tail area and arm to the c.g. have increased less rapidly than the moment of inertia. Both of these trends result in a decrease in the ability of the horizontal tail to produce airplane angular acceleration.

Methods that determine airplane motion from elevator motion satisfactorily account for the geometric and aerodynamic differences between airplanes, but the methods are tremendously complicated to use, depend on an arbitrary elevator motion, and are extremely critical to minor changes in the pattern of motion. It is satisfactory at low speeds to assume that the elevator is moved as rapidly as possible to the maximum possible deflection as limited by elevator stops or stick force, held at that deflection as needed to develop the maximum load factor, and then reversed to some specified deflection as rapidly as possible. However, at high speeds, what is physically possible becomes psychologically improbable. For instance, in a recent study on a high-speed airplane, extremely high angular accelerations were possible if the maximum load factor were developed in less than 0.2 sec. However, the stick motion is so critical that the continuance of up-elevator motion for 0.02 sec. or three-quarters of one degree more than the critical value would result in exceeding the maximum load factor by 40 per cent. It is certain that the probability of such elevator manipulation is low. Pilots would be restrained in such maneuvers by the danger of exceeding the airplane design load factor. This reduced probability is recognized in some of the current regulations by specifying an angular acceleration inversely proportional to the air speed or by specifying at high speeds an angular acceleration that is a given percentage of the low-speed value.

A formula for $\ddot{\theta}$ which recognizes the variations between airplanes but which uses an empirical constant to be determined statistically is presented below:

$$\ddot{\theta} = B\left[\left(\frac{d\delta_e}{dt}\right)\frac{(dC_L/d\alpha)_t}{(dC_L/d\alpha)_w}\left(\frac{d\alpha}{d\delta}\right)\left(\frac{S_t l_t}{I_y}\right)\left(n\frac{W}{S_w}\right)\left(\frac{i}{V_e}\right)\right]^{1/2} \quad (2)$$

where $\ddot{\theta}$ is in radians per second per second and B is either $+2.5$ or -3.5; $d\delta_e/dt$ is the maximum rate of elevator deflection in degrees per second (discussed further below); $dC_L/d\alpha$ is the lift curve slope of the tail and wing, respectively; $d\alpha/d\delta$ is the elevator "effectiveness"; S_t is the horizontal tail area in square feet, l_t in feet, and I_y in slug feet squared as defined in Eq. (1); n is the maximum load factor reached during the maneuver; W/S_w is the airplane wing loading in pounds per square foot, and V_e the airplane equivalent velocity in miles per hour during the maneuver. All the aerodynamic parameters are determined at the Mach Number of the maneuver.

The $+2.5$ and -3.5 values for B are empirical and subject to revision, although they appear to be approximately correct for data presently available. The plus 2.5 value occurs at the beginning of a maneuver, and the $\ddot{\theta}$ so determined should be used in Eq. (1) in combination with the $C_{M_{c.g.}}$ associated with a load factor of 20 to 50 per cent of the maximum load factor reached in the maneuver. In all cases, the load factor used in Eq. (2) in determining $\ddot{\theta}$ is the maximum load factor encountered in the maneuver, even though the balancing part of the tail load is determined at some lesser load factor. The -3.5 value for B occurs at the time of maximum load factor, and the tail load angular acceleration increment so determined is combined with balancing tail load at the maximum load factor of the maneuver.

In comparing experimental data with this formula, the maximum rate of elevator deflection $d\delta_e/dt$, which occurs during the period immediately preceding the peak value of $\ddot{\theta}$, should be used in the expression. For computing a value of $\ddot{\theta}$ for use in design, it is suggested that a value of $d\delta_e/dt$ of 75° per sec. be used, even though higher rates are physically possible. The higher rates do not seem to result in appreciably higher loads. However, if the elevator rate is restricted to some lesser value, as may be the case in power-operated controls, the lesser value should be used. It is also possible that the 75° per sec. rate should be lower for extremely large airplanes, such as transports or bombers, but it is believed that the lower load factor to which these large airplanes are designed will reduce the $\ddot{\theta}$ in the proper proportion through the n term in the Eq. (2).

To date, all experimental data compared with this formula have been within the limits of the $+2.5$ and -3.5 values for B, as have all calculated values made from elevator deflections consistent with the philosophy of this method. The writer would be interested in learning of values of loads or angular accelerations higher than those determined by the equations above.

A Note on Detached Shock Waves

E. V. Laitone
University of California, Berkeley, Calif.
March 15, 1949

In reference 1, a Taylor series expansion is obtained for the distance of a detached shock wave in front of a body of revolution. It would be of interest to compare these results with those of reference 2, wherein a simple approximation locates the distance (S) of the normal portion of the detached shock wave ahead of the nose of the body (see Fig. 1). This approximation assumes that the subsonic velocity on the streamline along the axis of symmetry approaching the stagnation point downstream of the detached shock wave is the same as for incompressible flow with the proper boundary conditions. Because of symmetry,

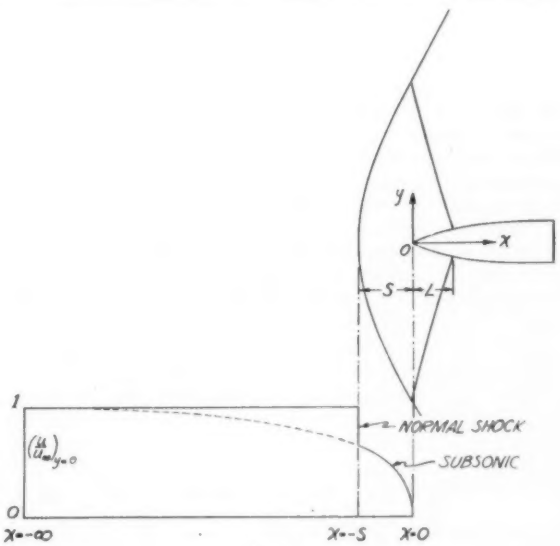

Fig. 1.

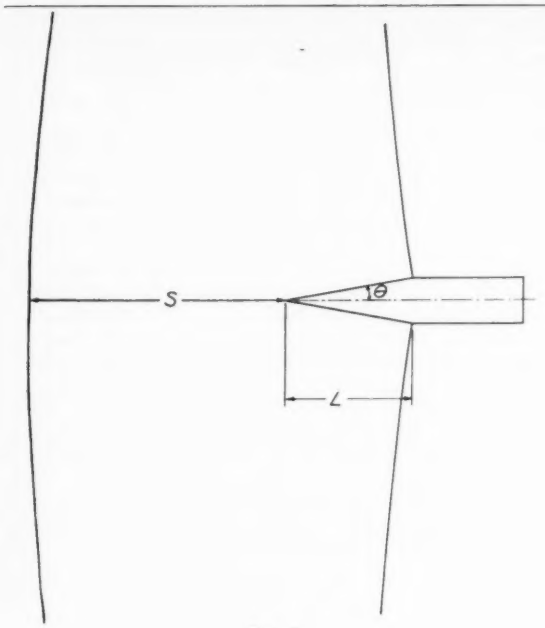

FIG. 2.

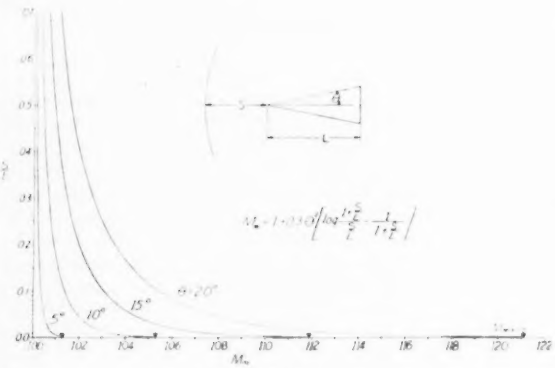

FIG. 3.

the portion of the detached shock wave through which this streamline passed was a normal shock wave. For each free-stream supersonic Mach Number (M_∞), this normal shock wave produces a known decrease to a subsonic velocity. This locates the normal portion of the detached shock wave as shown in Fig. 1. Since the distance L of the sonic line could not be easily determined, its effect was generally neglected in reference 2.

Applying the method of reference 2 to a sharp nose slender body one obtains along the streamline leading to the stagnation point

$$\frac{1}{\gamma+1}\left[\frac{2}{M^2_\infty}+(\gamma-1)\right]=\frac{u}{u_\infty}=1-\frac{1}{2}\int_0^L\frac{y'(x)y(x)dx}{(S+x)^2} \quad (1)$$

for a body of revolution and

$$1-\frac{4}{\gamma+1}(M_\infty-1)\approx\frac{u}{u_\infty}\approx 1-\frac{1}{\pi\sqrt{M_\infty{}^2-1}}\times\int_0^L\frac{y'(x)dx}{(S+x)} \quad (2)$$

for a two-dimensional body. These subsonic velocity variations include only the first order compressibility effects as obtained from linearized theory (see, for example, reference 3). An additional approximation in Eq. (2) is that $(M_\infty - 1)$ is small so that behind the normal shock wave

$$\sqrt{1-M^2}=\sqrt{M_\infty{}^2-1}$$

as shown in reference 2.

Now, in reference 4, it is shown that Eq. (1) can be rigorously applied to the limiting case of a very slender cone as the supersonic free-stream Mach Number approaches unity. For a cone the sonic line is always formed near the shoulder of the cone. In the limiting case of a slender cone near a free-stream Mach Number of unity, this sonic line approaches a limiting value given by a straight line normal to the cone axis and extending an unlimited distance from the shoulder of the cone (see Fig. 2). Similarly, the limiting value approached by the detached shock wave is another straight line normal to the cone axis but an unlimited distance ahead of the nose of the cone as indicated in Fig. 2. For this case the subsonic flow region is effectively of unlimited extent, and it is shown in reference 4 that the boundary conditions are satisfied by Eq. (1) for $y(x) = \theta x$ and $y'(x) = \theta$, so that

$$1-\frac{\theta^2}{2}\left\{\log\left(\frac{1+(S/L)}{S/L}\right)-\frac{1}{1+(S/L)}\right\}=\frac{1}{\gamma+1}\times\left[\frac{2}{M_\infty{}^2}+(\gamma-1)\right]\approx 1-\frac{4}{\gamma+1}(M_\infty-1) \quad (3)$$

The additional approximation in Eq. (3) assumes that $(M_\infty - 1)$ is small so only its first power is retained (see reference 2).

Then, for air, we have $\gamma = 1.400$, so Eq. (3) may be written

$$M\approx 1+0.3\theta^2\left\{\log\left[\frac{1+(S/L)}{S/L}\right]-\frac{1}{1+(S/L)}\right\} \quad (4)$$

This variation of the detached shock wave location (s) with the free-stream Mach Number (M_∞ is shown in Fig. 3 for various values of the semivertex angle (θ) of a conical nose of length L. The minimum values of the free-stream Mach Number for which a conical shock wave becomes attached to the conical nose are also shown in Fig. 3 by means of a small arrow.

REFERENCES

[1] Dugundji, John, *An Investigation of the Detached Shock in Front of a Body of Revolution*, Journal of the Aeronautical Sciences, Vol. 15, No. 12, pp. 699–705, December, 1948.

[2] Laitone, Edmund V., and Pardee, Otway O., *Location of Detached Shock Waves in Front of Bodies Moving at Supersonic Speeds*, N.A.C.A. Research Memorandum No. A7B10 May 6, 1947 (N.A.C.A–A.C.R., 1945).

[3] Sauer, Robert, *Theoretical Gas Dynamics*, pp. 39 and 47; J. W. Edwards, Ann Arbor, 1947.

[4] Laitone, E. V., *The Detached Shock Wave in Front of a Conical Nose at Supersonic Speeds*, paper presented at the 1948 Annual Meeting of the American Physical Society, January 27, 1949.

Errata—Aerodynamic Forces on an Oscillating Flap at Supersonic Speeds

John W. Miles
Department of Engineering, University of California at Los Angeles
April 13, 1949

THE FOLLOWING ERRORS have been found in my paper (JOURNAL OF THE AERONAUTICAL SCIENCES, Vol. 15, No. 9, pp. 565–568, September, 1948).

(a) The ordinates of Figs. 4 and 5 should be labelled $[2/(1-c)]^2k^2R_{b\beta}$ and $[2/(1-c)]^2k^2I_{b\beta}$, respectively.

(b) Eq. (20) should read

$$A'_{ja}(K,M,c) = \left(\frac{1-c}{2}\right)\left(1+\frac{j}{k}\right)A'_{ba}(k,M,c) - \left(\frac{1+c}{2}\right)^{j}\left[A_{aa}\left(\frac{1+c}{2}k,M\right) + A_{ca}\left(\frac{1+c}{2}k,M\right)\right]$$

(c) Eq. (22) should read

$$A_{ja}(k,M,c) = A_{aa}(k,M) + cA_{ca}(k,M) - \left(1+\frac{j}{k}\right)\left(\frac{j+c}{2}\right)\left(\frac{j+c}{2}\right)^{3}\left[A_{ab}\left(\frac{1+c}{2}k,M\right) + A_{cb}\left(\frac{1+c}{2}k,M\right)\right] - \left(\frac{1+c}{2}\right)^{j}\left[A_{aa}\left(\frac{1+c}{2}k,M\right) + A_{ca}\left(\frac{1+c}{2}k,M\right)\right]$$

The numerical results given in the paper are rather inaccurate (particularly those for R_{ba} and I_{ba}), and more accurate results are referenced in a recent report by Biot, et al.[1]

REFERENCE

[1] Karp, S. N., Shu, S. S., Weil, H., and Biot, M. A., *Aerodynamics of the Oscillating Airfoil in Compressible Flow*, F-TR-1167-ND (October, 1947) and F-TR-1195-ND (June, 1948), Hq., A.M.C. Wright Field, Dayton, Ohio.

A Method for Accelerating the Convergence of an Iteration Procedure

Gabriel Isakson
Aero-Elastic and Structures Research Laboratory, Massachusetts Institute of Technology, Cambridge, Mass.
April 4, 1949

IN MOST PROBLEMS in which an iteration or successive approximation procedure is used in order to obtain a solution, the rate of convergence decreases as the iteration proceeds. Consequently, high orders of accuracy become increasingly difficult to achieve, and a large number of iterations may be required. In such problems a great deal of time and labor may be saved if the values in a small number of successive approximations can be used to predict the final correct value.

In the present method the assumption is made that the successive values obtained in an iteration procedure follow closely the form of a simple exponential approaching its asymptote. That is, if one value is considered as being the first in a series, the value obtained after the nth subsequent iteration is given by,

$$x = X + Ae^{-an} \tag{1}$$

where X is the asymptotic value and A and a are constants. If x_0, x_1, and x_2 are three values obtained in successive iterations, we may write,

$$x_0 = X + A \tag{2}$$

$$x_1 = X + Ae^{-a} \tag{3}$$

$$x_2 = X + Ae^{-2a} \tag{4}$$

Subtracting Eq. (3) from Eq. (2) gives,

$$x_0 - x_1 = A\,(1 - e^{-a}) \tag{5}$$

Subtracting Eq. (4) from Eq. (3) gives,

$$x_1 - x_2 = Ae^{-a}(1 - e^{-a}) \tag{6}$$

Dividing Eq. (6) by Eq. (5),

$$(x_1 - x_2)/(x_0 - x_1) = e^{-a} \tag{7}$$

Substituting Eq. (7) into Eq. (5) we obtain,

$$A = \frac{x_0 - x_1}{1 - [(x_1 - x_2)/(x_0 - x_1)]} = \frac{(x_0 - x_1)^2}{x_0 - 2x_1 + x_2} \tag{8}$$

Substituting Eq. (8) into Eq. (2) yields, finally,

$$X = x_0 - [(x_0 - x_1)^2/(x_0 - 2x_1 + x_2)] \tag{9}$$

It is thus seen that the asymptotic value may be simply determined from three successive approximations. This asymptotic value will not, in general, be the true value being sought, but it will frequently lie much closer to it than the three values from which it was derived. If greater accuracy is required, the value obtained in this way may be used as the starting point for subsequent iterations and further acceleration.

It should be noted that the calculation involves small differences between successive approximate values, so that a fairly large number of significant figures must be carried if accuracy is to be achieved.

The method has been applied successfully in the matrix iteration procedure for determining the natural mode shapes and frequencies of vibration of an elastic system. The convergence of the mode coefficients to their correct value is accelerated in this manner, and it has been found that in many cases two or more significant figures are gained in each acceleration cycle. It is frequently necessary to defer the acceleration till five or six iterations have been performed, since the variation in the first two or three iterations is sometimes erratic.

In some iteration solutions successive values oscillate about an asymptote. In such cases the acceleration cannot be applied directly to successive values but may be applied to alternate values. A simple rough test for the applicability of the method is that the difference between the second and third values should be of the same sign and somewhat smaller than the difference between the first and second values in the sequence.

It is interesting to note that Aiken's δ^2 process,[1] developed specifically for application to matrix iteration in the solution of characteristic value problems, yields the same expression as Eq. (9).

REFERENCE

[1] Aitken, A. C., *Studies in Practical Mathematics*, Part III, p. 269: Proceedings of the Royal Society of Edinburgh, 1936–1937.

On the Compressibility Correction Factor for Axially Symmetric Bodies

W. H. Dorrance
Research Associate in Aerodynamics, Aeronautical Research Center, University of Michigan, Ann Arbor, Mich.
March 31, 1949

SEVERAL PAPERS have appeared dealing with the problem of the application of the Prandtl-Glauert method to subsonic compressible flow over three-dimensional bodies.[1–4] Attempts have been made using this notion to establish a compressibility correction factor for three-dimensional bodies similar to the familiar compressibility correction factor $(1 - M^2)^{-1/2}$ applied to two-dimensional bodies. It is generally agreed that the Prandtl-Glauert method will not yield a universal correction factor for three-dimensional bodies which is independent of the shape of the body. It is also generally agreed that the effects of compressibility on the surface pressures of a body in a subsonic stream become less pronounced as the body is made more slender. This latter behavior has been illustrated by examining the maximum surface velocity in the field of flow about ellipsoids while varying thickness ratios, aspect ratios, and free-stream subsonic Mach Number.

The statement is made by Sauer[5] that, to a first approximation, the surface pressures over a slender axially symmetric body

of revolution situated in a compressible stream remain unchanged from the surface pressures experienced in an incompressible stream at the same velocity. This statement is supported by an analysis employing appropriate source-sink distributions to approximate the presence of a body in the stream.

The mechanisms of this particular analysis remain somewhat obscure. The purpose of this note is to present a clearer illustration of the statement that to a first approximation there is no effect of compressibility on the surface pressures of a slender axially symmetric body in a subsonic stream.

The partial differential equation of continuity for the perturbation velocity potential in an incompressible stream in cylindrical coordinates is, for axially symmetric flow:

$$\frac{\partial^2\phi'}{\partial x'^2}+\frac{\partial^2\phi'}{\partial r'^2}+\frac{1\partial\phi'}{r'\partial r'}=0 \tag{1}$$

where ϕ' = antigradient of perturbation velocities. A general solution of Eq. (1) is

$$\phi'=-\frac{1}{4\pi}\int_{-c/2}^{c/2}\frac{f(\xi)d\xi}{\sqrt{(x'-\xi)^2+r'^2}} \tag{2}$$

where $f(\xi)$ is a function representing the strength distribution of sources and sinks distributed continuously along the x-axis between the vertex of any given body at $x'=-c/2$ and the end of the body at $x'=c/2$.

Prandtl and Glauert are credited with introducing the following affine transformation relating the incompressible space x', r', ω' with a compressible space x, r, ω

$$\left.\begin{aligned} x &= x' \\ r &= 1/\beta\, r' \\ \omega &= \omega' \\ \phi &= K\phi' \end{aligned}\right\} \tag{3}$$

where K is any multiplying factor.

Employing this transformation in conjunction with Eq. (1), there results the linearized partial differential equation of continuity for the perturbation velocity potential in a compressible stream for axially symmetric flow.

$$\beta^2\frac{\partial^2\phi}{\partial x^2}+\frac{\partial^2\phi}{\partial r^2}+\frac{1}{r}\frac{\partial\phi}{\partial r}=0 \tag{4}$$

where $\beta=\sqrt{1-M^2}$ and M = free-stream Mach Number. Corresponding to Eq. (2), a solution to Eq. (4) using transformation (3) is

$$\phi=-(K/4\pi)\int_{-c/2}^{c/2}f(\xi)\,d\xi/\sqrt{(x-\xi)^2+\beta^2r^2} \tag{5}$$

Eq. (5) for slender bodies is subject to the boundary condition that the flow at the body surface must be tangent to the body surface.

$$\phi_r/(U+\phi_x)=(\phi_r/U)_{r\to 0}=\tan\theta \tag{6}$$

where θ = angle between tangent to surface of body and x-axis and U = free-stream velocity.

If the given body is to retain its shape no matter what the variation of free-stream Mach Number, then

$$\tan\theta=(\phi_r/U)_{r\to 0}=\text{constant} \tag{7}$$

Returning to Eq. (5)

$$\phi_r=\frac{K\beta^2r}{4\pi}\int_{-c/2}^{c/2}\frac{f(\xi)d\xi}{[(x-\xi)^2+\beta^2r^2]^{3/2}} \tag{8}$$

This integral is to be evaluated as r approaches a small quantity hereafter designated as $r\to\epsilon$. This can be done in a more lucid manner than the process employed by Sauer.[5]

$$\phi_r=\frac{K}{4\pi r}\int_{-c/2}^{c/2}\frac{f(\xi)\,(d\xi/\beta r)}{\{[(x-\xi)/\beta r]^2+1\}^{3/2}} \tag{9}$$

let

$$\frac{x-\xi}{\beta r}=t,\qquad \frac{x+(c/2)}{\beta r}=a,\qquad \frac{x-(c/2)}{\beta r}=b$$

then

$$\phi_r=-\frac{K}{4\pi r}\int_a^b f(x-\beta rt)\frac{dt}{(t^2+1)^{3/2}} \tag{10}$$

Eq. (10) is evaluated now as $r\to\epsilon$ by taking advantage of the mean value theorem. As $r\to\epsilon$, $a\to\infty$, $b\to-\infty$, and $f(x-\beta rt)\to f(x_1)$, where x_1 is some value of x between $x=c/2$ and $x=c/2$

$$(\phi_r)_{r\to\epsilon}=\frac{-Kf(x_1)}{4\pi r}\int_{\infty}^{-\infty}\frac{dt}{[t^2+1]^{3/2}}=\frac{Kf(x_1)}{2\pi r} \tag{11}$$

Eq. (11), with eq. (7), yields

$$Kf(x_1)/2\pi r=U\tan\theta \tag{12}$$

Eq. (12) illustrates that no compensating factor K containing Mach Number is needed in the equation to preserve the required independence of Mach Number.

Within the rigor of the linearization implied in Eq. (4), the expression for the ratio of the compressible stream pressure coefficient to the incompressible stream pressure coefficient at any subsonic free stream velocity U is

$$(C_{p_m})_{r\to\epsilon}/(C_{p_0})_{r'\to\epsilon'}=u/u' \tag{13}$$

From Eqs. (2) and (5) for slender bodies with $K=1$,

$$(\phi'_{x'})_{r'\to\epsilon'}=(\phi_x)_{r\to\epsilon}=\frac{1}{4\pi}\int_{-c/2}^{c/2}\frac{\pm f(\xi)d\xi}{(x-\xi)^2} \tag{14}$$

and therefore,

$$(C_{p_m})_{r\to\epsilon}=(C_{p_0})_{r'\to\epsilon'} \tag{15}$$

The practical importance of this knowledge lies in the consideration of the effects of thickness ratio or aspect ratio on the compressibility phenomena. Simply stated, the more slender the body, the less apparent are the effects of compressibility. Thus the airflow over fuselages will be less influenced by the consideration of the compressibility effects than will the airflow over wing and tail surfaces with higher aspect ratio.

References

[1] Goethert, B., *Plane and Three-Dimensional Flow at High Subsonic Speeds*, N.A.C.A. T.M. No. 1105, Reprint, October, 1946.

[2] Goethert, B., *Several Remarks on Prandtl's Rule With Regard to Two- and Three-Dimensional Flow*, U.S.A.A.F. Translation No. F-TS-1514-RE April, 1947.

[3] Lees, Lester, *A Discussion of the Application of the Prandtl-Glauert Method to Subsonic Compressible Flow over a Slender Body of Revolution*, N.A.C.A. T.N. No. 1127, September, 1946.

[4] Hess, Robert V., and Gardner, Clifford S., *Study by the Prandtl-Glauert Method of Compressibility Effects and Critical Mach Number of Ellipsoids of Various Aspect Ratios and Thickness Ratios*, N.A.C.A. T.N. No. 1792, January, 1949.

[5] Sauer, R., *Theoretical Gas Dynamics*, pp. 36–51; reprinted by Edward Brothers, Ann Arbor, 1947.

Structural Design for Minimum Weight

H. L. Cox

National Physical Laboratory, Teddington, Middlesex, England

April 2, 1949

I HAVE READ with great interest Mr. Shanley's paper (in the March, 1949, issue of the JOURNAL OF THE AERONAUTICAL SCIENCES) on the "Principles of Structural Design for Minimum Weight." The conclusions regarding the most economical de-

sign for tubes in bending are particularly interesting. It seems that, if the allowable stress decreases with t/D when that ratio tends to zero and if it tends to an upper limit when t/D is moderately large, the optimum working stress and the optimum value of t/D depend only on the material and the form of construction and not at all on the value of the bending moment. Moreover, it appears that the optimum stress cannot differ much from about half the upper limiting value. Broad conclusions of this nature are obviously of great value to designers, so that it would be worth while to extend the analysis to further representative types of construction.

A point that is insufficiently emphasized in Mr. Shanley's reference 2 is that the frame spacing in itself does not seriously affect the structure weight of a stiffened panel—that is, the difference in weight between two optimum structures, one with a few fairly heavy frames (ribs) and the other with more numerous lighter ones, is not marked. If this conclusion may be applicable also to stiffened tubes in bending, and it seems that it should be, the effect of frame spacing in itself may be less than appears from Fig. 21.

It is gratifying to note that the nomenclature and notation for analysis of problems in design are becoming standardized. For my part I shall be glad to adopt "structural index" in preference to "structure loading coefficient"; but I cannot refrain from pointing out a lapse by Mr. Shanley himself at the bottom of the second column on page 138!

In conclusion, I must express my entire concurrence in all Mr. Shanley's conclusions and recommendations.

Effect of Rotary Inertia on Higher Modes of Vibration

Henry E. Fettis
Air Materiel Command, Wright-Patterson Air Force Base, Dayton, Ohio

March 24, 1949

THE PROBLEM OF THE EFFECT of rotary inertia on the transverse bending vibration modes of aircraft wings is one that is frequently neglected when analyses are made. Perhaps one reason is the lack of a convenient method for accounting for this additional effect. In a recent note (JOURNAL OF THE AERONAUTICAL SCIENCES, Vol. 15, No. 7, p. 425) Professor Scanlan has presented a simple and straightforward method of handling this problem. In this investigation, as well as in others where the question of rotary inertia is mentioned, the results are confined to the effect on the primary mode only, for which the effect on frequency and mode shape is negligible even when the inertia is extremely large. The reader is thus led to the erroneous conclusion that the additional work involved is not warranted in view of the slight change that results. However, when the effect is included in the second and higher modes, it is found that a surprisingly large change occurs both in the frequency and in the mode shape. To illustrate this, Professor Scanlan's example is employed, and the second modes are computed for varying amounts of inertia.

From the theory of matrices, it is known that the primary mode of the matrix may be suppressed by subtracting from the original matrix the matrix

$$\begin{bmatrix} \delta_F(1,4) \\ \delta_F(2,4) \\ \delta_F(3,4) \\ \delta_F(4,4) \\ \delta_F(4,4) \end{bmatrix} \begin{bmatrix} m_1 & & & & \\ & m_2 & & & \\ & & m_4 & & \\ & & & m_4 & \\ & & & & I_4 \end{bmatrix} \begin{matrix} \{y_1^{(1)},\ y_2^{(1)},\ y_3^{(1)},\ y_4^{(1)},\ y_4'^{(1)}\} \\ \\ \\ \\ (y_4^{(1)} = 1) \end{matrix}$$

where $[y_i^{(1)}]$ is the first mode.

By carrying out this reduction process and iterating the second mode matrices for various values of the tip weight moment of inertia, the following results are obtained:

I	0	3,000 lb.in.^{2}	27,000 lb.in.^{2}	36,000 lb.in.^{2}
$y_1^{(2)}$	2.11	1.48	0.531	0.464
$y_2^{(2)}$	3.82	2.82	1.225	1.096
$y_3^{(2)}$	1.00	1.00	1.00	1.00
$y_4^{(2)}$	−4.98	−3.53	−0.632	−0.304
$y_4'^{(2)}$	...	−0.275	−0.111	−0.091
ω_2	3,310 c.p.m.	3,047 c.p.m.	1,961 c.p.m.	1,791 c.p.m.
Per cent change	...	10	40	46

The reduction in frequency is now seen to be nearly 50 per cent for I = 36,000 lb.in.,^{2} and the effect on the mode shape is also large. The deflections are normalized to unity at station 3 rather than at the tip, since the tip amplitude approaches zero as I is increased. It is, in fact, possible to obtain zero deflection at the tip without the presence of an infinite mass, a result that could not occur if rotary inertia were neglected. This is brought out by computing the second mode for I = 54,000 lb.in.,^{2} which yields the following shape:

$$\begin{aligned} y_1^{(2)} &= 0.379 \\ y_2^{(2)} &= 0.951 \\ y_3^{(2)} &= 1.000 \\ y_4^{(2)} &= 0.097 \\ y_4'^{(2)} &= -0.066 \end{aligned}$$

(ω_2 = 1.575 cycles per min.). In this case all the tip amplitude is positive, while for I = 36,000 the tip amplitude is negative, indicating that for some intermediate value of I the tip amplitude will be zero.

The Rolling and Yawing Moments Due to Yaw of Unswept Wings

R. F. Anderson
Northrop Aircraft, Inc., Hawthorne, Calif.

March 24, 1949

IN MAKING ESTIMATES of the rolling and yawing moments due to yaw of wings with sweep, the increment due to sweep is

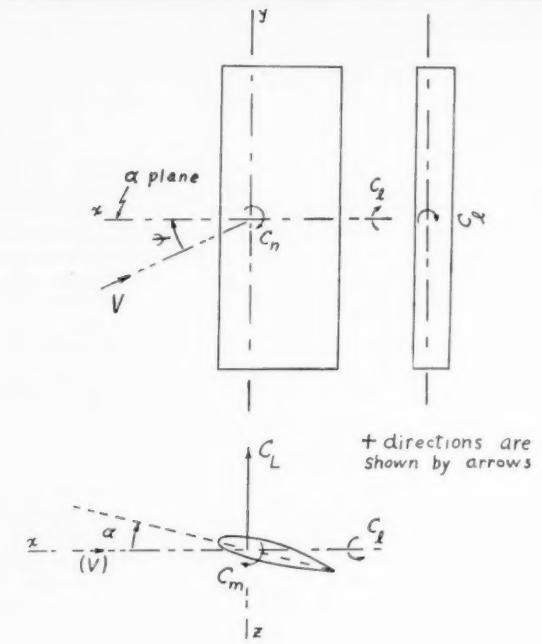

Fig 1. Axes and conventions.

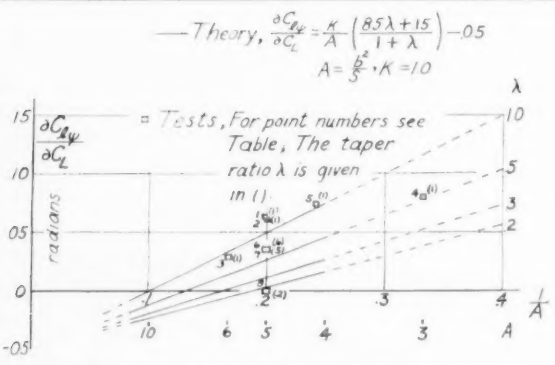
—Theory, $\frac{\partial C_{l_\psi}}{\partial C_L} = \frac{K}{A}\left(\frac{8.5\lambda+15}{1+\lambda}\right) - .05$
$A = \frac{b^2}{S}$, $K = 1.0$
□ Tests, For point numbers see Table, The taper ratio λ is given in ( ).
$\frac{\partial C_{l_\psi}}{\partial C_L}$
radians
λ
A

Fig2 The rolling moment derivative of unswept wings

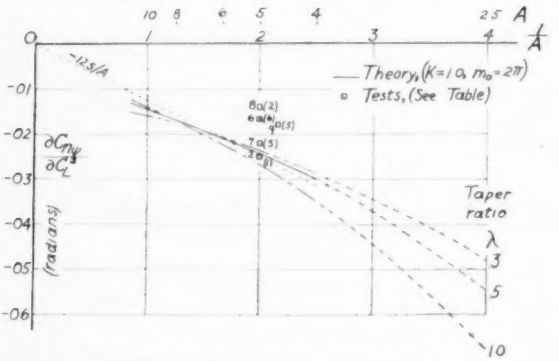

Fig3 The yawing moment derivative of unswept wings

usually added to the value for the unswept wing. For an unswept wing at an angle of yaw, there is an unsymmetrical lift distribution.[1] Rolling and yawing moments result, and formulas for their values have been obtained by Weissinger.[1] However, reference 1 contains errors, and, although corrections were made in reference 2, it is not readily available in clearly printed form. Certain errors were also made in American reports. It is the purpose of this letter to give the correct formulas and to make comparisons with some experimental data.

Symbols

- α = angle of attack measurement in the plane of symmetry, rad.
- ψ = angle of yaw, rad. (see Fig. 1 for positive direction)
- A = aspect ratio
- c_r = root chord
- c_t = tip chord
- λ = taper ratio = c_t/c_r
- K = a constant depending on the spanwise flow component (tip shape)
- C_L = lift coefficient
- C_l = rolling moment/qSb, stability axes (see Fig. 1)
- C_{l_ψ} = $\partial C_l/\partial\psi$
- C_{l_0} = the rolling moment coefficient at zero lift
- C_{m_0} = the pitching moment coefficient at zero lift (about the stability axis)
- C_n = yawing moment/qSb
- C_{n_ψ} = $\partial C_n/\partial\psi$
- C_{n_0} = the yawing moment coefficient at zero lift
- m = the wing lift curve slope in radians (at zero yaw)
- m_0 = the airfoil section lift curve slope, rad.

The Rolling Moment

In carrying out the integrations to find the rolling moment, errors were made on page 51 of reference 1. A value of a constant of 0.29 was obtained instead of 0.15. The constant is given correctly in references 2 and 3, and the formula for the rolling moment derivative is then

$$\frac{\partial C_{l_\psi}}{\partial C_L} = \frac{K}{A}\left\{\frac{1 + 0.15\,[(c_r/c_t) - 1]}{(c_r/c_t) + 1}\right\} - 0.05 \qquad (1)$$

This is for a wing with linear taper, and K is a constant that depends on tip shape (spanwise flow component). If the taper ratio is now defined as $\lambda = c_t/c_r$, then Eq. (1) may be written:

$$\frac{\partial C_{l_\psi}}{\partial C_L} = \frac{K}{A}\left(\frac{0.85\,\lambda + 0.15}{1 + \lambda}\right) - 0.05 \qquad (2)$$

The sign and symbol conventions are shown in Fig. 1.

For an elliptical wing,[1]

$$\frac{\partial C_{l_\psi}}{\partial C_L} = 0.27\left[\frac{K}{A} - \frac{\ln(4\pi A) - 2}{A + 4}\right] \qquad (3)$$

Weissinger states that the value of K may vary between 1.0 and 1.5. For rectangular wings of aspect ratio 5, a value of 1.2 gave reasonable agreement with tests[2] (with the yawing moment also considered).

A comparison of the theory and a few tests is shown in Fig. 2. In the formula, K was taken equal to 1.0 for convenience in computing. The lines are drawn dashed beyond aspects ratios 4 and 12, since the formula is valid only between those limits. The test data are for the initial straight portion of the C_l curves—i.e., from $C_L = 0$ to about 0.5. The theory and tests are in reasonable agreement if it is considered that for swept wings the discrepancies are small compared to the effect of sweep.

The Yawing Moment

Weissinger's formula for the yawing moment due to yaw contains a constant 0.02 in reference 1, which is corrected to 0.084 in references 2 and 3. Conversion from the half span to the span gives 0.042, and the formula for the yawing moment derivative may be written:

TABLE OF TEST DATA PLOTTED ON FIGS. 2 AND 3

Pt. No.	A.R.	c_t/c_r	Section[3]	Tip Shape	Reference	Remarks
1	5.02	1.0	23012	Revolved	*T.N. 1046*, Fig. 38[1]	No tares
2	5	1.0	23012	Revolved	Jacobs, U.M. 2069	Table 2, page 16[2]
3	6	1.0	0012	Square	*RM L7D23*[1]	Fig. 36
4	3	1.0	0012	Square	*RM L7D23*[1]	Fig. 36
5	4.13	1.0	23012	Revolved	*T.N. 1046*, Fig. 38[1]	No tares
6	5	0.6	23012	Revolved	Jacobs, *U.M. 2069*	Table 2[2]
7	5	0.5	0012	Revolved	Weissinger, *U.M. 1392*	Fig. 7
8	5	0.2	23012	Revolved	Jacobs, *U.M. 2069*	Table 2[2]
9	4.62	0.5	0015 to 23009	Revolved	McCormack, *RM A6K15*[1]	Fig. 22

[1] N.A.C.A. Reports.
[2] Rolling moment, Fig. 16; yawing moment, Fig. 17.
[3] N.A.C.A.

$$\frac{\partial C_{n\psi}}{\partial C_L{}^2} = -\left[\frac{K}{A}\left(\frac{0.85\lambda + 0.15}{1+\lambda}\right) - 0.05 + 0.042 \times \frac{A(1+\sqrt{1/\lambda})}{A+2}\right]\frac{1}{m} \quad (4)$$

This is for a wing with linear taper and no flaps or camber The value of m may be taken as the lift curve slope of the unyawed wing (in radians). In Eq. (4) the substitution

$$\alpha C_L = C_L{}^2/m$$

has been made.

For the elliptical wing the formula is:

$$\frac{\partial C_{n\psi}}{\partial C_L{}^2} = -0.27\left[\frac{K}{A} + \left(\frac{A-2}{A+2}\right)\frac{\ln(4\pi A) - 2}{A+4}\right]\frac{1}{m} \quad (5)$$

where the sign after K/A has been changed from $-$ to $+$ from reference 1 to reference 2.

A comparison of a few tests with the theory as given by Eq. (4) is shown in Fig. 3. A value of $K = 1.0$ was again used for convenience. Values of m were obtained from reference 4 using $m_0 = 2$.

In Fig. 3 the agreement between theory and tests is not so good as for the rolling moment. This is unfortunate in view of the fact that the yawing moment due to yaw of the unswept wing is large compared to the increment due to sweep.

The calculated yawing moment (Fig. 3) does not vary much with taper ratio for aspect ratios—say, between 5 and 8. This suggests the use of a constant factor for making rough estimates. For example, the relation $\partial C\sqrt{n_\psi}/\partial C_L{}^2 = -0.125/A$ could be used. This line is drawn on Fig. 3.

A similar relation due to Hoerner[5] was given on page 29 of reference 6. Even though Hoerner's formula agrees with some tests, its derivation was erroneous.

The foregoing formulas apply strictly to wings without camber or flaps—i.e., to wings for which $C_{m_0} = 0$. For wings with camber or flaps, zero lift terms should be added. The rolling moment increment[2,3,7] is given approximately by

$$\partial C_{l_0}/\partial\psi = C_{m_0}/A \quad (7)$$

Fair experimental verification was obtained in reference 2, Fig. 5. However, agreement was not so good in reference 3.

The value of $\partial C_{n_0}/\partial\psi$ is not given explicitly but would appear to be related to the distribution of profile drag along the span.

REFERENCES

[1] Weissinger J., *Der schiebende Tragfluegel bei gesunder Stroemung*, L.G.L. Bericht S.2, Preisausschreiben, 1938/39.

[2] Weissinger, J., *Ergaenzungen und Berichtigungen zur Theorie des schiebenden Fluegels*, Vorabdrucke, Jahrbuch 1943 der deutschen Luftfahrtforschung.

[3] Thiel, G., and Weissinger, F., *Six-Component Measurements on a Straight and a 35° Swept-Back Trapezoidal Wing with and without Split Flap*, N.A.C.A. T.M. No. 1107, 1947.

[4] Swanson, R. S., and Crandall, S. M., *Lifting-Surface-Theory Aspect-Ratio Corrections to the Lift and Hinge Moment Parameters for Full-Span Elevators on Horizontal Tail Surfaces*, N.A.C.A. T.N. No. 1175, February, 1947.

[5] Hoerner, S., *Forces and Moments on a Yawed Airfoil*, N.A.C.A. T.M. No. 906.

[6] Toll, T. A., and Queijo, M. J., *Approximate Relations and Charts for Low-Speed Stability Derivatives of Swept Wings*, N.A.C.A. T.N. No. 1581.

[7] Multhopp, H., *Die Anwendung der Tragflugeltheorie auf Fragen der Flugmechanik*, L.G.L. Bericht S.2, Preisausschreiben, 1938/39.

Importance of Intermolecular Forces at Low Specific Volumes in the Steady, One-Dimensional Flow of a Gas

Lester Lees

Associate Professor of Aeronautical Engineering, Princeton University, Princeton, N.J.

April 4, 1949

IN THE READERS' FORUM for March, 1949 (pages 190–191), Prof. J. D. Schetzer calls attention to the effect of variations in the specific heats with temperature on the gas dynamic relations for one-dimensional flow. However, in presenting the results of the calculations, no mention is made of the effects of intermolecular forces, as expressed in the dependence of internal energy on volume, or the dependence of enthalpy on pressure. Particularly at low specific volumes, these effects can easily be large enough so that under certain conditions the "corrections" to the perfect-gas relations are of opposite sign to those predicted by Professor Schetzer's calculations. For example, in an isentropic expansion the enthalpy change is given by

$$dH = c_p dT + (\partial H/\partial_p)_T dp = V dp$$

The relation between the differential temperature and pressure variations is

$$dT = \left\{\left[\frac{T(\partial V/\partial T)_p - V}{c_p}\right] + \frac{V}{c_p}\right\} dp$$

where the quantity in brackets in the Joule-Thomson coefficient. Thus, whether the pressure change for a given temperature change is smaller or larger than that which would be calculated from perfect-gas relations depends upon the sign of the Joule-Thomson coefficient, and its magnitude relative to V/c_p. Similarly, the differential change in volume depends upon the magnitude of the quantity

$$c_V/[1 + (1/p)(\partial U/\partial V)_T]$$

as compared with the value of $c_V{}^{(\infty)}$ for a perfect gas.

In order to investigate the effects of intermolecular forces, we have calculated the isentropic expansion of air from rest for various initial conditions, assuming that the gas obeys the Beattie-

Bridgman equation of state.* In one case the initial stagnation temperature is 1,500°R. and the initial pressure 495 lbs. per sq.in. absolute; at $M = 5.0$, we find $p/p_0 = 0.00187$, as compared with $p/p_0 = 0.00189$ for a perfect gas with $\gamma = 1.4$. In this case the "correction factor" is 0.989 rather than 0.830, as given by Professor Schetzer for $M = 5.0$, local $T = 520°R$. The difference is explained by the fact that Professor Schetzer's calculations are based on the tables of Keenan and Kaye, which were prepared for a pressure of 1 lb. per sq.in. atmosphere and which neglect the dependence of internal energy on volume and of enthalpy on pressure. At high temperatures $c_v^{(\infty)}$ and $c_p^{(0)}$ are both larger than the perfect-gas values; consequently, if one neglects the Joule-Thomson effect and puts $(\partial U/\partial V)_T = 0$, the volume and pressure changes for a given temperature change are larger than that predicted by the perfect-gas relations, and the "correction factors" for an isentropic expansion are less than unity. Evidently, such a procedure is justified only if the pressures are low—i.e., specific volumes are large. One may conclude that no universal correction factors independent of specific volume exist (as Professor Schetzer is undoubtedly aware), and the one-dimensional flow calculations must be carried out for a series of representative values of pressure and temperature.

* A report is in preparation.

Relations Between Viscous and Structural Damping Coefficients

(Continued from page 410)

case of Eq. (20), however, the ellipse remains the same regardless of changes in frequency. It is a well-known fact that in any given structure under static test, as the load is slowly cycled through its range of values and load-deflection diagrams plotted covering the entire cycle, a definite hysteresis loop is obtained which bears considerable similarity to the ellipse described by Eqs. (20). This hysteresis loop shows no evidence of reducing to zero as the rapidity of loading is decreased to extremely low values. This agrees at least qualitatively with Eqs. (20). There is also evidence to indicate that the size of the hysteresis loop does depend on the rapidity of loading. However, it is outside the scope of the present paper to discuss these deviations of an actual structure from the assumed damping laws.

The damping in a structure is frequently defined by the ratio of the area of the ellipse given by Eqs. (21) and (22) to the strain energy of the structure at its extreme displacement. The strain energy is $(1/2)kx_0^2$, and the area ratios are:

$$\pi c\omega x_0^2/[(1/2)kx_0^2] = 2\pi c\omega/k \qquad (23)$$

$$\pi kgx_0^2/[(1/2)kx_0^2] = 2\pi g \qquad (24)$$

If the damping in a structure does follow the mechanism implied by the assumption of the complex stiffness, then the equivalent viscous damping coefficient is a linear function of the forcing frequency and must increase at the same rate that the frequency decreases.

Eqs. (23) and (24) define a "per cent energy loss due to damping," in that of the total strain energy present at an extreme displacement the proportion given by Eqs. (23) or (24) is dissipated in completing a cycle of vibration. This per cent loss can be a sizable figure even for relatively small amounts of damping. For example, for a value of $g = 0.10$ (corresponding to $\lambda = 0.05$) $2\pi g$ becomes 0.628, or nearly 63 per cent of the strain energy present at the beginning of a cycle is dissipated in the course of that cycle.

References

[1] Theodorsen, T., and Garrick, I. E., *Mechanism of Flutter*, N.A.C.A. Report No. TR685, 1940.

[2] Coleman, R. P., *Damping Formulas and Experimental Values of Damping in Flutter Models*, N.A.C.A. T.N. No. TN751, February, 1940.

[3] Den Hartog, J. P., *Mechanical Vibrations*, 3rd Edition, p. 53; McGraw-Hill Book Company, Inc., New York, 1947.